ORNL/TM-11781

ornl

OAK RIDGE
NATIONAL
LABORATORY

MARTIN MARIETTA

Tritium Proof-of-Principle Pellet Injector

P. W. Fisher

MANAGED BY
MARTIN MARIETTA ENERGY SYSTEMS, INC.
FOR THE UNITED STATES
DEPARTMENT OF ENERGY

ORNL/TM-11781
Dist. Category UC-424

Fusion Energy Division

TRITIUM PROOF-OF-PRINCIPLE PELLET INJECTOR

P. W. Fisher

Date Published—July 1991

NOTICE: This document contains information of a preliminary nature. It is subject to revision or correction and therefore does not represent a final report.

Prepared for the
Office of Fusion Energy
Budget Activity No. AT 15 01 02 7

Prepared by
OAK RIDGE NATIONAL LABORATORY
Oak Ridge, Tennessee 37831-6285
managed by
MARTIN MARIETTA ENERGY SYSTEMS, INC.
for the
U.S. DEPARTMENT OF ENERGY
under contract DE-AC05-84OR21400

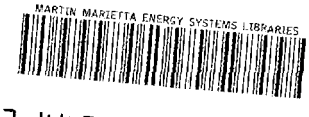

CONTENTS

LIST OF FIGURES v
LIST OF TABLES vii
ABSTRACT ix
1. INTRODUCTION 1
2. EXPERIMENT 3
2.1 SYSTEM HARDWARE 3
2.1.1 Gun Assembly 3
2.1.2 Pellet Diagnostic Line 7
2.1.3 System Flow 11
2.1.4 Interfaces between TSTA System and Glovebox 17
2.1.5 Process Control and Data Acquisition 18
2.2 SYSTEM OPERATION 21
2.2.1 TSTA Requirements 22
2.2.2 Calibrations 22
2.2.3 General Operation 23
2.3 TRITIUM ANALYSIS 28
3. RESULTS AND DISCUSSION 31
3.1 PELLET SIZE 32
3.1.1 Deuterium Fill Data 32
3.1.2 Tritium Fill Data 34
3.1.3 Equilibrium Fill Model 37
3.2 PELLET VELOCITY 50
3.2.1 Diagnostics 50
3.2.2 Correlation with Theory 51
3.3 BREAKAWAY PRESSURE 55
3.4 PELLET EROSION 57
3.5 SYSTEM RELIABILITY 62
4. CONCLUSIONS AND RECOMMENDATIONS 64
REFERENCES 65

FIGURES

2.1. TPOP experiment 4
2.2. Diagram of TPOP gun 5
2.3. Photograph of TPOP gun 6
2.4. Helium-3 separator 8
2.5. Gun assembly in glovebox 9
2.6. Gun and pellet diagnostic line 10
2.7. Overall system flow diagram 12
2.8. Glovebox layout 13
2.9. Gun feed gas manifold 15
2.10. Storage gas manifold 16
2.11. Interfaces between pellet injector and TSTA 18
2.12. TPOP control and data acquisition system 19
2.13. Deuterium and tritium vapor pressure 22
2.14. Tritium fill path produced by program T2FILL 24
2.15. Helium-3 separation flow path 25
2.16. Gun filling flow path 27
2.17. Uncertainty in ^3He analysis 31
3.1. Deuterium pellet size as a function of heat sink location 33
3.2. Deuterium pellet size as a function of temperature and equilibrium fill pressure 33
3.3. Time dependence of deuterium pellet formation 34
3.4. Deuterium pellets at various times during formation 35
3.5. Trtium pellet size as a function of temperature and pressure 36
3.6. Time dependence of tritium pellet formation 37
3.7. Predicted ratio of backpressure to feed pressure 38
3.8. Geometry for pipe gun pellet formation equilibrium model 39
3.9. Finite difference node arrangement 40
3.10. Effect of number of nodes on pellet size 44
3.11. Deuterium pellet size as a function of temperature and pressure 45
3.12. Deuterium pellet size for pellets formed by filling from the breech 46
3.13. Tritium pellet size for pellets formed by filling from both ends of the barrel and by filling from the breech 47
3.14. Pellet shape with 1 K isotherms for a deuterium pellet 48

3.15. Pellet shape with 1 K isotherms for a tritium pellet 48
3.16. Deuterium pellet formed at 10 K 49
3.17. Effect of feed pressure above the triple-point pressure on pellet length 50
3.18. Breech pressure and velocity diagnostics for a typical shot 51
3.19. Pellet velocity as a function of peak breech pressure 52
3.20. Pellet velocity as a function of initial acceleration 54
3.21. Typical breakaway pressure curves 56
3.22. Shear strength of D_2 and T_2 determined from breakaway pressure data 58
3.23. Video images of several deuterium pellets 59
3.24. Relative size of a video image of a rectangular grid pattern. 60
3.25. Pellet diameter as a function of velocity 61
3.26. Pellet fractional mass loss, based on diameter reduction, as a function of velocity 62
3.27. Number of cycles for TPOP system components 63

TABLES

2.1. Tritium analysis data 29
3.1. Physical property data 42
3.2. Breakaway pressure data 57

ABSTRACT

The tritium proof-of-principle (TPOP) experiment was designed and built by Oak Ridge National Laboratory (ORNL) to demonstrate the formation and acceleration of the world's first tritium pellets for fueling of future fusion reactors. The experiment was first used to produce hydrogen and deuterium pellets at ORNL. It was then moved to the Tritium Systems Test Assembly at Los Alamos National Laboratory for the production of tritium pellets. The injector used in situ condensation to produce cylindrical pellets in a 1-m-long, 4-mm-ID barrel. A cryogenic ^{3}He separator, which was an integral part of the gun assembly, was capable of lowering ^{3}He levels in the feed gas to <0.005%. The experiment was housed in a glovebox for tritium containment. Nearly 1500 pellets were produced during the course of the experiment, and about a third of these were pure tritium or mixtures of deuterium and tritium. Over 100 kCi of tritium was processed through the experiment without incident. Tritium pellet velocities of 1400 m/s were achieved with high-pressure hydrogen propellant. The design, operation, and results of this experiment are summarized.

1. INTRODUCTION

Injection of high-velocity pellets of hydrogen isotopes is an efficient means of fueling fusion devices or confinement experiments.[1–5] To date, injection systems on fusion experiments have used pellets of either hydrogen or deuterium.[6] However, future fusion devices, such as the Burning Plasma Experiment[7] (formerly the Compact Ignition Tokamak) and the International Thermonuclear Experimental Reactor[8] (ITER), as well as fusion reactors, will depend heavily on tritium and deuterium-tritium (DT) pellet fueling.

The tritium proof-of-principle (TPOP) experiment was conceived and carried out to begin the study of tritium pellet fueling for future devices by demonstrating the feasibility of tritium pellet production and acceleration. A tritium pellet injection system was designed and built at Oak Ridge National Laboratory (ORNL), where it was used to produce hydrogen and deuterium pellets. It was then moved to the Tritium Systems Test Assembly (TSTA) at Los Alamos National Laboratory (LANL) and used to produce tritium pellets. All design work was carried out in close collaboration with TSTA personnel to ensure compatibility of interfaces and operations with the TSTA test loop.

The design of the TPOP experiment was complicated by the limited information on the properties (especially the mechanical properties) of solid tritium,[9] which made it impossible to determine conclusively whether any of the existing pellet injector concepts could be successfully applied to the generation of tritium pellets. The radioactive decay of tritium is accompanied by several phenomena that could affect pellet injector design and performance. Tritium has an internal heat generation term (0.977 W/mol T), not present in other hydrogen isotopes, that could affect pellet formation and strength. The natural decay product of tritium, ^{3}He, grows at a rate of 0.015 mol %/d. Small amounts of helium could affect the thermal conductivity and strength of the solid.[10] In Ref. 11, Souers reported that very low concentrations of ^{3}He seriously impede the transfer of tritium into small capsules by cryopumping action. These capsules were similar in size to the freezing zone that must be filled by cryopumping in pellet injectors. According to Souers,[11] the lowest ^{3}He level that can be achieved in tritium with uranium bed processing is 0.12%; it was anticipated that much lower concentrations than this would be required for the TPOP experiment. Added to these concerns are requirements for radiation-compatible materials for tritium-wetted gun components and double containment for all tritium handling equipment. All of these effects were taken into account during the design process, and their impacts on design, operation, and performance were evaluated as part of the TPOP program.

Existing pellet injector designs were reviewed and evaluated for their applicability to the TPOP experiment. In an early injector developed by Milora and co-workers,[12–15] pellets were formed at a fill station by direct condensation of hydrogen from the gas phase and then transported to the gun barrel in a disk-shaped carrier, which sheared off any excess solid when it was rotated from the fill station to the firing position. Lafferanderie and co-workers[16] later used an approach that they termed in situ condensation, in which a 6-mm-OD pellet was frozen in a 6-mm-long cooled section at the breech end of a barrel in a position ready for firing. This concept simplifies gun design because it eliminates all moving parts inside the gun; however, since the pellet length is not mechanically constrained, pellet size is more difficult to control. By attaching heaters to the barrel next to the cooled barrel section, it was possible to made reproducible pellets up to 8 mm long in this gun. Combs and co-workers[17] used a similar concept to produce 4-mm-OD pellets by attaching heater collars to the outside of the gun barrel near the 4-mm-long freezing zone; ≈8-mm-long pellets were produced. Sorenson and co-workers[18] described a gun for producing 2-mm-OD pellets; the barrel is a continuous stainless steel tube with copper rings soldered to the outside of the barrel to set the length of the pellet formation zone (2 mm) and the temperature gradient to the pellet. Pellets on the order of 3 mm long were produced in this gun.

An adaptation of the in situ condensation approach, incorporating a continuous stainless steel gun barrel, was adopted as a point of departure for the TPOP design, with the goal of producing 4-mm-OD pellets with an aspect ratio of one. The entire experimental apparatus was designed and built to be compatible with tritium and was enclosed in a glovebox for tritium containment. A cryogenic ^{3}He separator was incorporated as an integral part of the TPOP assembly.

The success of this effort has been demonstrated by the results from the TPOP experiment. Nearly 1500 pellets were produced during the course of the experiment, about a third of which were pure tritium or mixtures of deuterium and tritium. Pellet length was successfully controlled without heater collars on the gun barrel. Over 100 kCi of tritium was processed through the experiment without incident. Tritium pellet velocities of 1400 m/s were achieved with high-pressure hydrogen as the propellant. The cryogenic ^{3}He separator was capable of lowering ^{3}He levels in the feed gas to <0.005%.

Previous publications have reported TPOP system design and operation on TSTA[19] and some results from operation with deuterium[20] and tritium.[21] Here we summarize the work to date. The TPOP experiment is described in Sect. 2, and results are presented in Sect. 3. Conclusions and recommendations are given in Sect. 4.

2. EXPERIMENT

Figure 2.1 is a photograph of the TPOP experiment as it appeared during operations with hydrogen and deuterium feed gas in the ORNL Fusion Energy Division. The gun, the injection line, and the gas handling system were housed in a glovebox for tritium containment. With very few exceptions (noted below), tritium-wetted surfaces were all metal (usually stainless steel). All interfaces between the glovebox and the outside world (tritium, nitrogen, helium, electrical, control, vacuum connections, etc.) were through panels in the top of the glovebox. Operation of the entire experiment was controlled remotely from the console at right in Fig. 2.1. High-speed data acquisition was accomplished through a MicroVAX II computer (not shown) and CAMAC interfaces located at the back of the control console. The system and its operation are described in detail in Sects. 2.1 and 2.2. Tritium analysis is described in Sect. 2.3.

2.1 SYSTEM HARDWARE

2.2.1 Gun Assembly

Figure 2.2 is a diagram of the TPOP gun assembly, which is housed in a guard vacuum chamber consisting of a front flange and a shell, and Fig. 2.3 is a photograph of the assembly with the guard vacuum shell removed. The entire gun assembly and all its associated feedthroughs are mounted on the front flange of the guard vacuum enclosure. Principal components include the gun barrel, the copper plate that forms the freezing zone for the pellets, the gun cryostat, and the ^{3}He separator.

The gun barrel is a continuous 4-mm-ID, 1-m-long stainless steel tube with a wall thickness of 0.4 mm (0.016 in.). The position of the thermal short between the gun barrel and the front flange of the guard vacuum was used to help control the pellet length. The heater collars shown in Fig. 2.3 were used only during initial experiments and then removed.

The gun barrel was silver soldered to a 3-mm-thick copper plate to form the freezing zone for the pellets. (A 1-mm-thick copper insert was added to make the freezing zone 4 mm long during the final phase of tritium testing.) The temperature of the copper plate was measured by two silicon diodes (Lakeshore DT-470-CU-12) mounted directly on the plate with brass studs. The joint between the gun barrel and the copper plate was carefully machined to remove all solder from the barrel and form a sharp corner between the barrel and the copper plate. A Cajon VCR fitting was attached to each end of the barrel to form an all-metal sealed interface with the injection line at the muzzle end and

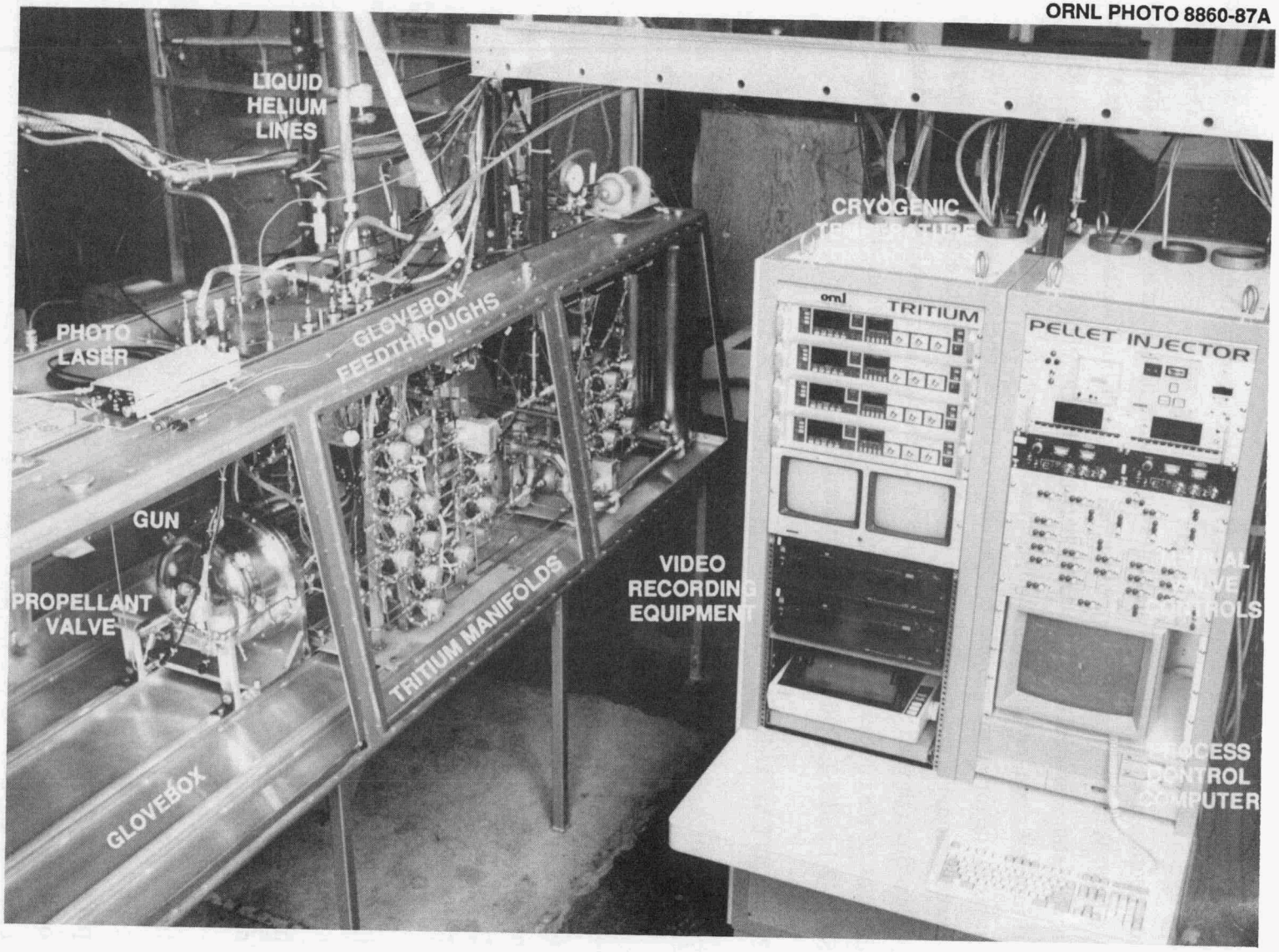

Fig. 2.1. TPOP experiment.

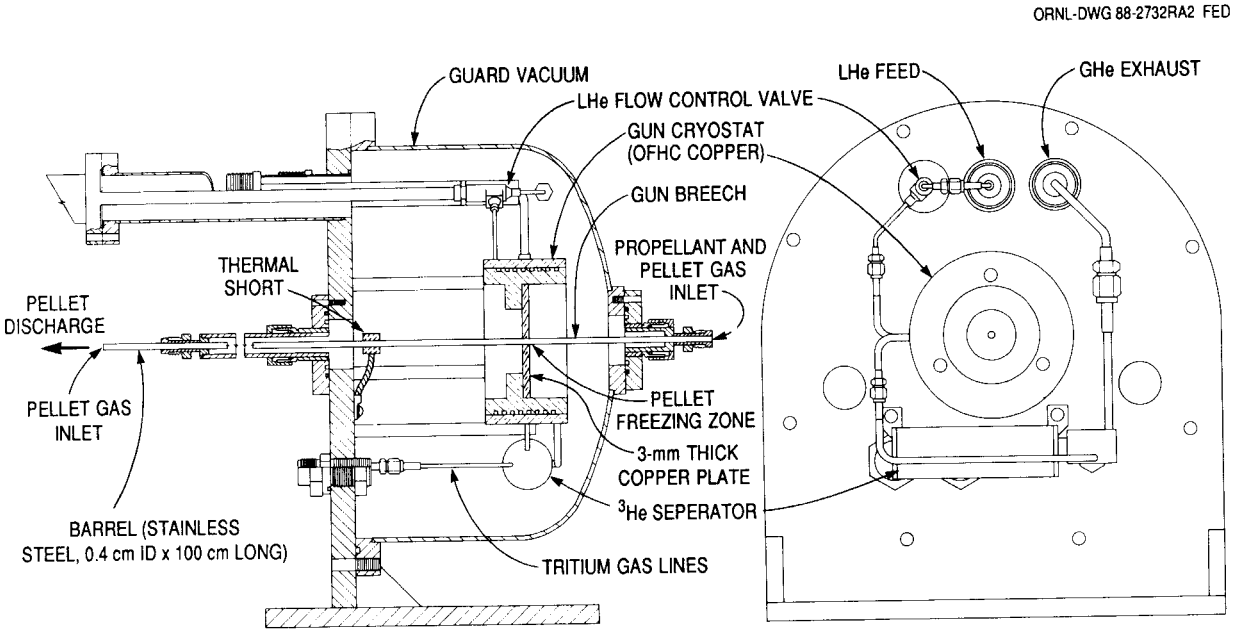

Fig. 2.2. Diagram of TPOP gun.

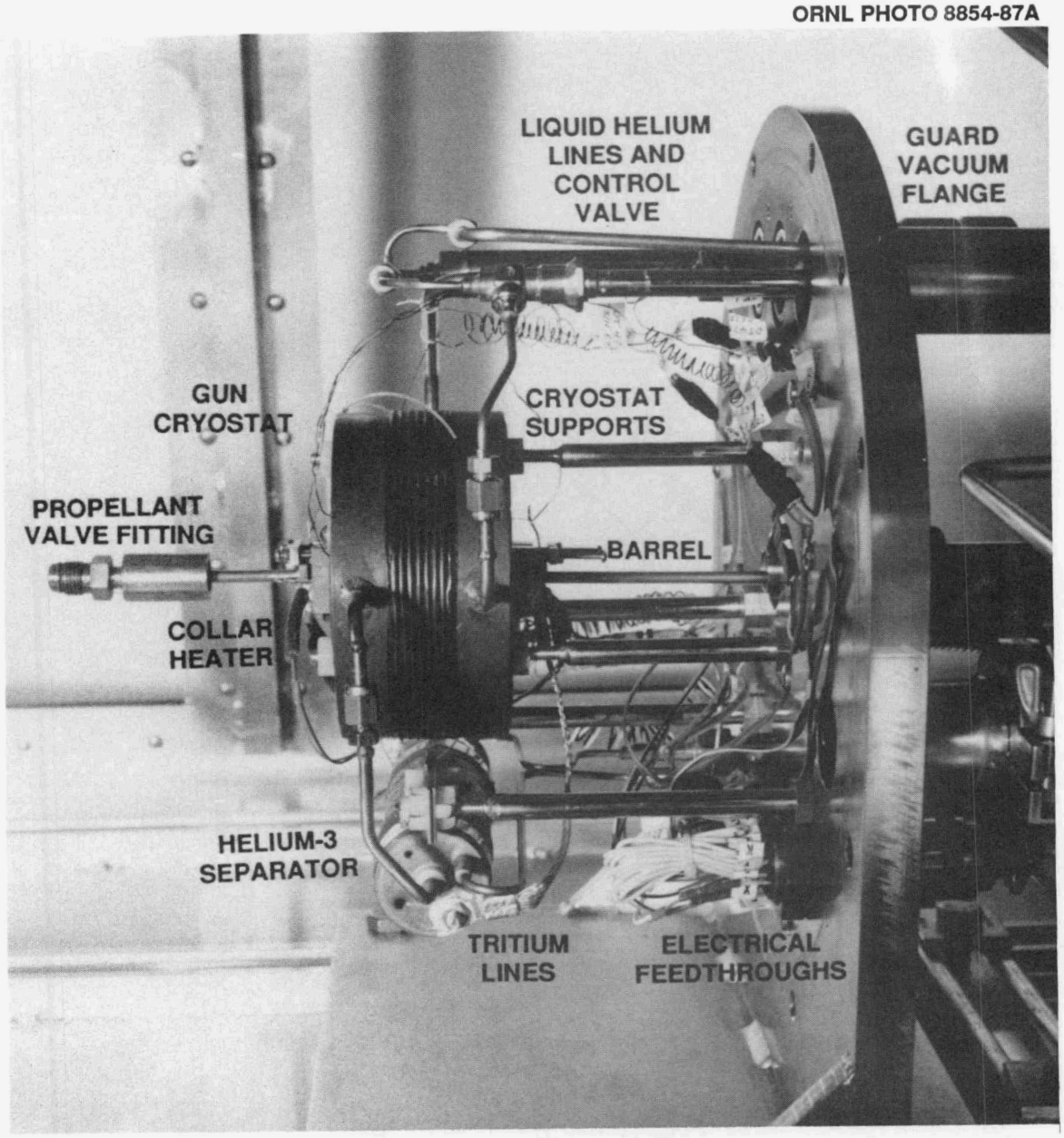

Fig. 2.3. Photograph of TPOP gun.

the propellant valve at the breech end. The breech region (from the freezing zone to the end of the fitting for the propellant valve) is 14 cm long.

A 1.91-cm-OD (0.075-in.-OD) sleeve was soldered near each end of the barrel just inboard of the VCR fittings. These sleeves slide through the O-ring seals on the guard vacuum chamber to form the guard vacuum interface. The copper plate was bolted to the gun cryostat, and the interface of this joint was coated with silver-loaded grease to improve heat transfer. The entire barrel assembly could be removed from the system by

disassembling these few mechanical joints, which were easily remade, without disturbing any other parts of the system.

The gun cryostat is a 12.7-cm-OD (5-cm-OD) block of oxygen-free, high-conductivity (OFHC) copper that has 0.318- by 0.318-cm (0.125- by 0.125-in.) square cooling channels with a 0.635-cm (0.25-in.) spiral pitch machined into it. A 50-Ω Nichrome heater was wrapped around and epoxied to the perimeter of the cryostat for temperature control.

Liquid helium entered and exited the guard vacuum chamber through bayonet fittings. The liquid helium passed through a flow control valve, then through the cryostat, and finally through the ^{3}He separator before it was discharged.

The ^{3}He separator is basically a small copper counterflow heat exchanger. A diagram is shown in Fig. 2.4. Helium coolant passes through the 1.27-cm-ID (0.5-in.-ID) central cooling channel, which has a spiral baffle to enhance heat transfer. Tritium is cryopumped into the external finned surfaces, which have a large volume (139 cm^3) to keep the ^{3}He pressure low during filling and a wide entry region to prevent obstruction by condensed tritium.

Figure 2.5 shows the gun assembly mounted in the glovebox. The gun barrel, guard vacuum enclosure, helium feed lines, pellet gas valve, and propellant valve are visible. Cajon VCR fittings were used for all external gas connections. The propellant valve is a fast solenoid valve (<1-ms opening time) developed by Milora and co-workers,[22] which has operated at 20.6 MPa (3000 psi). It is all metal except for the Vespel stem tip. A Conflat-type seal was used for the main body. The pellet gas valve admitted feed gas to the gun breech during pellet formation. Breech pressure was measured with a quartz piezoelectric transducer (PCB 105B22, 0 to 5000 psi). A similar valve was located at the muzzle end of the barrel, as shown in Fig. 2.6. These bellows valves (Nupro HB series), which also have Vespel stem tips, have an operating pressure of 24.1 MPa (3500 psi). The Teflon-coated bellows-to-body gasket on the original valve was replaced with a silver-coated gasket for tritium service.

2.1.2 Pellet Diagnostic Line

The pellet diagnostic line shown in Fig. 2.6 provided several means for measuring pellet velocity and photographing pellets. The two diagnostic stations shown, which were 80.5 cm apart, were essentially identical; each had a velocity gate and a photographic station. Pellets were viewed through Ceramaseal sapphire windows with a 2.54-cm (1-in.) clear viewing diameter. The windows were mounted on 7-cm-OD (2.75-in-OD) Conflat

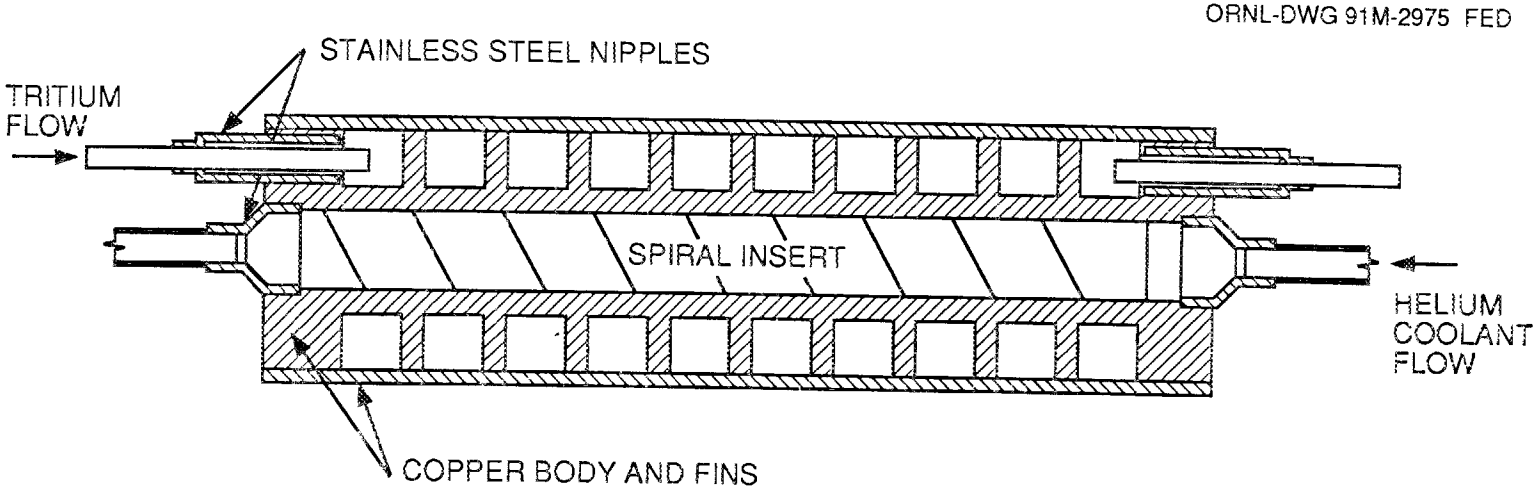

Fig. 2.4. ^{3}He separator.

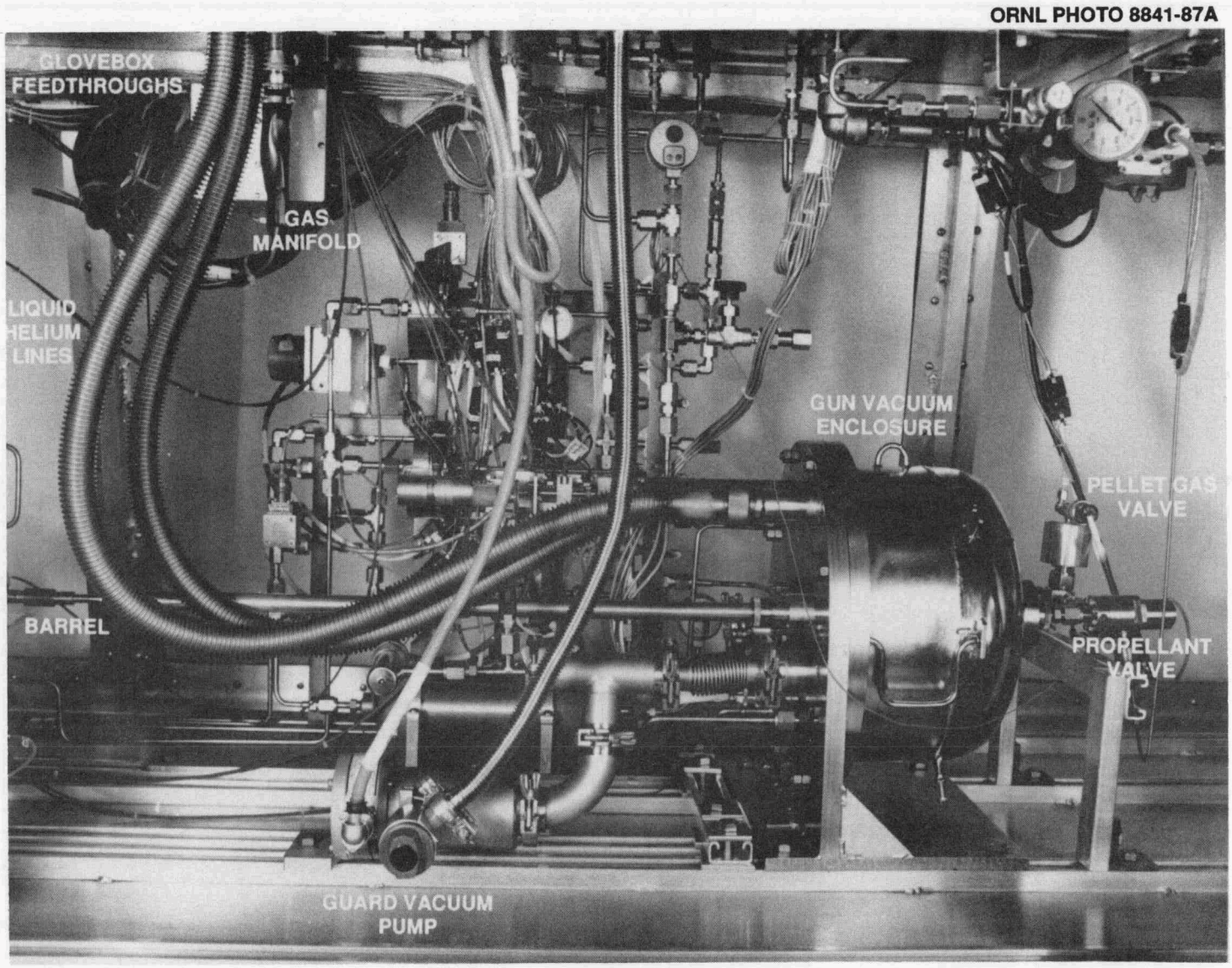

Fig. 2.5. Gun assembly in glovebox.

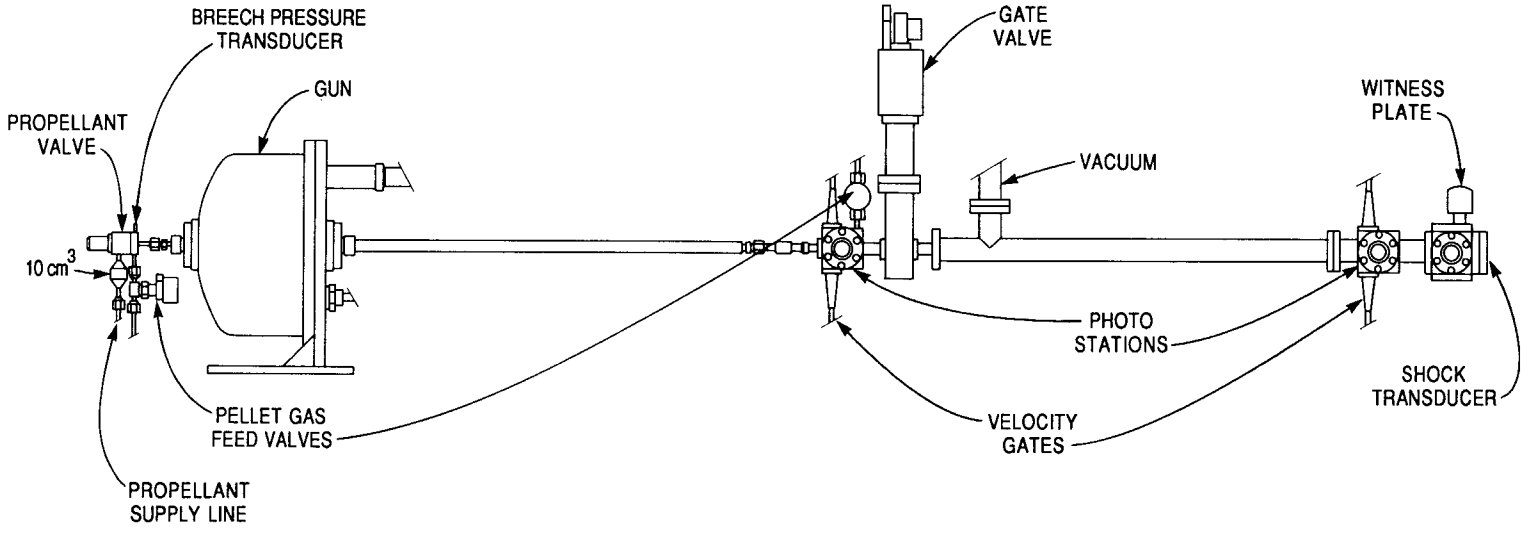

Fig. 2.6. Gun and pellet diagnostic line.

flanges and had a working pressure range from high vacuum to 2.1 MPa (300 psi). The velocity gates used 1-mm optical fibers to form light beams that, when interrupted, indicated the presence of a pellet. Ensing-Bickford radiation-hard and hard-clad silica fiber cables were used. The cladding was stripped back, and the silica fibers were brought into the vacuum system through 1-mm holes. Fibers were potted into Mini-Conflat fittings with Varian TorrSeal epoxy. The gap between transmitting and receiving fibers through which the pellets passed was 1.27 cm (0.5 in.). At the first diagnostic station, two light gates, separated by 1 cm along the pellet flight path, provided a velocity estimate, which was used to set the time of the first photograph. At the second diagnostic station, three light gates cut perpendicularly across the pellet flight path at the end of the guide tube to allow for pellet dispersion. Interruption of any one gate could be used to calculate velocity and to set the time for the second photograph.

The gate valve in the pellet line (PV1 in Fig. 2.7) separated the gun from the vacuum system during pellet formation. This pneumatically actuated (with spring closing), all-metal gate valve (VAT Series 48) had DN 16 CF (Mini-Conflat) flanges.

At the end of the pellet line, a piezoelectric shock transducer (PCB 305A03) was mounted on the outside of a 7-cm (2.76-in) Conflat flange to detect the time at which the pellet reached the end of the diagnostic line. The multiple light gates and impact signals from the shock transducer allowed independent measurement of the pellet speed. A piezoelectric force transducer (PCB 208A12), with its electrical connector concentric to the mounting stud, was mounted on the inside of the same flange (the vacuum seal was made with TorrSeal epoxy). This transducer was intended to provide a measurement of pellet impact force, from which the pellet mass could have been determined through the velocity; however, signals from the transducer showed wide positive and negative swings (like a shock transducer) and could not be used to determine force.

The witness plate at the end of the diagnostic line gave a positive indication of pellet position by recording an impact crater in a soft metal target. The plate was mounted on a rotary bellows seal valve operator so that it could be rotated from the pellet path to a sapphire window for viewing.

2.1.3 System Flow

Figure 2.7 is a flow diagram of the TPOP system, including the gun assembly, the guard vacuum, the pellet diagnostic line, the feed gas manifolds, the glovebox, and the required utilities. The locations of these major components are shown in Fig. 2.8.

The glovebox was made of aluminum with Lexan windows; it had an internal volume of 3 m^3. The system was modularized as much as possible so that subassemblies

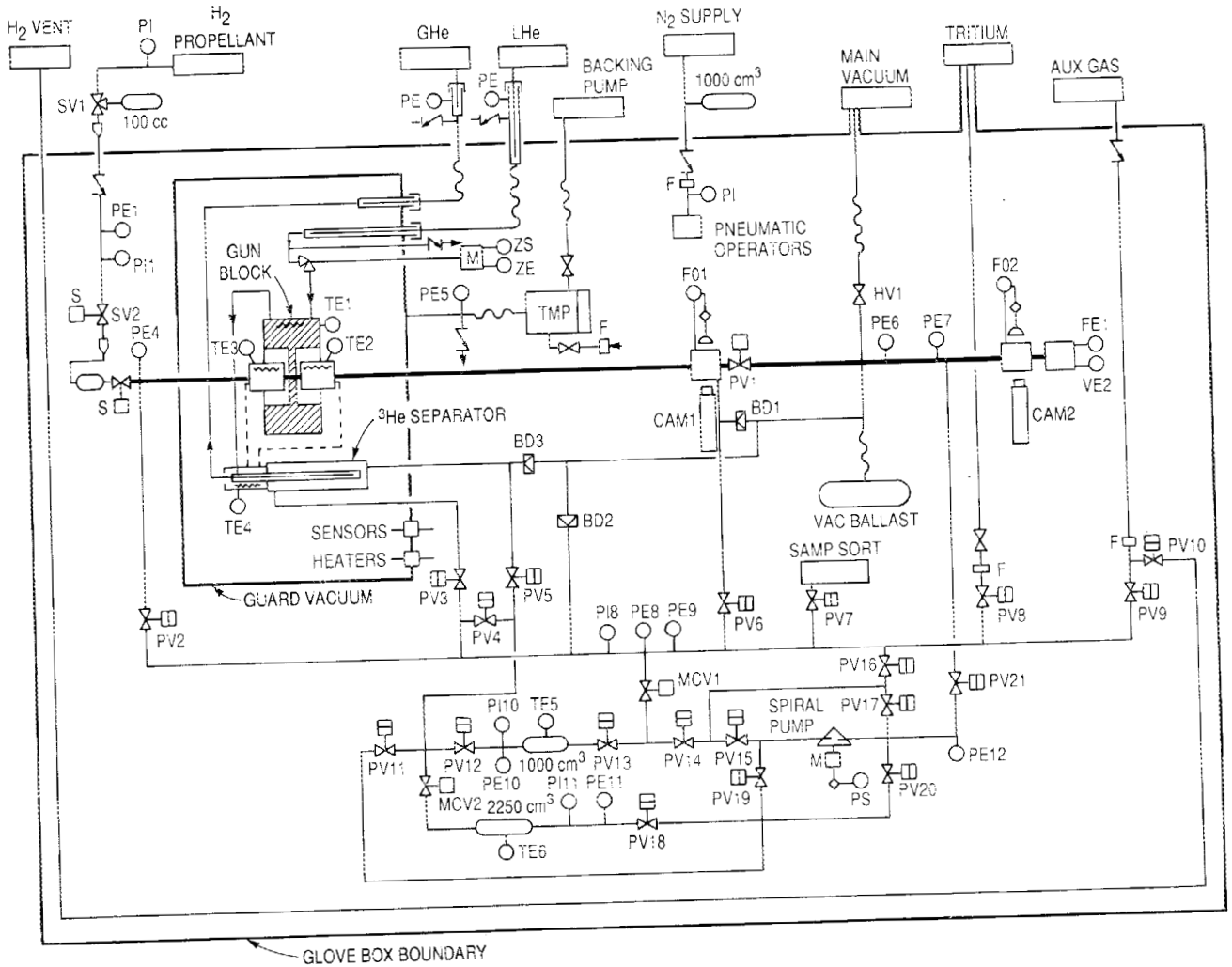

BD - BURST DISK
CAM - CCD CAMERA
F - FILTER
FE - FORCE ELEMENT
FO - FIBER OPTIC
HV - HAND VALVE
M - MOTOR
MCV - MOTOR CONTROL VALVE
PE - PRESSURE ELEMENT
PI - PRESSURE INDICATOR
PV - PNEUMATIC VALVE
S - SOLENOID
SV - SOLENOID VALVE
TE - TEMPERATURE ELEMENT
VE - VIBRATION ELEMENT
ZS - POSITION SWITCH
ZE - POSITION ELEMENT

Fig. 2.7. Overall system flow diagram.

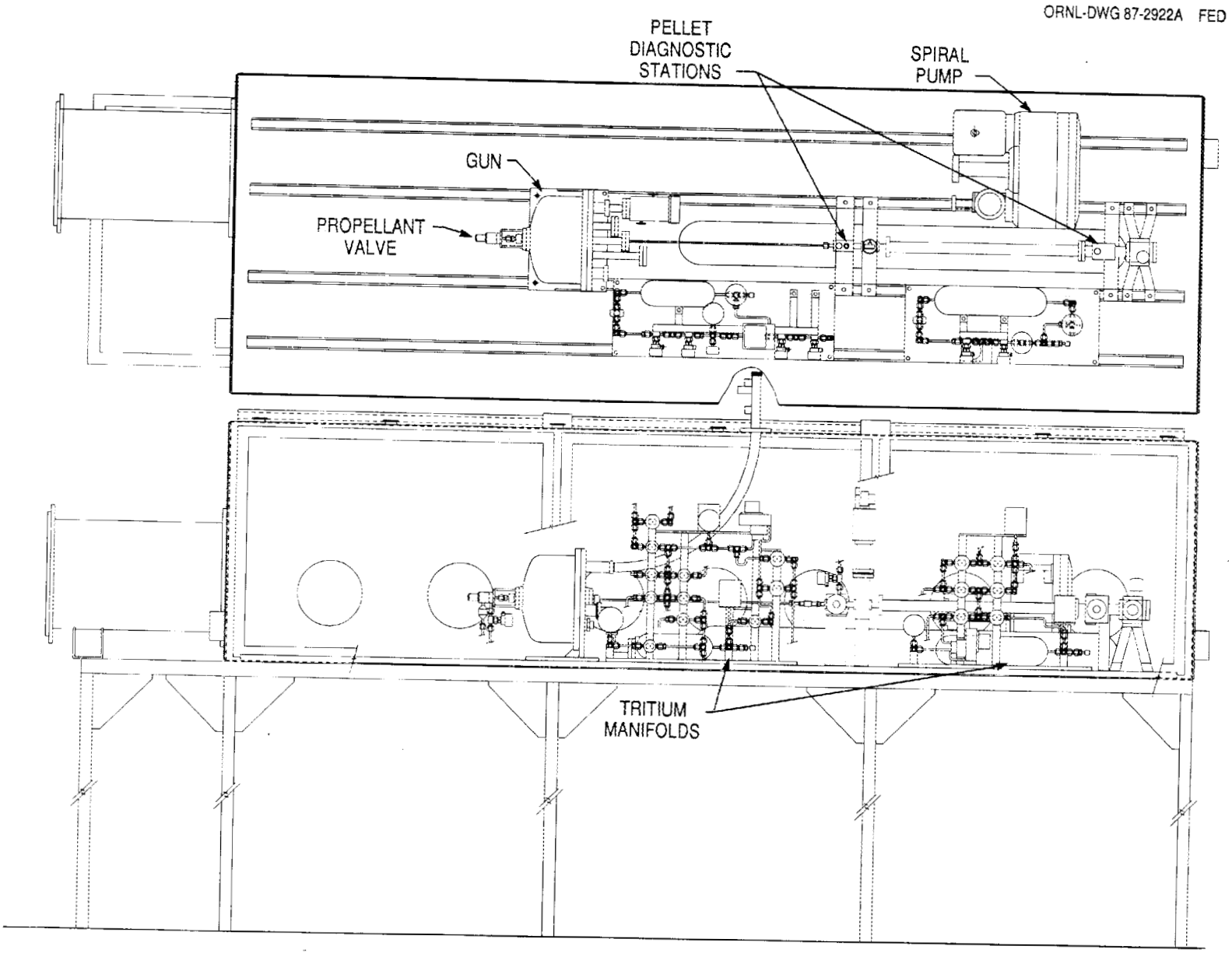

Fig. 2.8. Glovebox layout.

could be fabricated and tested before installation in the glovebox. Components were arranged to provide maximum space for maintenance and expansion. Subassemblies were attached to the glovebox with Unistrut strips that were welded to the floor and ceiling of the glovebox.

The gate valve in the pellet line (PV1), the pellet gas valve (PV2), and the valve at the muzzle end of the barrel (PV6) are described in Sect. 2.1.1. Valves PV3–PV5 and PV7–PV20 were located on two pellet feed gas (tritium) manifolds, shown in Figs. 2.9 and 2.10. The manifold in Fig. 2.9 supplied pellet feed gas to the gun and tritium to the ^{3}He separator, received feed gas (both tritium and auxiliary gas) from external sources, and served as a gas sampling location. The manifold in Fig. 2.10 provided 2250 cm^3 of storage for the pellet feed gas and internal pumping and vacuum interfaces for the feed gas system. Both manifolds were constructed entirely of stainless steel with welded, silver-soldered, or Cajon VCR joints. Shutoff valves were pneumatically actuated, normally closed valves (Nupro BK series) with Vespel tips. Valve positions were determined by reading pressure switches (Whitman-P119) attached to each valve's pneumatic supply line. Each manifold had a motor control valve (MCV1 and MCV2 in Fig. 2.7) for metering gas delivery and for use as a pressure control element. These control valves were all metal with stepper motor drive (MKS Type 245). Pressures were indicated locally with absolute-pressure, variable-reluctance transducers (Validyne AP10) with AND-10050 pressure fittings sealed with Natorq silver-plated metal boss seals.

Valve PV21, located near the spiral pump, was a pneumatically actuated, spring-closing, all-metal, right-angle valve (VAT Series 37) with DN-16-CF (Mini-Conflat) flanges. This valve established flow between the manifolds and the external vacuum system via the pellet diagnostic line. The system's internal vacuum pump was a Normetex 15-m^3/h all-metal spiral pump, backed by a Normetex two-stage, all-metal diaphragm pump with a maximum discharge pressure of 100 kPa (1 atm). These pumps were outfitted with Conflat flanges for tritium service. The interface valve between the main vacuum line and the pellet diagnostic line was an all-metal, in-line hand valve (VAT Series 50) with DN-CF-35 (2.75-in.-OD) Conflat flanges. All VAT valves had position-indicating switches. A 30-L vacuum ballast tank attached to the main vacuum line helped to keep the system pressure low during shots. Aluminum bursting disks were provided for overpressure protection of nodes that could receive high-pressure gas or trap cryogenically condensed gas; these disks vented to the downstream vacuum system, not to the glovebox, to ensure tritium containment in case of failure. Reverse buckling rupture disks (BS&B Safety Systems RF-90), mounted in nominal 2.54-cm (1-in.) safety heads (RB-7FS) modified by adding VCR fittings, were used for this purpose.

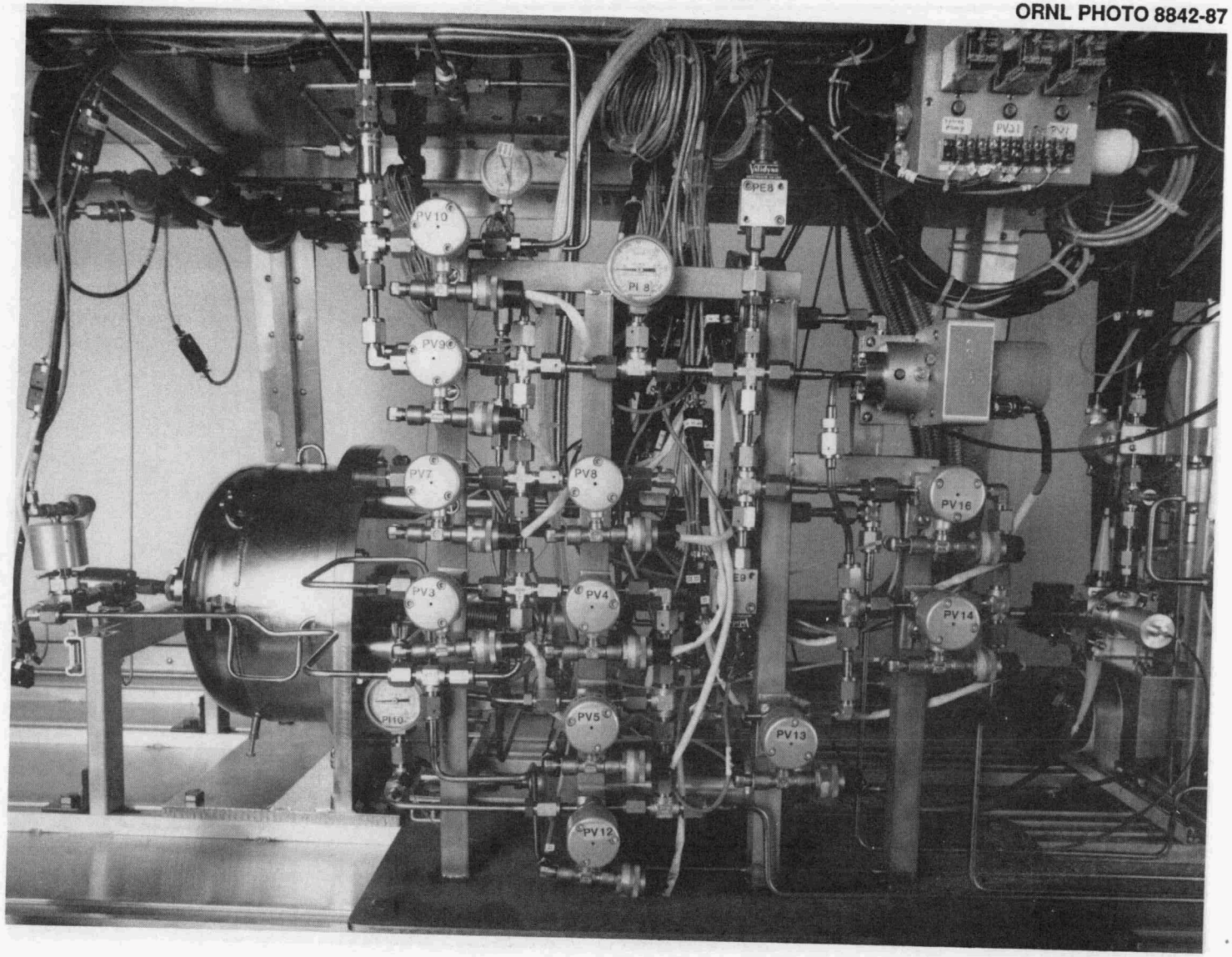

Fig. 2.9. Gun feed gas manifold.

ORNL PHOTO 8835-87

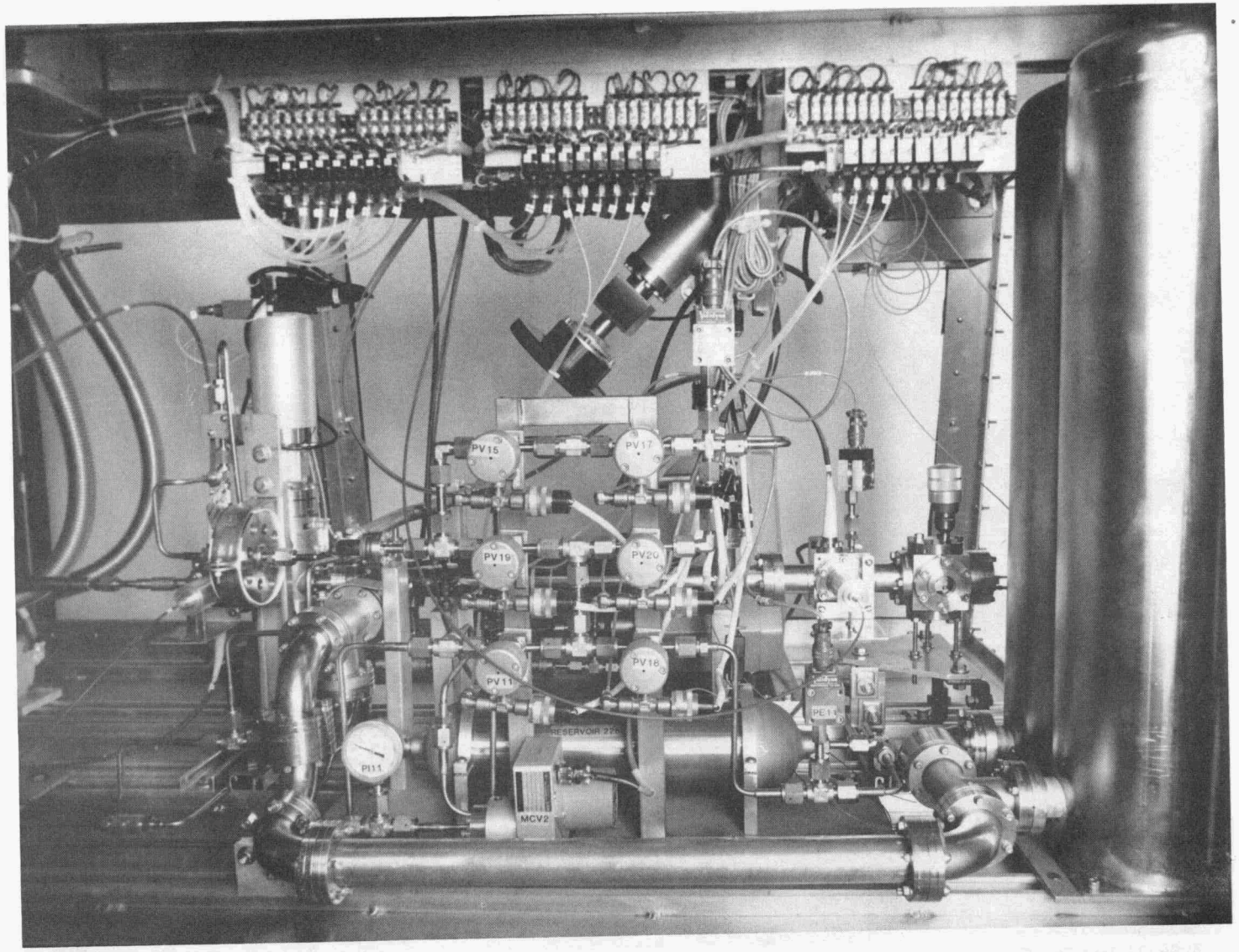

Fig. 2.10. Storage gas manifold.

All components in the propellant gas feed system were rated for operating pressures above 36 MPa (5200 psi). A three-way valve (SV1) separated the propellant supply line from the experiment, limiting the maximum gas volume that could be released to the glovebox to 100 cm^3, which is not enough to cause an overpressure hazard. Valves SV1 and SV2 were solenoid valves (Circle Seal SV20 series) with position-indicating switches. A snubber in the line after each of these valves limited the flow rate of high-pressure gas. Pressure was measured with a 0- to 24-MPa (0- to 3500-psi) pressure transducer (Dynisco Series 800). Supply pressure was measured with a 34.45-MPa (5000-psi) full-scale, calibrated Bourdon tube gage (Pressure Products). A hydrogen monitor (100 ppm full scale in nitrogen, International Sensor Technology AG3100) was located inside the glovebox to detect hydrogen leaks. All cryogenic temperatures were measured with silicon diodes (Lakeshore DT-470-CU-12).

2.1.4 Glovebox to TSTA System Interfaces

Figure 2.11 shows the major interfaces between the TPOP experiment and the TSTA facility. All interface feedthroughs (both mechanical and electrical) were located in two stainless steel panels that replaced two of the three windows on the top of the glovebox. Tritium was supplied to the glovebox from a product container (PC) in the TSTA load-in/load-out (LIO) system through a 0.635-cm-OD (0.25-in.-OD) copper line, which was doubly contained throughout its entire length. The main vacuum interface was connected with the TSTA transfer pump system (TP1) by a 3.8-cm-OD (1.5-in.-OD) stainless steel line, also doubly contained throughout its entire length. The TP1 system used a Normetex 15-m^3/h spiral pump backed with a two-stage metal bellows pump to transfer gas from the pellet injector to an empty PC in the LIO glovebox. Guard vacuum exhaust went to the TSTA house vacuum system.

The glovebox was automatically purged with nitrogen and pressure was controlled by a standard TSTA secondary containment enclosure control system (SEC). The gas supplied for operation of pneumatic valves was also nitrogen. Tritium levels were measured by a TSTA tritium monitor. Purge gas was routed to the tritium waste treatment system (TWT) whenever tritium levels exceeded 1 mCi/m^3. The glovebox was also equipped with a pressure relief bubbler connected to the TSTA stack. Two quick-disconnect fittings in the glovebox floor accommodated a portable tritium monitor used for tritium leak checking of equipment inside the glovebox. Liquid helium coolant was supplied from dewars to the glovebox through a transfer line with a bayonet fitting. Gaseous helium exhaust was routed directly to the TSTA stack through another transfer

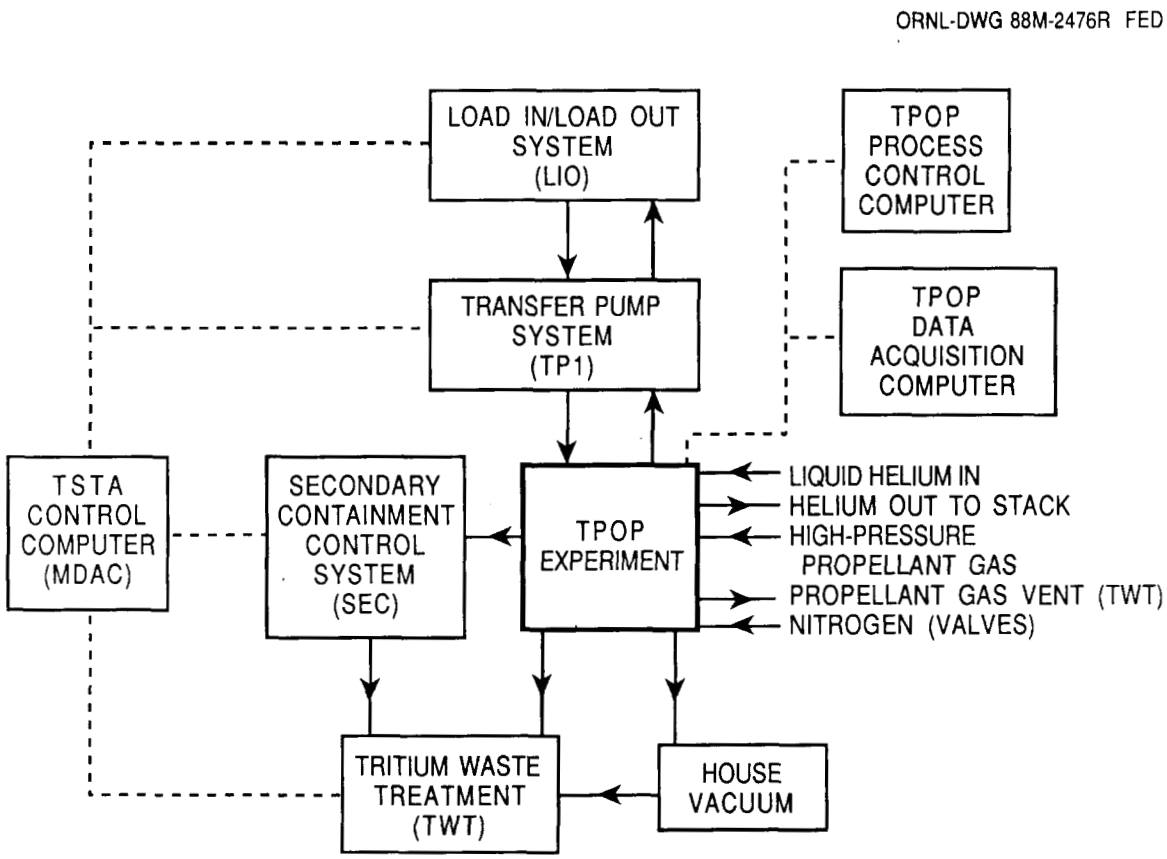

Fig. 2.11. Interfaces between pellet injector and TSTA.

line. All vented process gas that left the glovebox went to the TSTA TWT system. All utility gases (propellant, auxiliary gas, and nitrogen) entered the glovebox through check valves to prevent any backflow contamination of these supplies with tritium.

2.1.5 Process Control and Data Acquisition

Three separate computer systems were involved in TPOP operation. The TSTA master data acquisition computer (MDAC) controlled all of the functions of TSTA systems shown in Fig. 2.11 (LIO, TP1, SEC, etc.). The TPOP process control system, an NCR-PC8 personal computer (PC/AT) using a program called THE FIX from Intellution, controlled all systems in the TPOP glovebox. The TPOP experiment was operated in the TSTA facility with close cooperation of a TSTA operator who controlled all TSTA systems through MDAC while the TPOP experiment was running. A MicroVAX II computer was used for high-speed data acquisition from TPOP.

Figure 2.12 is a block diagram of the TPOP control and data acquisition system. All routine operations inside the glovebox were controlled by equipment outside the glove-

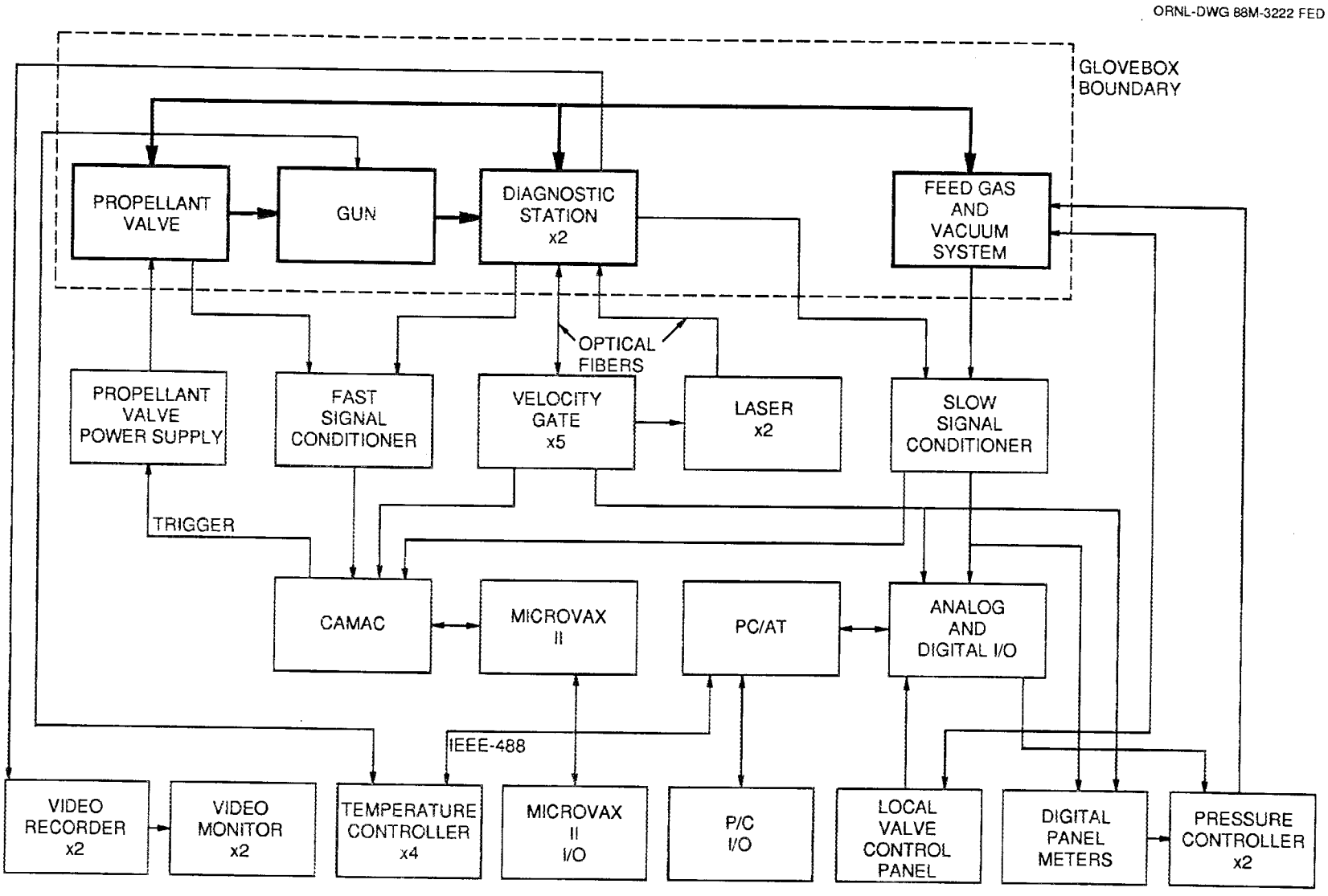

Fig. 2.12. TPOP control and data acquisition system.

box. In general, the operator worked only with the equipment shown along the bottom row in Fig. 2.12. Controls for this equipment (with the exception of the MicroVAX II input/output) were located on the front panel of the control console in Fig. 2.1. Valves in the experiment could be controlled either through a manual control panel or through the process control computer (but not through both simultaneously). THE FIX controlled all digital and analog input and output functions through an Analog Devices micro-Mac-4000 unit. The PC/AT also operated the Lakeshore DRC-91C cryogenic temperature controllers from THE FIX through an IEEE-488 bus using a program written in the C language especially for this purpose. Another C program recorded the number of times each valve was operated, the number of times the pump was operated, and the total time of pump operation for reliability studies. These data were recorded even if the system was being operated from the manual control panel. THE FIX was configured to allow the operator to see and control the entire process in manual mode from the PC/AT, see and control the gun temperatures, read and trend analog inputs (temperatures, pressures, etc.), and execute the program that was required to automatically run the system. All normal operations, such as tritium transfer to the glovebox, ^{3}He separation, gun filling, etc., were carried out automatically by these programs. Pressures in the system were controlled by MKS-245 pressure controllers. The setpoint pressures for these controllers came from the PC/AT, and the control-point pressures came directly from the digital panel meter gage readouts.

Signals from the light gates, shock transducers, and pressure elements were digitized by the CAMAC system. Fast signals were digitized at a rate of 0.5 MHz. The MicroVAX II computer collected fast transient data from the CAMAC modules, provided the trigger for the fast valve that fires the pellet, and collected a snapshot of all analog data values just before each shot. After the runs were completed, programs were run to plot the transient data, analyze the data to determine pellet velocity, and report pretrigger analog values. Velocities were calculated from the resulting time-of-flight information for three segments of the pellet path: between the first and second light gates, between the first light gate and the first indication of shock at the end of the diagnostic line, and between the second light gate and the first indication of shock. The analog circuit that controlled the light gates and photo triggers also calculated velocity from the light gates and produced an analog signal that was proportional to velocity. This signal was read by the PC/AT. Pellet images were recorded on VHS videotape by Panasonic AG-1950 video recorders using Panasonic WV-CD51 charge-coupled device (CCD) cameras. Images were backlighted by light from Laser Science VSL-DYE lasers with Coumarin 481 dye,

located outside the glovebox. Each 3-ns flash from a laser was carried through 1-mm optical fiber to a photo station, where it "froze" the image of the pellet in flight.

Hard-wired interlocks were built into the valve operating and firing systems to prevent two accidents with serious consequences. First, because transfer of tritium to any external system when the TSTA tritium supply was open to the TPOP gas manifolds could result in loss of large amounts of tritium, interlocks closed the tritium fill valve (PV8 in Fig. 2.7) whenever any valve to an external system (PV2, PV6, PV7, PV9, or PV21) was not closed. In addition, the propellant valve was prevented from firing into a closed system or into the gas manifolds by interlocking the fast valve power supply so that it could not be fired if the vacuum system valves HV1 and PV1 were not open or if fill valve PV2 or PV6 was not closed. The Normetex diaphragm pump was also protected against overpressure, which could occur if the system was improperly operated, by a pressure switch (Whitman Controls E120) that monitored the pump's exhaust pressure and cut its power if the pressure exceeded half the rated discharge pressure of 48 kPa (7 psig).

2.2 SYSTEM OPERATION

2.2.1 TSTA Requirements

Before any equipment was installed and operated in the TSTA facility, a standard operating procedure document, "Tritium Single Shot Pellet Injector" (TSTA Procedure TTA-SOP-110), and a test plan document, "Tritium Single Shot Pellet Injector Test Plan for Phase I Experiments" (TTA-TP-110-1), were written and approved by TSTA personnel. These documents covered all aspects of TPOP design, interfaces with the TSTA system, safety analysis, personnel training requirements, installation procedures, tritium leak testing procedures, and experimental procedures for pellet runs. Operators were required to read and understand these documents before working on the experiment. They were also required to read and have a working knowledge of the following documents: TSTA Organization Chart, MST-3 Safety Policy, TSTA Operating Procedures and Rules, TSTA Emergency Plan (TTA-EP-100-1), and Working With Tritium (TTA-SOP-100-3).

2.2.2 Calibrations

The span of the pressure transducers was set against a mercury barometer shortly after the experiment was installed at TSTA. Before each day's work, the entire system was evacuated and all pressure gages were zeroed. Figure 2.13 shows measured vapor

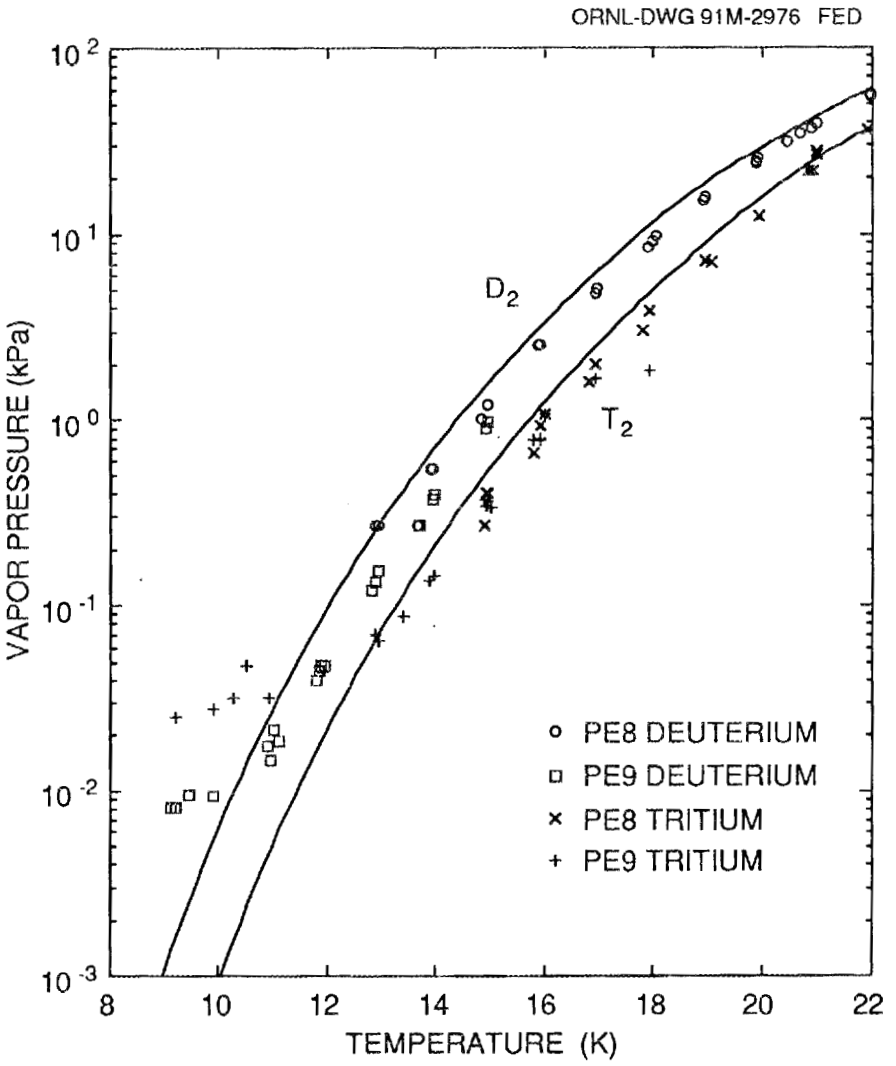

Fig. 2.13. Deuterium and tritium vapor pressure.

pressures of deuterium and tritium condensed in the ^{3}He separator. Vapor pressure curves show about a 0.5 K translation from the reported values.[9] This offset is a reasonable temperature gradient to expect across the separator, which had cooling along the centerline and a temperature transducer mounted on the outside, where the coolant exits. The pressure plateau observed at low pressure was probably due to helium in the system. Volumes of each node in the gas handling system were measured with an external calibrated volume prior to operation. Pressure-volume data were used to calculate inventories in the system and the amount of material delivered to the gun during pellet formation.

2.2.3 General Operation

Feed gas preparation

Tritium was transferred to the TPOP experiment in batches. Usually one to two batches were required for a day's operation (about 25 pellets per batch). Before a transfer, the TSTA operator mounted a PC of tritium in the LIO glovebox and established a flow path to the TPOP glovebox. A program named T2FILL was then run from THE FIX. This program measured the pressure in tritium line, calculated an intermediate fill pressure based on the final desired fill pressure (entered by the operator), and transferred tritium from the PC until the intermediate pressure was reached. The flow path is shown in Fig. 2.14. The spiral pump draws tritium into the storage reservoir through MCV1. When the intermediate setpoint is reached, T2FILL stops the flow of tritium by closing MCV1 and ends. When T2FILL ended, the TSTA operator shut the hand valve on the PC and started a program called T2FILL2. This program transferred all the remaining tritium from the line into the storage reservoir.

The tritium obtained from TSTA contained from 3% to 16% ^{3}He, which had to be removed from the tritium before it could be used to produce pellets.The TSTA operator established the main vacuum exhaust route through TP1 into an empty PC in the LIO glovebox. The ^{3}He separator was cooled to <12 K. If the gas was to be analyzed, a sample cylinder was attached to the sample port and evacuated, then rinsed with deuterium and evacuated several times to remove all traces of helium from the previous sample. Program HE3-SEP was then run to carry out the separation. This program established a flow path between the storage reservoir and the ^{3}He separator by opening valves PV5, PV11, and PV18, as shown in Fig. 2.15. The temperature in the separator rose slightly (to >20 K) as the separator condensed the feed gas; after it returned to 12 K (typically within 30 s), the vacuum system was opened to the other side of the separator (by opening PV3) to draw off ^{3}He and lower the separator pressure to allow transfer of the remaining tritium from the reservoir. At this point the separator was isolated from the feed reservoir by closing PV5. The separator was then heated to 15 K and the ^{3}He was swept out to the vacuum with a small amount of tritium (tritium vapor pressure = 4 torr at 15 K) for a period of 4 min. Low ^{3}He levels could not be obtained if the separator was operated at lower temperatures (<15 K) during this period, either because of flow limitations from the separator or because of cryotrapping of ^{3}He in the solid tritium. At this point PV3 was closed to isolate the separator from the system. The balance of the system (excluding the separator), including both reservoirs and all lines, was carefully

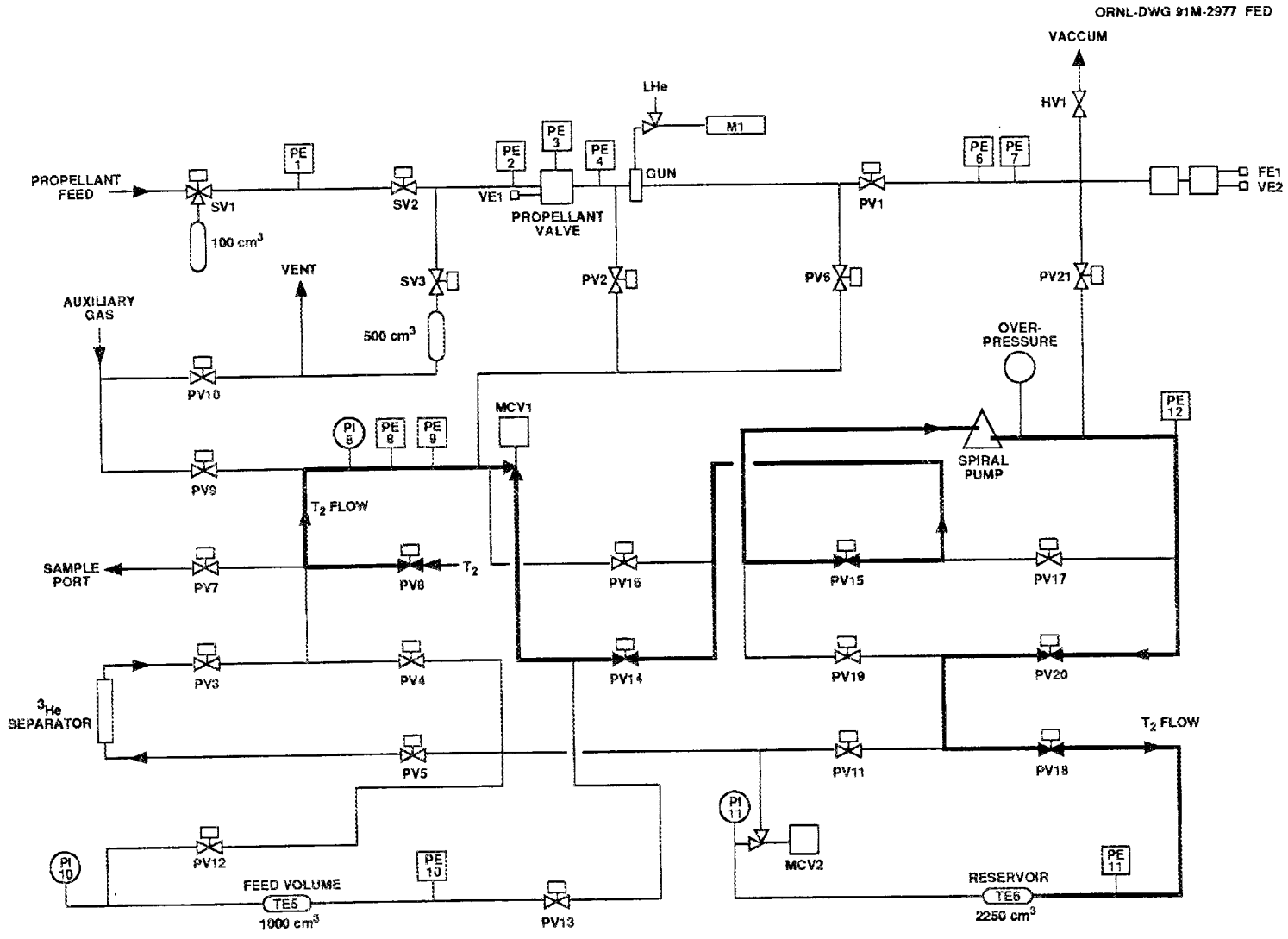

Fig. 2.14. Tritium fill path produced by program T2FILL.

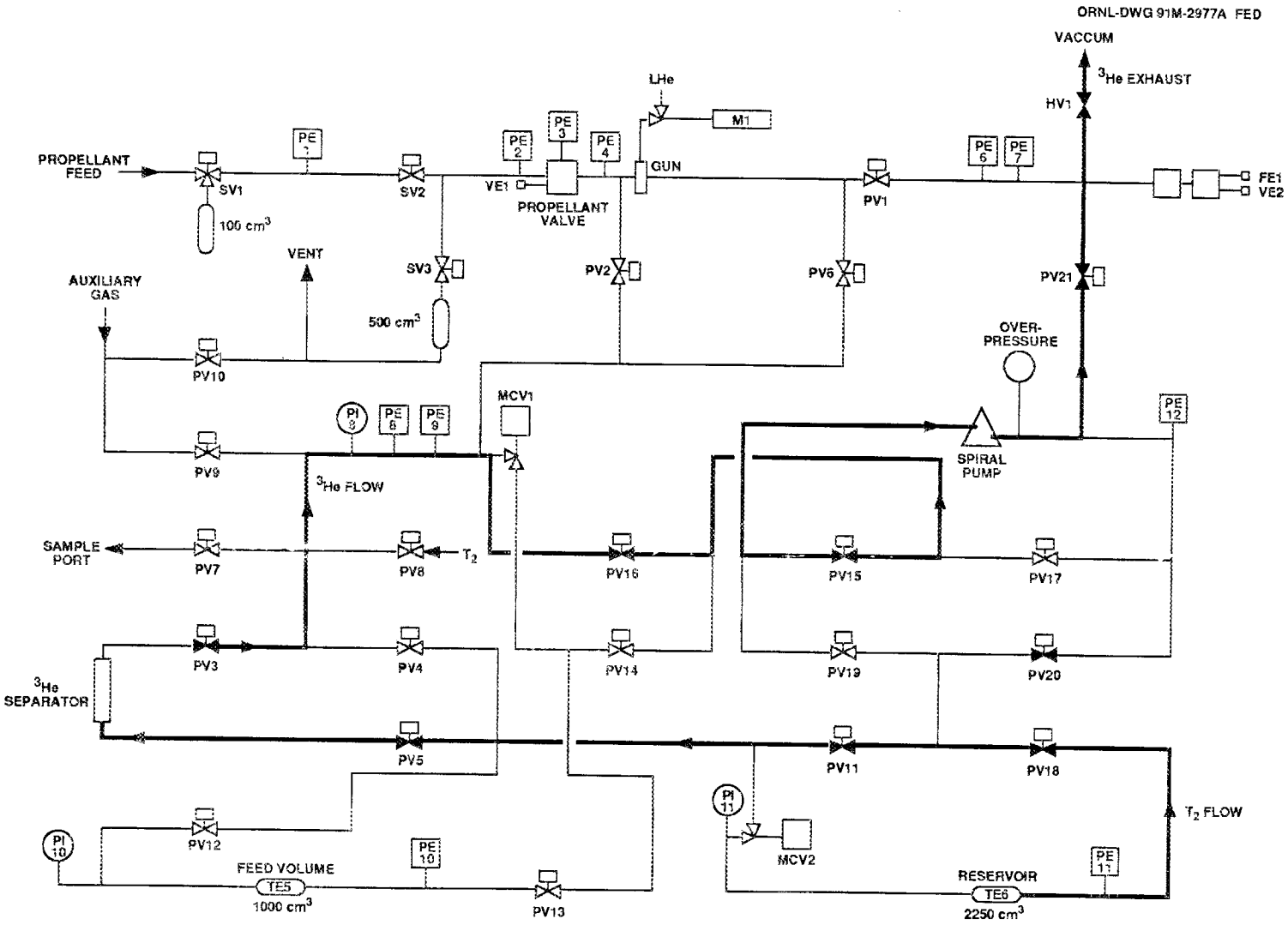

Fig. 2.15. ^{3}He separation flow path.

rinsed with deuterium and evacuated to remove all traces of residual ^{3}He. Flow from the separator was then routed to the storage reservoir through the spiral pump, and the tritium was transferred by heating the separator. Typically, more than 95% of the initial tritium charge was recovered for use in pellet production after the separation. At this point a sample was taken for analysis by mass spectroscopy.

To prepare a gas mixture of deuterium and tritium, the desired amount of tritium was transferred into the glovebox, treated to remove ^{3}He, and stored in the reservoir. The desired amount of deuterium was then admitted from the auxiliary gas line into the feed volume, and a program named MIXGAS was run. This program circulates the gas in a loop through both reservoirs by using the spiral pump, interrupting the flow several times so that all the gas accumulates in one reservoir to help promote mixing. Samples of this gas may also be taken for analysis by mass spectroscopy.

Pellet formation and firing

Pellets were usually formed with the feed gas at constant pressure, using a program called CONSTPRES. For each shot, the operator entered the desired pressure and started the program. Because gas from the vacuum system condensed in the gun after each shot, the temperature of the cryostat was raised for a short time to evaporate this material before refilling. If the feed gas reservoir pressure was too high, the program automatically used the spiral pump to transfer gas back to the storage reservoir. Pressure in the feed volume was automatically controlled with MCV2, as shown in Fig. 2.16.

During filling, the gun was isolated from the vacuum line by closing PV1. Pellets could be formed by filling from the breech, accomplished by opening PV2; from the barrel muzzle, accomplished by opening PV6; or from both ends simultaneously, accomplished by opening both valves. All three methods were used during the TPOP experimental program; however, the preferred method was filling from the breech. Changing the fill method required slight changes in CONSTPRES. Filling was considered complete when the feed gas pressure and the vapor pressure of the pellet were in equilibrium. The program determined this point by monitoring the feed reservoir pressure (PE11). When this pressure did not change for a period of 30 s, the filling operation was terminated by closing all feed valves, waiting for a short period, then opening the gun to vacuum through PV1.

Pellet firing was controlled from the MicroVAX computer through a program called ARCHIP, which triggered the propellant valve power supply, read the fast data from the CAMAC modules, plotted the data on the screen for the operator, and stored the data in permanent archive files, which were later stored on TK50 tapes. Hard copies of the plots

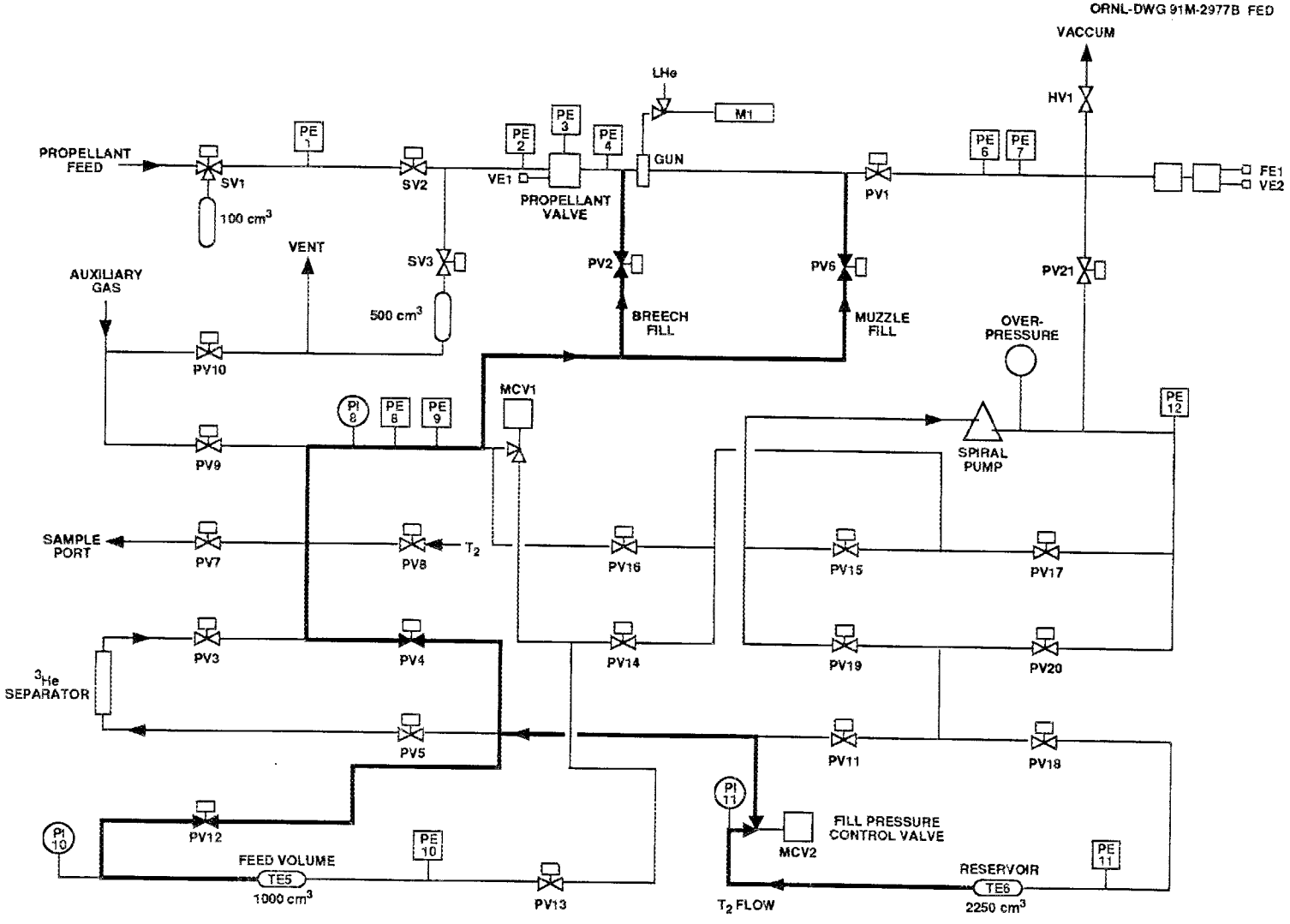

Fig. 2.16. Gun filling flow path.

were also made by printing the SHOT____.TKF files. Pretrigger values of all transducers were read by a CAMAC module and stored in a file called PRE_TRIGGER.DAT, which was also printed out after each day's runs. Pellet velocities were calculated from the fast CAMAC data for light gates and shock signals by running a program named ANALYZE. Hard copies of all of his information were placed in notebooks with photographs of the pellets for each of the 1500 shots.

2.3 TRITIUM ANALYSIS

Tritium analysis was performed by TSTA personnel using a Nuclide Model 6-60 magnetic sector mass spectrometer. The spectrometer had an ion bombardment source that used 70-V electrons and an electron multiplier detector. Although mass spectrometry was the best analytical technique for measuring trace amounts of ^{3}He in tritium, some uncertainty was associated with the analysis because ^{3}He and T have the same atomic weight (3.0160) and cannot be resolved into separate peaks. Therefore, a correction based on the T_2, DT, and HT parent peak heights and their respective cracking patterns must be made to the ^{3}He peak. Nevertheless, TSTA personnel estimate that reported ^{3}He values should be good to within about ±10% (±0.5% for hydrogen) and have a lower limit of detectability of 0.005% ^{3}He in pure tritium.

Table 2.1 shows the results of sample analysis on the tritium used in these experiments. The correction to the ^{3}He peak creates a significant problem, as shown by the negative results for the last few samples in the table. To get a better estimate of the ^{3}He levels in these samples, the residual pressure was measured after freezing all the tritium onto the ^{3}He separator. These data confirm that the ^{3}He composition was <0.005% for these samples. (Similar measurements were not made on earlier samples.) The precision of the analysis was estimated from the four cases for which duplicate analyses were performed on a sample. The standard deviation for these samples was expressed as a percentage of the mean and is plotted as a function of the mean in Fig. 2.17, which indicates that the standard deviation was on the order of 25% in the region of interest (near zero). Another estimate was obtained from the measured hydrogen levels for samples from the same PC because hydrogen was also a trace constituent. (Deuterium was not used for sample-to-sample comparisons because it was used to rinse the system and was, therefore, a possible contaminant.) This estimate showed about the same behavior as that of ^{3}He with the exception of a point for PC847, which had a reduced standard deviation of about 150% (which is off the graph). Checks for internal consistency within the data set indicate that the mass spectrometer analysis was not as accurate as anticipated, and in

Table 2.1. Tritium analysis data

Analysis number	Sample date	Date of MS	Feed PC number	Sample number	H, HDT base (%)	D, HDT base (%)	T, HDT base (%)	^{3}He by MS[a] (%)	^{3}He by PV[b] (%)	Comments
1	1/29/88	2/19/88	616	PC assay	0	0.550	99.450	12.693		Feed
2	5/25/88	5/25/88	616	P187-1	0.213	2.855	96.932	0.563		
3	5/25/88	5/26/88	616	P187-2	1.183	6.842	91.975	0.369		
4	5/25/88	5/26/88	616	P187-3	4.796	4.432	90.772	0.061		
5	8/18/88	8/18/88	616	P211-1	4.750	2.208	93.042	16.429		Feed
6	8/18/88	8/18/88	616	P211-2	4.689	3.089	92.223	0.750		
7	8/18/88	8/18/88	616	P212-3	4.250	5.096	90.654	0.190		2nd on prev
8	8/18/88	8/18/88	616	P212-4	4.171	5.175	90.655	0.346		
9	8/19/88	9/8/88	616	P213-5	4.861	7.010	88.129	0.877		3 consec. seps.
10	8/19/88	9/8/88	616	P213-6	4.845	5.361	89.794	0.825		2 consec. seps.
11	9/29/88	9/29/88	664	P233-1	0.096	0.650	99.254	11.600		Feed
12	9/29/88	9/29/88	664	P233-2	0.118	1.881	98.001	0		15 K evac
13	9/29/88	9/29/88	664	P233-3	0.112	3.307	96.581	0		2nd on prev
14	9/29/88	9/29/88	664	P234-4	0.165	5.644	94.191	0		16 K evac
15	9/30/88	9/30/88	664	P242-1	0.189	1.546	98.265	9.836		Feed
16	9/30/88	9/30/88	664	P242-2	0.194	2.703	97.103	0.187		
17	9/30/88	9/30/88	664	P243-3	0.130	50.146	49.724	0.163		DT mixture
18	11/1/88	11/2/88	664	P249-1	0.069	1.272	98.659	0		
19	11/2/88	11/2/88	664	P249-2	0.147	1.856	97.997	0.173		
20	11/3/88	11/4/88	784	P252-4	0.421	3.511	96.069	0.095		MS down
21	11/3/88	6/27/89	784	P253-5	0.566	98.281	1.153	0.071		1% T mixture

Table 2.1. (Continued)

Analysis number	Sample date	Date of MS	Feed PC number	Sample number	H, HDT base (%)	D, HDT base (%)	T, HDT base (%)	^{3}He by MS[a] (%)	^{3}He by PV[b] (%)	Comments
22	6/22/89	6/27/89	847	P273-1	0.021	1.307	98.672	0.326		
23	6/22/89	6/27/89	847	P273-1b	0.010	1.285	98.705	0.220		Duplicate
24	6/26/89	6/27/89	847	P275-1	0	1.686	98.314	0.049		
25	6/26/89	6/27/89	847	P275-1b	0.036	1.660	98.304	0.035		Duplicate
26	6/27/89	6/29/89	847	P279-1	0.031	2.173	97.796	0.607		
27	6/27/89	6/29/89	847	P279-2	0.016	2.233	97.751	0.071		
28	6/29/89	6/29/89	847	P283-2	0	1.305	98.695	0.221		
29	8/8/89	8/8/89	847	P292-1	0	0.551	99.449	3.133		Feed
30	8/8/89	8/8/89	847	P292-2	0.164	0.897	98.939	–0.013		
31	8/9/89	8/9/89	847	P6-1	0.191	1.070	98.739	–0.036	0.003	
32	8/10/89	8/10/89	847	P12-1	0	1.903	98.897	–0.008	0.003	
33	8/11/89	8/12/89	847	P18-1	0.236	50.489	49.276	0.158	0.003	DT mixture
34	8/14/89	8/14/89	847	P25-1	0.689	3.032	96.279	0.030	0.003	
35	8/15/89	8/15/89	847	P30-1	0	1.032	98.968	–0.009	0.002	
36	8/15/89	8/15/89	847	P34-1	0.037	0.844	99.120	–0.052	0.002	
37	8/16/89	8/16/89	847	P45-1	0.104	2.597	97.299	–0.058	0.002	

[a]MS = mass spectrometry.

[b]PV = pressure-volume measurement.

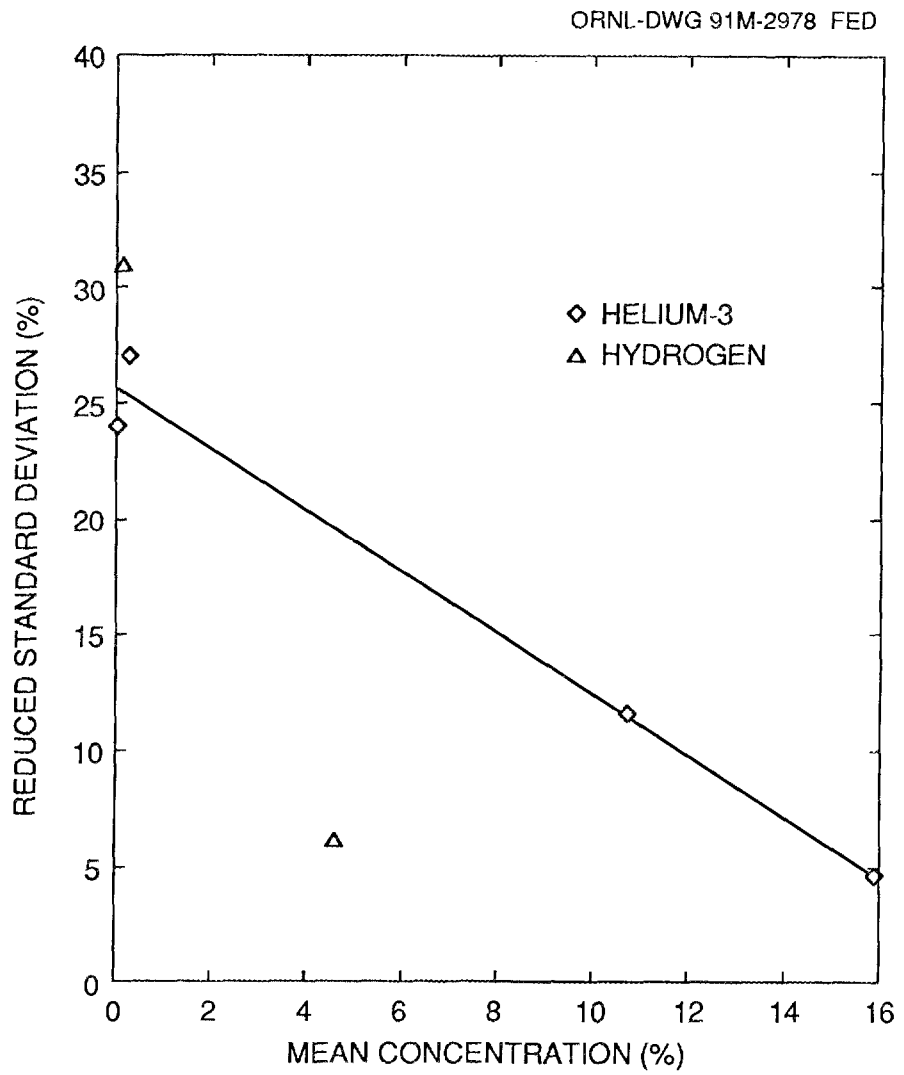

Fig. 2.17. Uncertainty in ^{3}He analysis. Diamonds: data from duplicate ^{3}He analysis. Triangles: data from H analysis for identical tritium feeds.

future work, pressure measurements within the TPOP system should be used to confirm the analysis.

3. RESULTS AND DISCUSSION

This experiment operated for several years at two separate locations, and the results published to date[20,21] have been presented in chronological order and have thus concentrated on specific hydrogen isotopes (H and D for operation at ORNL, T for operation at TSTA). Here we present the data according to the type of measurement or phenomenon,

so that differences and similarities between isotopes can be more easily observed. Of course, not every effect was measured with equal completeness for each isotope. In fact, practically no data were collected for hydrogen. Therefore, there are gaps in the data simply because time and priorities did not allow a more comprehensive study.

3.1 PELLET SIZE

Pellet size was controlled by several variables, including cryostat temperature, fill pressure, position of the thermal short on the barrel in front of the pellet (Fig. 2.2), and fill direction (i.e., from either end or both ends of the barrel). The data presented here are for pellets formed by filling from both ends or from the breech end until there was no change in feed gas reservoir pressure for 30 s, as described in Sect. 2.2.3. Filling from the front, or muzzle, end of the barrel produced pellets that generally suffered damage during acceleration, so no data are presented for these pellets. Apparently filling from the front leaves voids in the rear of the pellet; when these voids are filled with high-pressure gas during acceleration, the pellets tend to fracture or even explode as they emerge from the barrel. When pellets are formed from the rear or from both ends, there is a much greater probability that imperfections at the rear of the pellet will be "healed over" with condensing gas in the final stages of formation.

3.1.1 Deuterium Fill Data

Figure 3.1 shows the effect of heat sink (thermal short) location and equilibrium fill pressure on deuterium pellet size. With no heat sink, there was about a 90-cm conduction path to room temperature through the stainless steel barrel in front of the pellet. With the heat sink 10 cm from the pellet, the temperature gradient was about the same on both sides of the pellet. Deuterium pellets 4 mm in diameter and 4 mm long contain 6.2 kPa•L (47 torr•L) of gas. As shown in Fig. 3.1, moving the heat sink provides a coarse adjustment of pellet size that can be used to bring the operating curve into the desired range. Figure 3.2 shows the effect of cryostat temperature and equilibrium fill pressure on pellet size with the heat sink at 10 cm. These are typical of families of curves obtained with different heat sink locations. A wide range of pellet sizes can be produced by varying the temperature and pressure according to these curves. Filling the gun from both ends of the barrel produced pellets 15% to 35% larger than those made by filling from the breech only.

Figure 3.3 is a typical deuterium filling curve; in general, it took approximately 5 min to reach equilibrium during pellet formation. Figure 3.4 shows pellets formed at

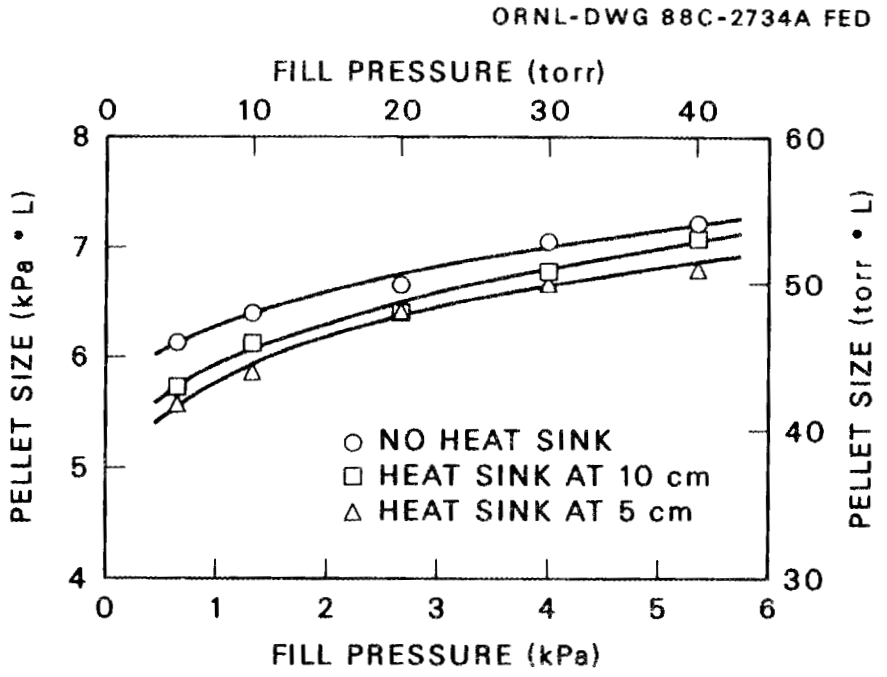

Fig. 3.1 Deuterium pellet size as a function of heat sink location.

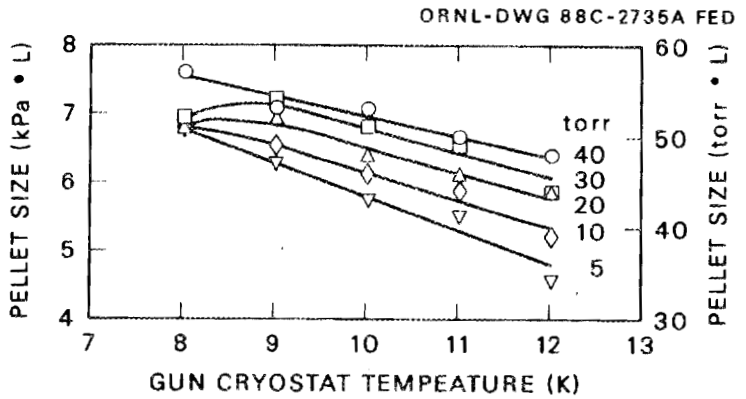

Fig. 3.2. Deuterium pellet size as a function of temperature and equilibrium fill pressure.

various times along the curve. Pellets first grow radially inward from the 3-mm-long freezing zone until closure occurs at the centerline. Then they appear to grow axially in the direction of fill. When the fill is from both directions, pellets naturally grow beyond the freezing zone in both directions. The pellet that was 87% of equilibrium size contains 6.2 kPa•L (47 torr•L) of deuterium and required only 100 s for formation. Thus, pellets with a specified length can be formed in shorter times by choosing equilibrium conditions

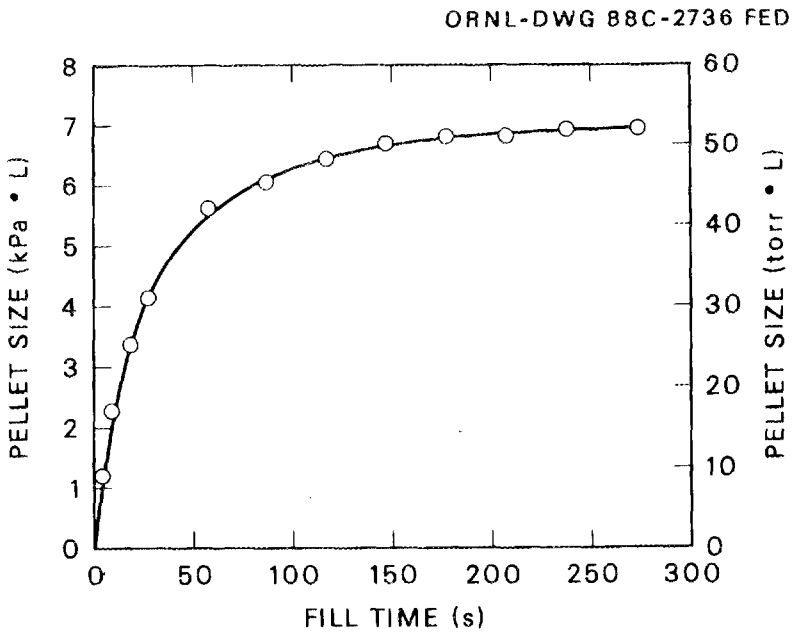

Fig. 3.3. T ime dependence of deuterium pellet formation.

for longer pellets. Fill time then becomes an important additional variable that can be used to control pellet length.

3.1.2 Tritium Fill Data

Figure 3.5 shows operating curves for production of tritium pellets with a 4-mm-long cooled section of barrel, with <0.005% ^{3}He, with filling from the breech end only, and with the heat sink 10 cm in front of the pellet. Pellets formed at 16 K could not be held for firing at temperature because they slid out of the barrel under the force of the gas trapped in the breech shortly after the barrel was opened to the vacuum system. The pressure behind the pellet at the time of release is not known but was probably very close to the fill pressure, which ranged from 4 to 8 kPa (30 to 60 torr). The contribution of the vapor pressure at 16 K is only 1.3 kPa (9.5 torr). The leak rate through the propellant valve was also very small, about 3×10^{-3} kPa•L/s (2×10^{-5} torr•L/s), and would lead to a pressure rise of only 0.3 kPa (2 torr) in 5 min. Release of the pellet at this low pressure could be due to either poor adhesion to the wall or very low shear strength. Since the pellet survived the trip down the diagnostic line, strength does not appear to be the problem. Although 4-mm deuterium pellets worked quite well, 5-mm-long (62-torr•L) tritium pellets appeared to be more robust than their 4-mm-long counterparts. The 8 K and 10 K curves fall in this range.

ORNL-PHOTO 2918-88 FED

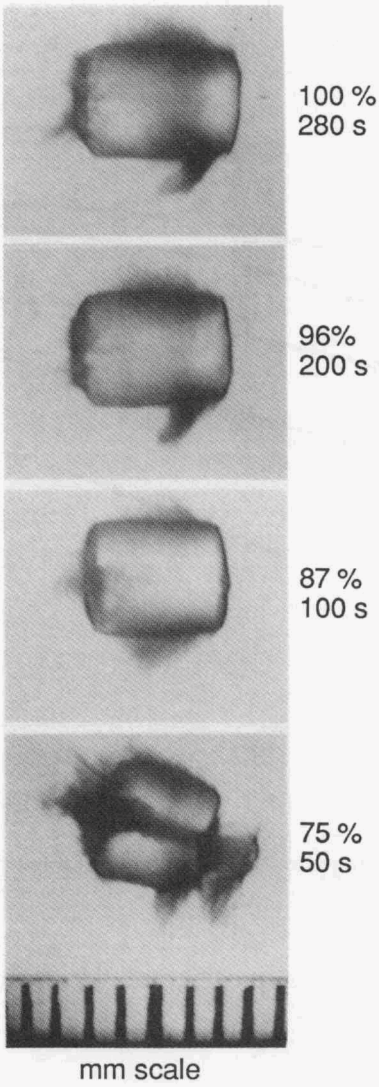

Fig. 3.4. Deuterium pellets at various times during formation.

The ^{3}He concentration had an effect on both the amount of gas condensed into a pellet and the rate of condensation. These effects were especially apparent when the pellet was formed by filling from both ends. Figure 3.6 compares fill rates for filling from the breech and from both ends. Although filling from both ends produces a longer pellet, the pellet forms more slowly because of a buildup of the noncondensible component ^{3}He at the point of pellet formation. Even at these low ^{3}He concentrations (0.002%), the back-pressure becomes significant as the pellet grows. This effect can be quantified by adapting the method of Souers[11] to the freezing zone of the barrel. The backpressure P can be

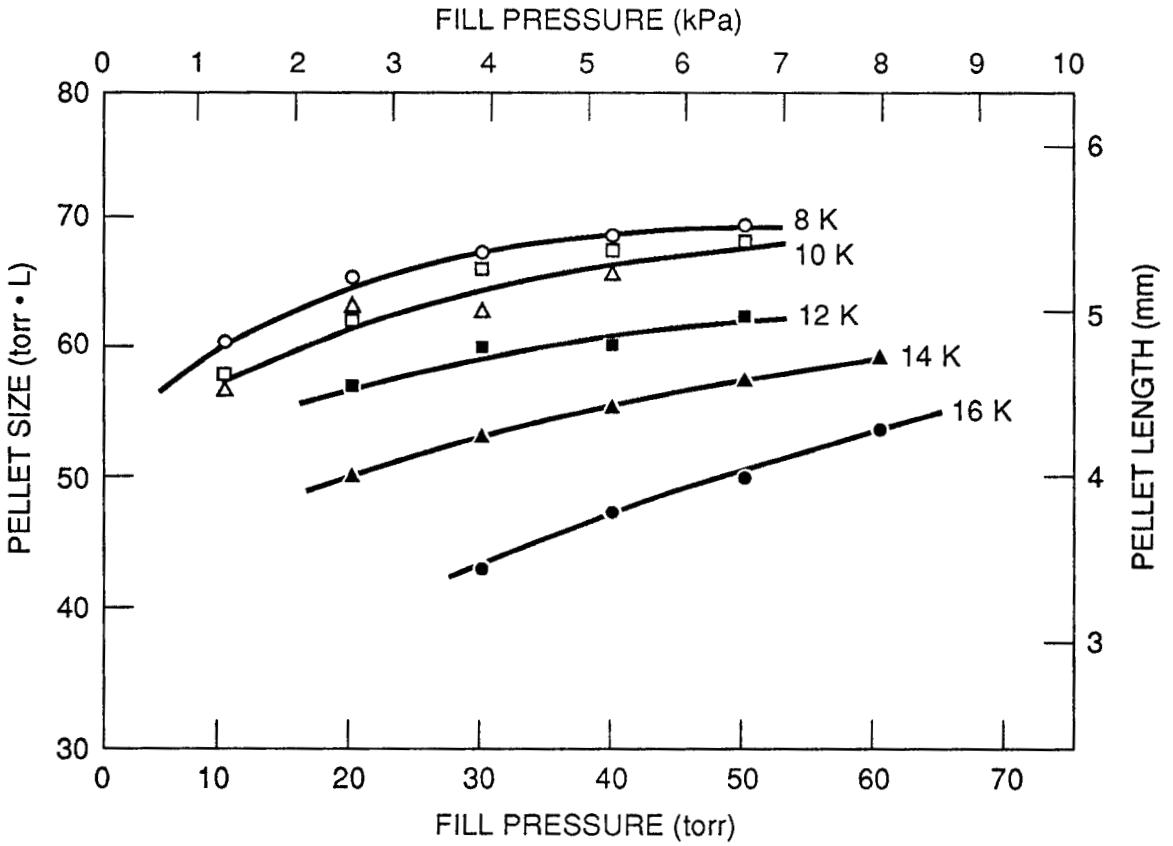

Fig. 3.5. Tritium pellet size as a function of temperature and pressure.

expressed as the sum of the partial pressure of ^{3}He at the pellet P_{He} and the vapor pressure of tritium $P^s_{T_2}$,

$$P = P_{He} + P^s_{T_2} \quad . \tag{3.1}$$

The partial pressure of ^{3}He can be expressed in terms of the fraction of the assumed fixed volume freezing zone f that is filled with solid tritium,

$$P = (\rho_s y_{He} RTf)/(1-f) + P^s_{T_2} \quad , \tag{3.2}$$

where ρ_s is the molar density of solid tritium, y_{He} is the mole fraction of ^{3}He in the feed (assumed small), R is the gas constant, and T is the temperature of the freezing zone. Figure 3.7 shows the ratio of the feed pressure to the backpressure as a function of the

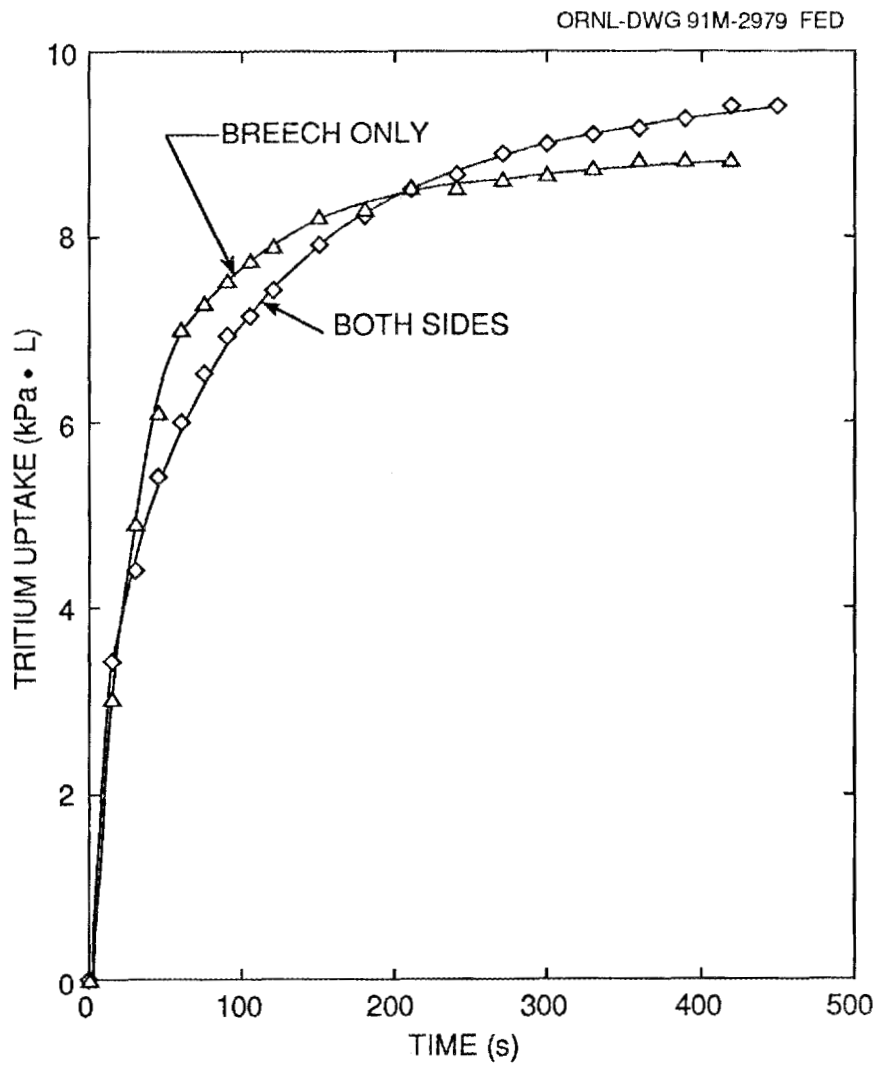

Fig. 3.6. Time dependence of tritium pellet formation.

fractional fill. When this ratio reaches one, the flow of feed gas due to the pressure gradient will stop, and tritium will be transferred to the pellet only by means of diffusion through the long feed line, which is a much slower process. Thus, pellet formation stops short of completion.

3.1.3 Equilibrium Fill Model

The ultimate size of a pellet being formed in a pipe gun can be calculated from a simple conduction heat transfer model when the system is in equilibrium with the feed gas at its final pressure. For this model, it is assumed that the pellet is symmetric about its axis and about the midplane of the freezing zone perpendicular to its axis, as illustrated in

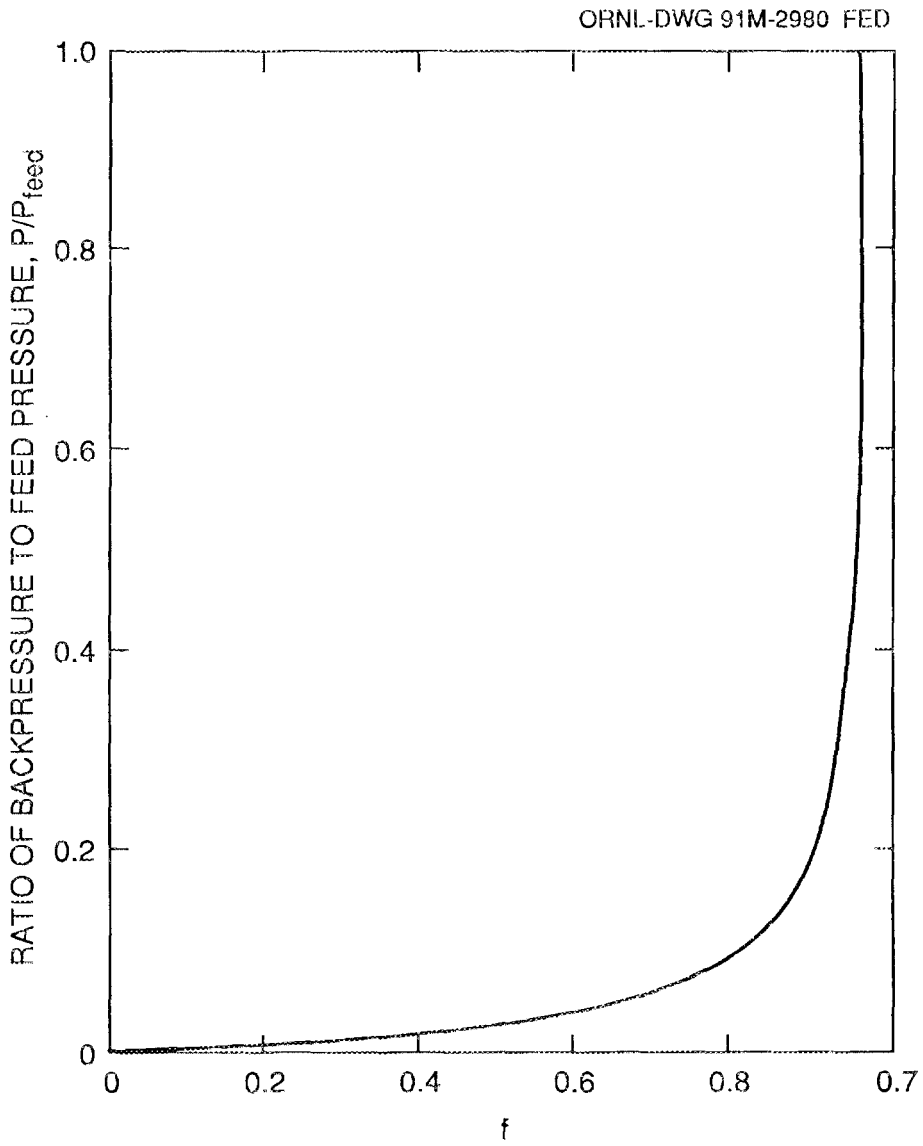

Fig. 3.7. Predicted ratio of backpressure to feed pressure as a function of fractional filling for two-sided fill under the conditions in Fig. 3.6.

Fig. 3.8 (equivalent to filling from both ends). The pipe gun has been modeled using the finite difference approach both with and without collar cryostats on each side of the pellet cryostat. Figure 3.9 shows the grid arrangements for the two configurations. Node temperatures T were determined by successive applications of the conduction equation between nodes, which for any node ij is given by

$$T_{ij}^{+} = \frac{q\rho_{ij}V_{ij} + \sum_{m}\left(k_{im}A_{im}/\Delta r\right)T_{im} + \sum_{n}\left(k_{nj}A_{nj}/\Delta x\right)T_{nj}}{\sum_{m}\left(k_{im}A_{im}/\Delta r\right) + \sum_{n}\left(k_{nj}A_{nj}/\Delta x\right)}, \tag{3.3}$$

Fig. 3.8. Geometry for pipe gun pellet formation equilibrium model. (a) No-collar model. (b) Model with collar cryostats.

where k is the effective thermal conductivity across the conduction path, A is the area for heat transfer between adjacent nodes, Δr and Δx are the distances to adjacent nodes in the radial and axial directions, V is the volume of the node, ρ is the density of material at the conditions of the node, and q is the heat generation rate, which is zero for all materials

ORNL-DWG 91M-2982 FED

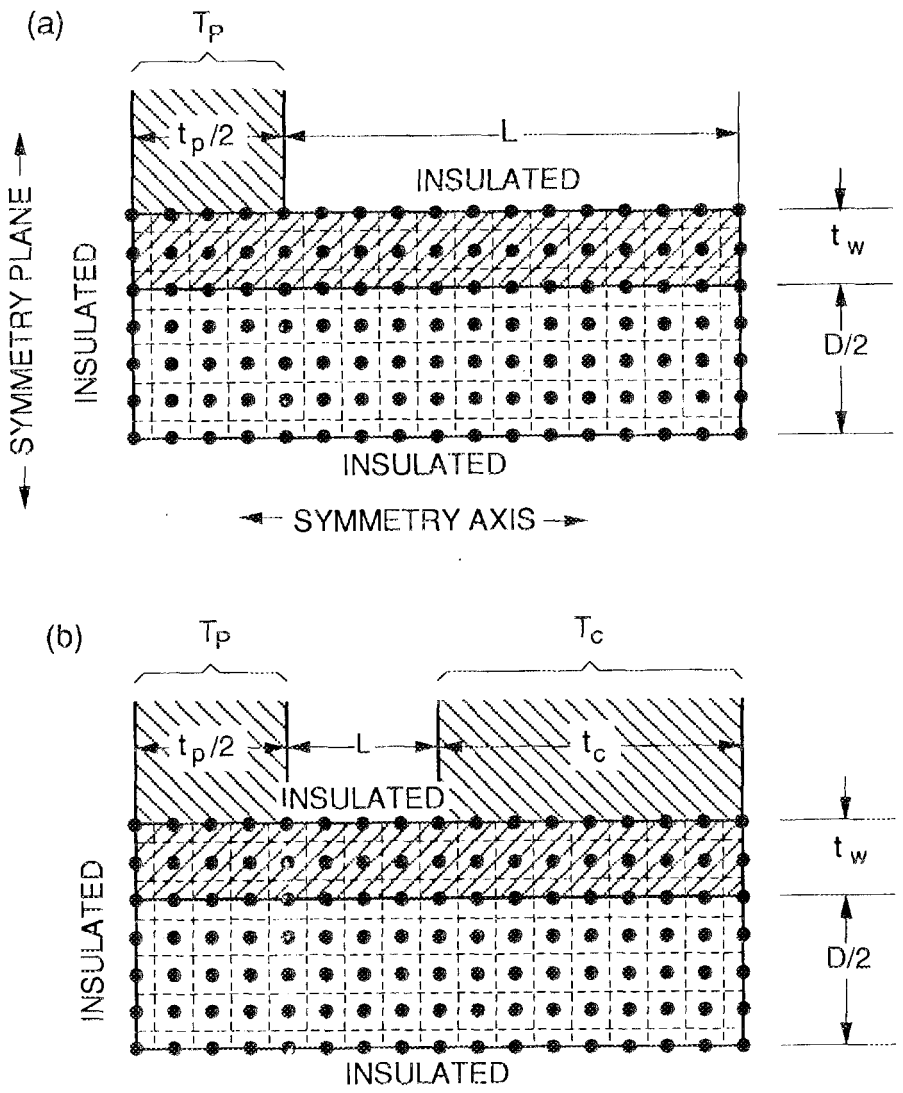

Fig. 3.9. Finite difference node arrangement. (a) No-collar model. (b) Model with collar cryostats.

other than tritium. New values of T are calculated to replace old values in storage until successive temperatures for all nodes agree to within 0.0001 K.

Boundary conditions for the models are illustrated in Fig. 3.9. Nodes in contact with constant-temperature cryostats were assumed to be at the temperature of the cryostat. It was assumed that there was no heat transfer across nodes of symmetry or from the exposed external surface of the barrel (i.e., no radiation or conduction heat transfer from the barrel to the surroundings). Adjacent nodes perpendicular to insulated boundaries were assumed to be at the same temperature. In the no-collar model, the distance L was two times the pellet cryostat thickness (i.e., $2t_p$). In the other model, the length of the collar t_c

$= t_p/2 + L$. With these spacings, application of both constant temperature and insulated boundary conditions at the end of the barrel gave identical results for pellet size. The temperature of the nodes at the end of the barrel in the no-collar case was determined by calculating the temperature gradient along the barrel from the pellet cryostat (at temperature T_p) to the location of the thermal short on the barrel (assumed to be at 300 K).

Table 3.1 gives the physical property relationships used in the calculations. Properties of the hydrogen isotopes were derived from Refs. 9 and 23, and properties of the metals were derived from Ref. 24. The decay heating rate of tritium is 0.977 W/(mol T). In the calculation, physical property data for a specific node were updated whenever the node temperature deviated more than 0.01 K from the temperature of the node at the last update. Effective thermal conductivities were calculated from

$$k_{im} = 2k_{ij}k_{mj}/(k_{ij} + k_{mj}) , \quad k_{nj} = 2k_{ij}k_{in}/(k_{ij} + k_{in}) , \tag{3.4}$$

where k_{ij}, k_{mj}, and k_{in} are the thermal conductivities calculated at the conditions of the specific nodes.

Runs for new conditions were started by assuming flat radial temperature profiles and a moderate number of nodes (e.g., 3 radial nodes in wall and 10 radial and axial nodes in the freezing zone). After this solution converged, results were used as initial conditions for running a case with more nodes. Most results reported here used 5 radial nodes in the barrel and 25 radial and axial nodes in the pellet freezing zone (3625 total nodes for the no-collar model). This two-step approach required less run time than starting a large number of nodes directly with flat profiles. Runs can also be started with results from previous runs at different feed pressures. Tests showed that the number of radial nodes in the barrel had little effect on pellet size; going from 3 to 6 radial nodes changed the pellet size by only 0.1% for a typical size pellet. Figure 3.10 shows the effect of the total number of nodes on the predicted pellet size; pellet size was not a strong function of grid size when more than 1500 nodes were employed.

Figure 3.11 shows predicted pellet size and experimental results for deuterium pellets formed by filling from both ends of the barrel with thermal shorts 10 cm from the cryostat (i.e., a symmetrical heat leak on both sides of the freezing zone). The agreement between theory and experiment is good. The size of pellets formed by filling from only one direction could also be estimated using the model. Photographs of pellets at various stages of growth (e.g., Fig. 3.4) show that pellets were truncated at the end of the freezing zone on the end opposite the feed. This effect can be approximated by adding half the

Table 3.1. Physical property data

Thermal conductivity k, $W \cdot mm^{-1} \cdot K^{-1}$

Stainless steel, $k = AT^B$

$T > 67$ K: $A = 1.37 \times 10^{-3}$, $B = 0.42$

$T < 67$ K: $A = 6.35 \times 10^{-5}$, $B = 1.15$

Brass, $k = AT^B$

$T > 46$ K: $A = 1.48 \times 10^{-3}$, $B = 0.76$

$T < 46$ K: $A = 4.96 \times 10^{-4}$, $B = 1.04$

Gaseous hydrogen, $k = AT^{0.902}$

H_2: $A = 1.04 \times 10^{-6}$ D_2: $A = 8.42 \times 10^{-7}$

HD: $A = 9.46 \times 10^{-7}$ DT: $A = 7.49 \times 10^{-7}$

HT: $A = 8.42 \times 10^{-7}$ T_2: $A = 6.50 \times 10^{-7}$

Solid hydrogen, $k = AT^{-1.3}$

H_2: $A = 16.4 \times 10^{-3}$ D_2: $A = 24.0 \times 10^{-3}$

HD: $A = 20.2 \times 10^{-3}$ DT: $A = 19.0 \times 10^{-3}$

HT: $A = 15.2 \times 10^{-3}$ T_2: $A = 14.0 \times 10^{-3}$

Liquid hydrogen, $k = A \cos[B(T - C)]$

H_2: $A = 1.25 \times 10^{-4}$, $B = 8.03 \times 10^{-2}$, $C = 23$

HD: $A = 1.30 \times 10^{-4}$, $B = 6.63 \times 10^{-2}$, $C = 25$

HT: $A = 1.32 \times 10^{-4}$, $B = 5.93 \times 10^{-2}$, $C = 26$

D_2: $A = 1.35 \times 10^{-4}$, $B = 5.24 \times 10^{-2}$, $C = 27$

DT: $A = 1.38 \times 10^{-4}$, $B = 4.71 \times 10^{-2}$, $C = 28$

T_2: $A = 1.41 \times 10^{-4}$, $B = 4.01 \times 10^{-2}$, $C = 30$

Vapor pressure P, torr

Solid hydrogen, $P = \exp[A - B/T + C \ln(T)]$

H_2: $A = 3.08950$, $B = 87.5045$, $C = 2.71994$

HD: $A = 4.39095$, $B = 113.784$, $C = 2.48948$

HT: $A = 4.95000$, $B = 127.063$, $C = 2.40929$

D_2: $A = 5.29874$, $B = 136.742$, $C = 2.34074$

DT: $A = 5.79620$, $B = 149.916$, $C = 2.27590$

T_2: $A = 6.19797$, $B = 161.969$, $C = 2.22868$

Liquid hydrogen, $P = \exp[A - B/T + C \ln(T)]$

H_2: $A = 4.75319$, $B = 83.5177$, $C = 1.98042$

HD: $A = 6.68995$, $B = 109.419$, $C = 1.57756$

HT: $A = 7.83671$, $B = 123.995$, $C = 1.34440$

D_2: $A = 7.73898$, $B = 130.249$, $C = 1.38962$

DT: $A = 9.32752$, $B = 147.349$, $C = 1.04950$

T_2: $A = 10.9220$, $B = 164.486$, $C = 0.707997$

Table 3.1. (Continued)

Density ρ, mol•mm^{-3}
Solid hydrogen, $\rho = A \exp(-BT^5)$
H_2: $A = 4.34 \times 10^{-5}, B = 1.48 \times 10^{-8}$
HD: $A = 4.65 \times 10^{-5}, B = 1.31 \times 10^{-8}$
HT: $A = 4.83 \times 10^{-5}, B = 1.23 \times 10^{-8}$
D_2: $A = 5.01 \times 10^{-5}, B = 1.14 \times 10^{-8}$
DT: $A = 5.18 \times 10^{-5}, B = 1.06 \times 10^{-8}$
T_2: $A = 5.34 \times 10^{-5}, B = 0.98 \times 10^{-8}$
Gaseous hydrogen, $\rho = P/(RTZ)$
$(R = 62.4 \times 10^6, Z = 1 + (P/RT)[b + (1.8 \times 10^{-9} - b^2)(P/RT)], b = AT^B)$
H_2: $A = -0.0113, B = -1.44$
HD: $A = -0.0159, B = -1.52$
HT: $A = -0.0196, B = -1.58$
D_2: $A = -0.025, B = -1.64$
DT: $A = -0.031, B = -1.70$
T_2: $A = -0.0395, B = -1.77$

symmetrical pellet volume to half the freezing zone volume (defined as the volume of the cooled section of barrel). Figure 3.12 shows predicted and measured pellet size for deuterium pellets formed by filling from the breech only. Again, the model predictions are quite good. The agreement between theory and experiment indicates that the assumptions of the heat transfer model and the physical properties were valid and can be used as a predictive tool for future design work.

Figure 3.13 shows predictions and experimental results for tritium pellets formed at 10 K. Here, the model worked well for filling from the breech only, but it predicted significantly larger pellets than those observed in the experiment with filling from both directions. This discrepancy demonstrates the strong effect of small amounts of ^{3}He (<0.005% for these data) on pellet formation. When pellets were filled from the breech, the volume of the barrel in front of the pellet provided significant space into which the ^{3}He was disengaged during most of the formation process. However, with filling from both ends the ^{3}He had no place to go and, therefore, it significantly slowed, and effectively stopped, pellet growth before equilibrium was reached. The model does not account for these dynamic effects.

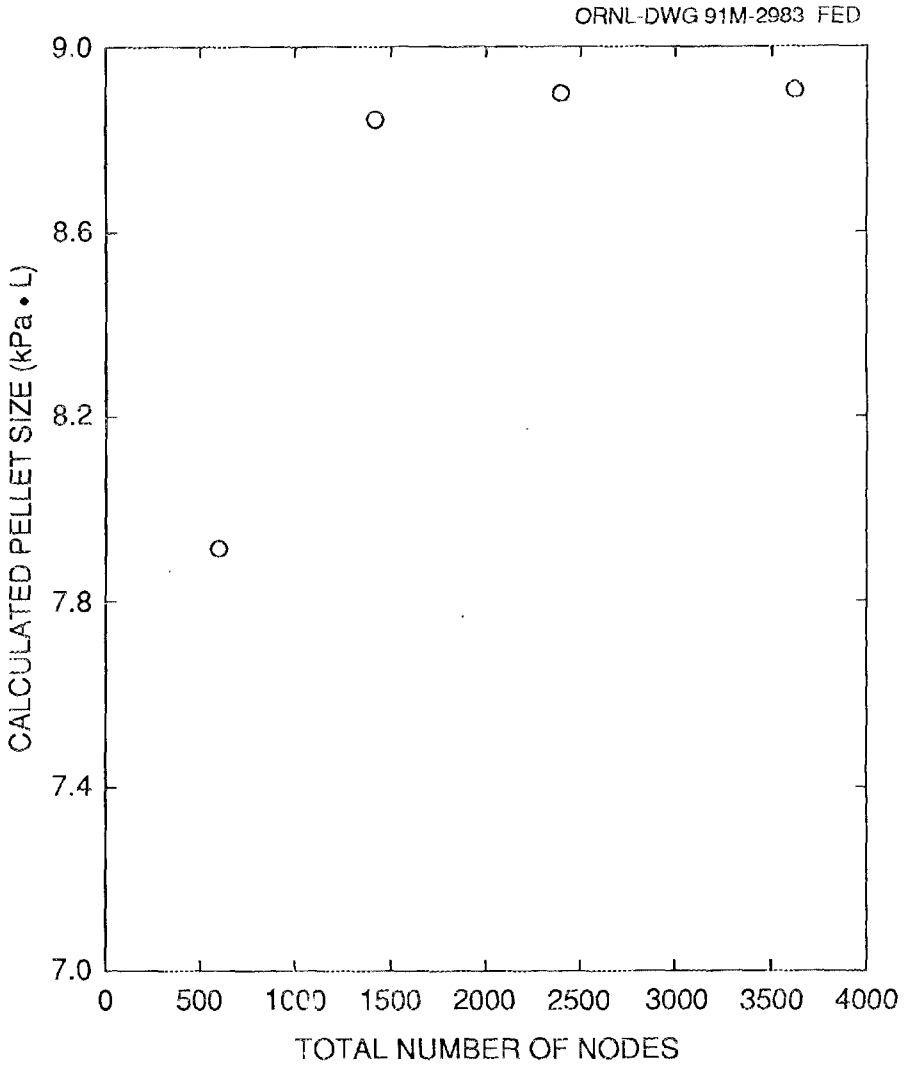

Fig. 3.10. Effect of number of nodes on pellet size.

Figure 3.14 shows predicted shapes and temperature profiles for a typical deuterium pellet, and Fig. 3.15 shows predicted shapes and temperature profiles for a typical tritium pellet. Both pellets were formed under the same conditions: with the pellet cryostat at 10 K and a 2.67-kPa (20-torr) feed. The cryostat was 3 mm thick for the deuterium pellet and 4 mm thick for the tritium pellet; these thicknesses represent the actual size of the freezing zone, which was enlarged for the final series of tritium runs. Tritium pellets support a larger temperature gradient within the pellet than do deuterium pellets because tritium has a higher sublimation temperature than deuterium at any given equilibrium pressure. The nose of the tritium pellet was blunter than that of the deuterium pellet because of internal heat generation. As pellet diameter increases, this effect will

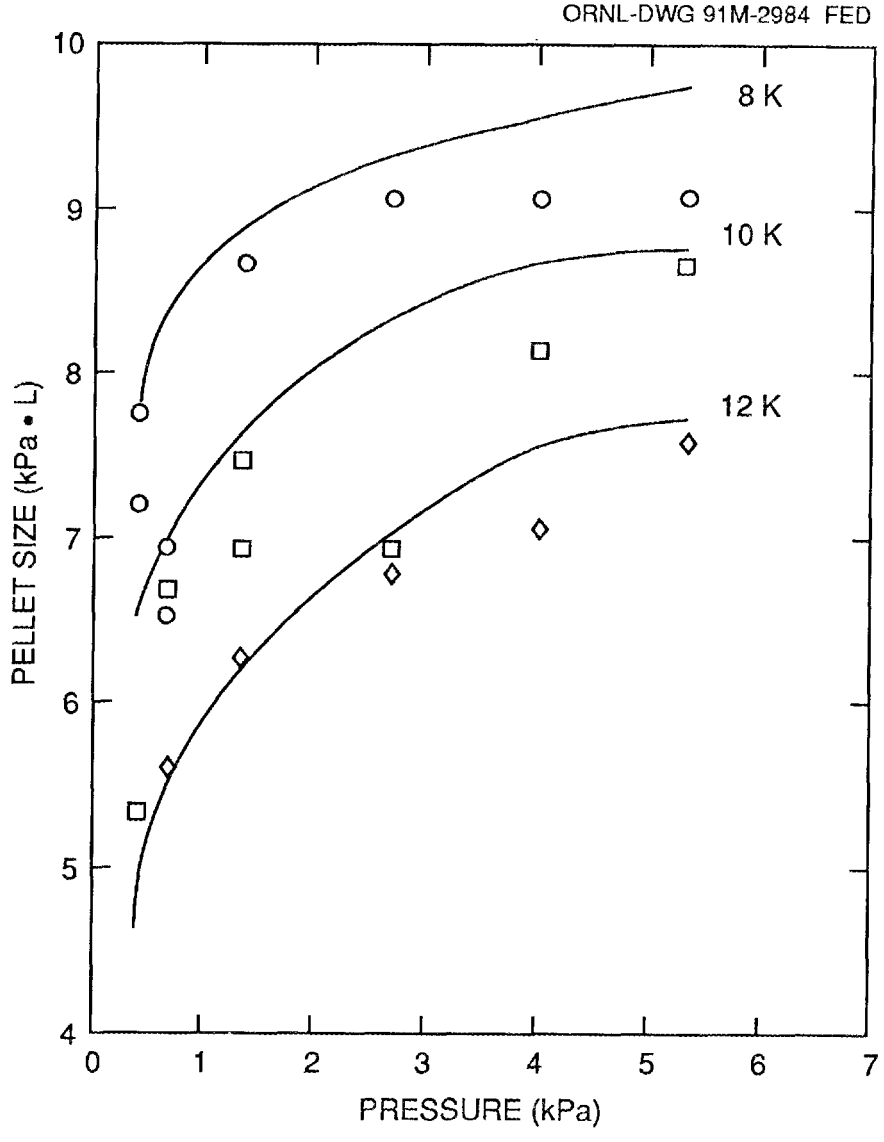

Fig. 3.11. Deuterium pellet size as a function of temperature and pressure for pellets formed by filling from both ends of the barrel with the thermal short about 10 cm in front of the pellet cryostat. Lines are model predictions.

eventually lead to the development of a hole in the pellet. However, the model has been run for tritium pellets as large as 12 mm in diameter with a 12-mm-long freezing zone without any indication of hole formation due to heating. Figure 3.16 shows a deuterium pellet and a tritium pellet formed by filling from both ends. The front ends of the pellets in Fig. 3.16 did not undergo erosion during acceleration. The actual pellet shapes were quite similar to those predicted (see Figs. 3.14 and 3.15), and tritium pellets were found to be blunter than deuterium pellets. Deuterium pellets also seemed to have a line of

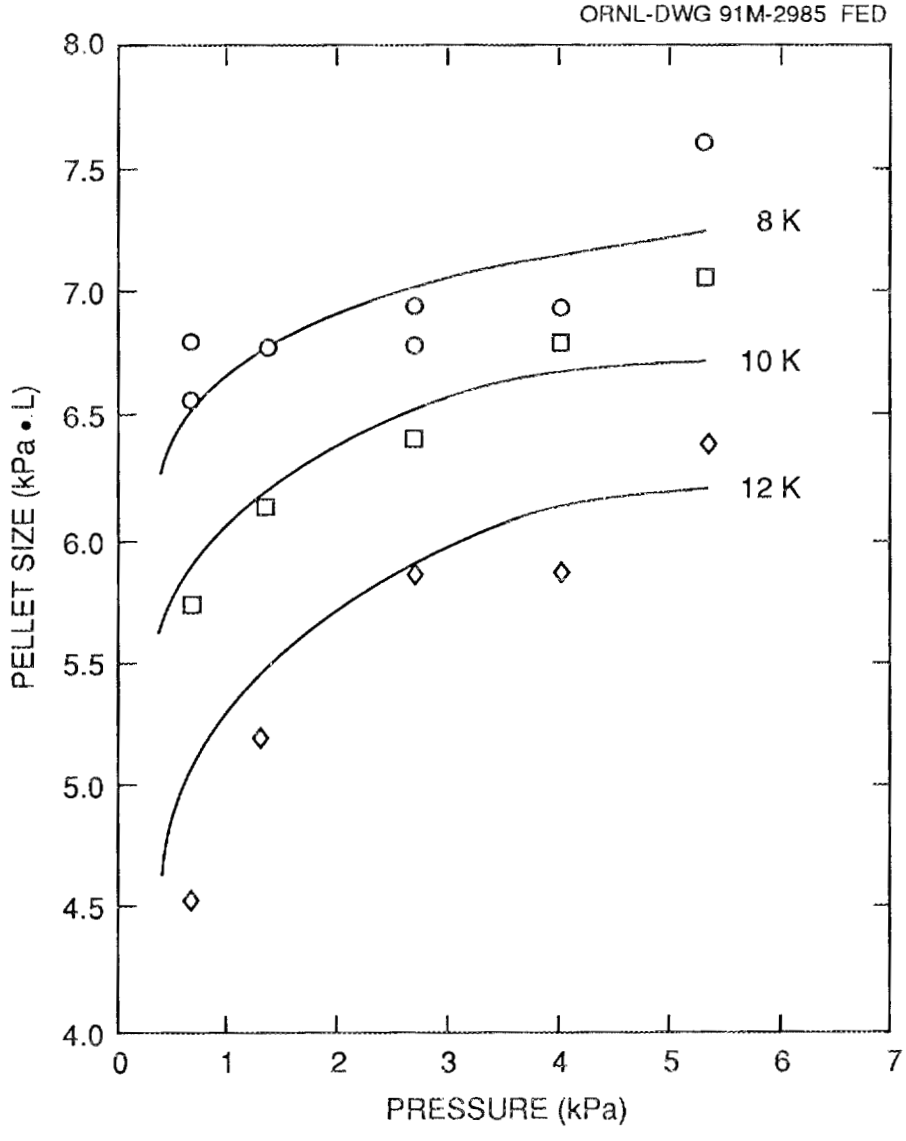

Fig. 3.12. Deuterium pellet size for pellets formed by filling from the breech direction. Lines are model predictions.

demarcation on their surface in a position corresponding to the end of the freezing zone. (Similar effects were obscured by the gas cloud in photographs of tritium pellets.) The model showed that axial temperature gradients along the barrel were very steep in this region and would truncate the pellet length if it were not for the very low thermal conductivity of the gas, which insulates the pellet from the wall and allows it to grow far beyond the freezing zone.

No systematic studies were made with feed gas above the triple-point pressure because results in this region were generally poor. Pellet shape was usually not well

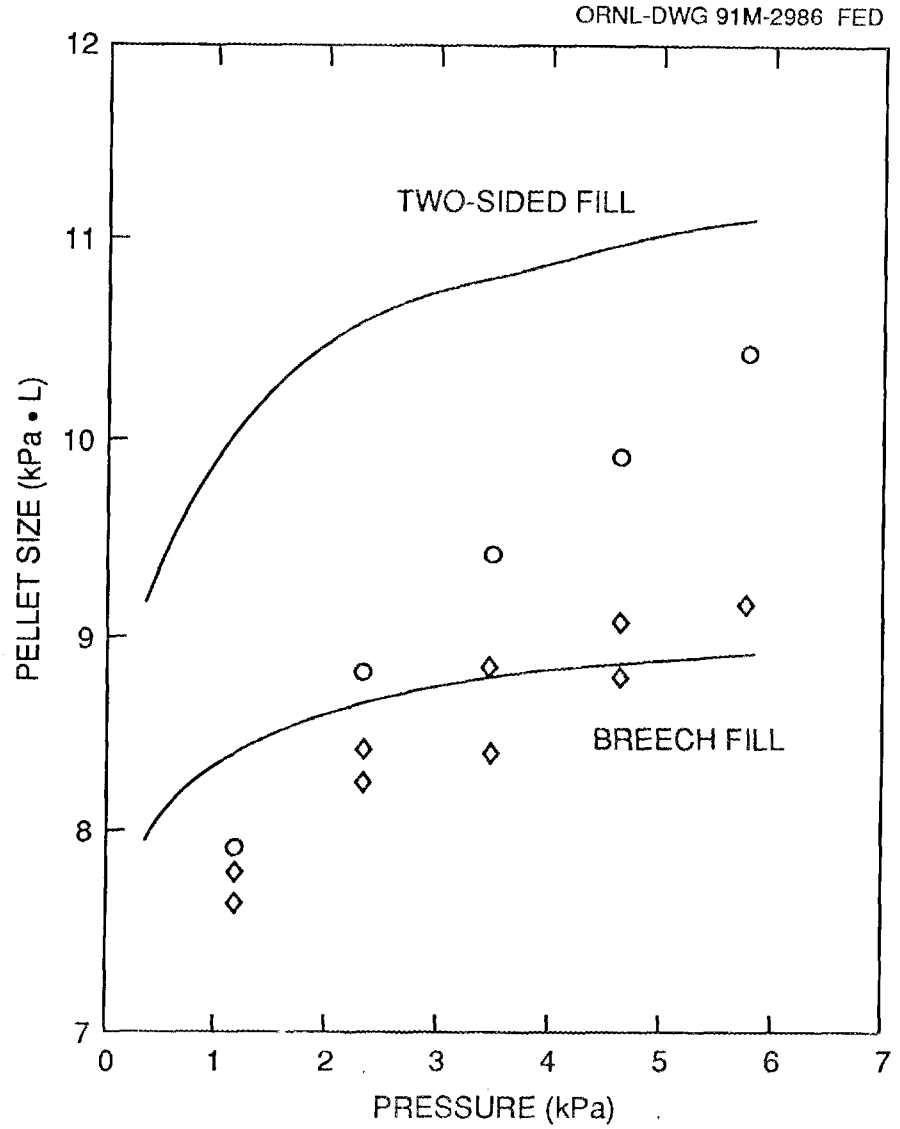

Fig. 3.13. Tritium pellet size for pellets formed by filling from both ends of the barrel (circles) and by filling from the breech on two different days (diamonds). Lines are model predictions.

defined by the freezing zone, and the gun actually took less feed gas than for pellets formed at much lower pressures. This was true for both deuterium and tritium. This behavior is explained in the model predictions shown in Fig. 3.17. Above the triple-point pressure, pellet length stabilizes at a value only slightly longer than the length of the freezing zone because liquid forms at the end of the pellet and transfers heat from the warm barrel to the pellet, which limits the pellet length. The amount of liquid present is virtually immaterial because a temperature rise of only a few kelvins is sufficient to melt

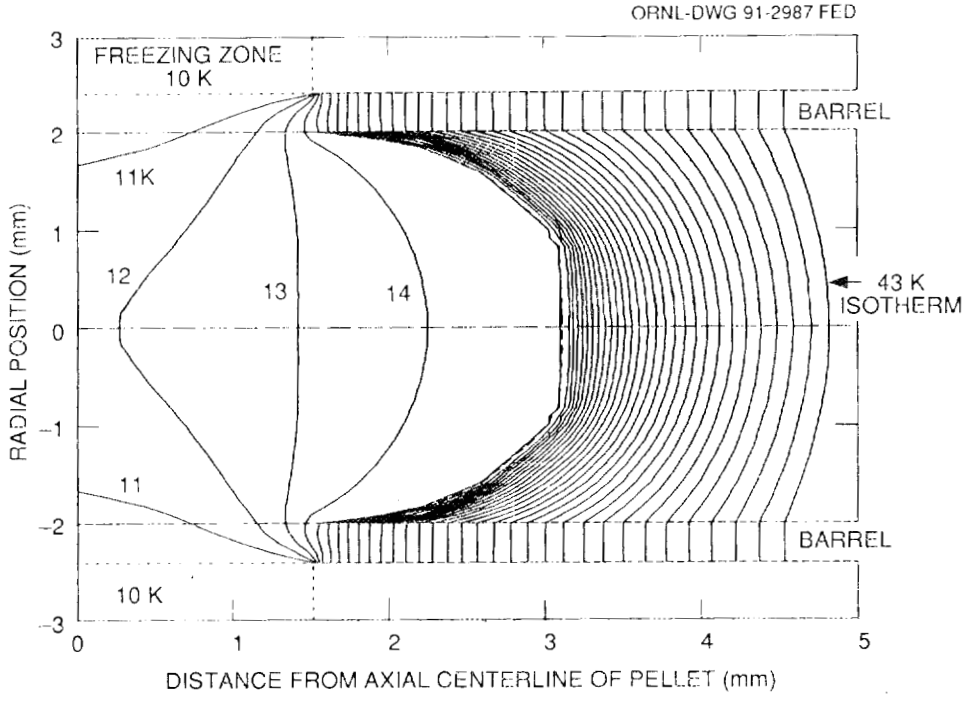

Fig. 3.14. Pellet shape with 1 K isotherms for a deuterium pellet formed at 10 K with equilibrium pressure of 2.67 kPa (20 torr) and a 300 K heat sink 10 cm from the freezing zone.

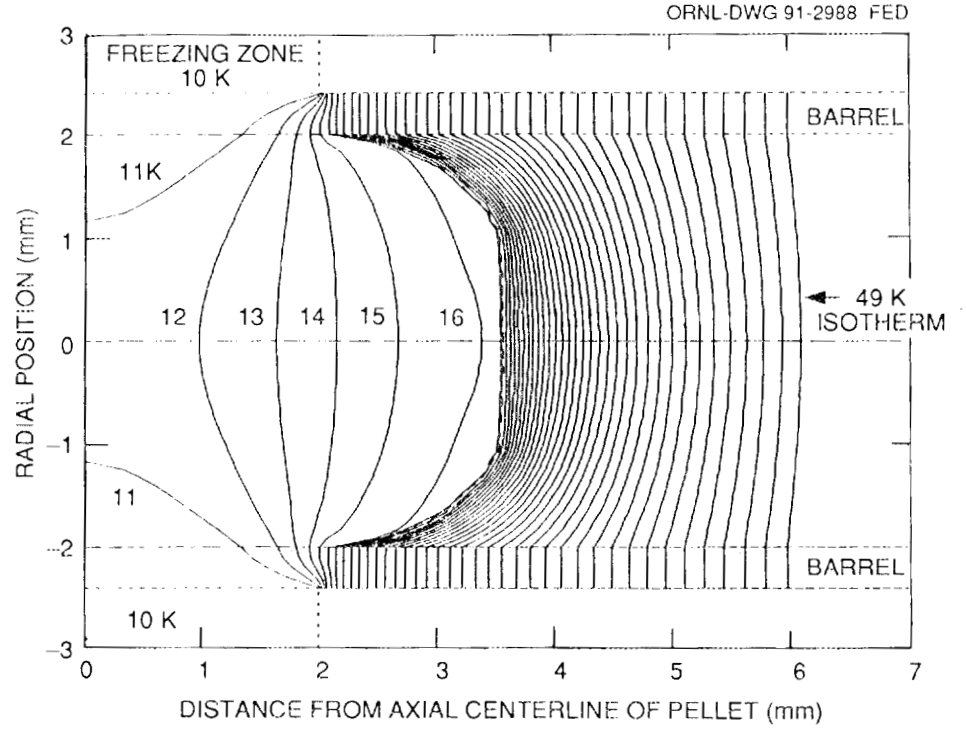

Fig. 3.15. Pellet shape with 1 K isotherms for a tritium pellet formed at 10 K with equilibrium pressure of 2.67 kPa (20 torr) and a 300 K heat sink 10 cm from the freezing zone.

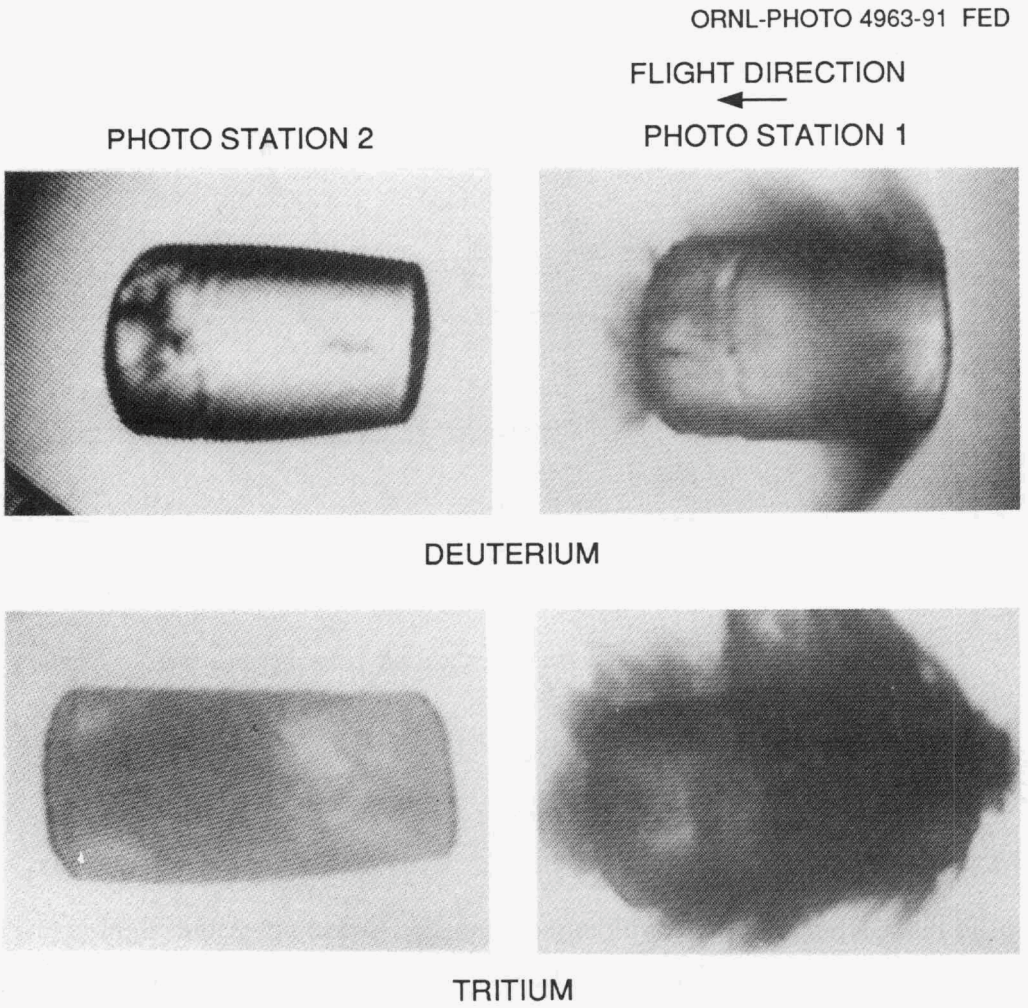

Fig. 3.16. Deuterium pellet formed at 10 K by filling the gun from both ends of the cryostat with a fill pressure of 4.0 kPa (30 torr) and a heat sink 10 cm from the cryostat.

the pellet, and this occurs in the barrel only a fraction of a millimeter from the edge of the cryostat. Thus, above the triple-point pressure, pellet length becomes independent of feed pressure. Since the cryostat in this gun was quite short, pellets formed under these conditions have a length-to-diameter ratio of less than one and do not perform well under acceleration. However, guns with longer cryostats might be capable of forming and accelerating pellets at these higher pressures. These model runs were made with collar cryostats mounted 10 mm on either side of the pellet, but the conclusion would be generally applicable for all types of pipe guns.

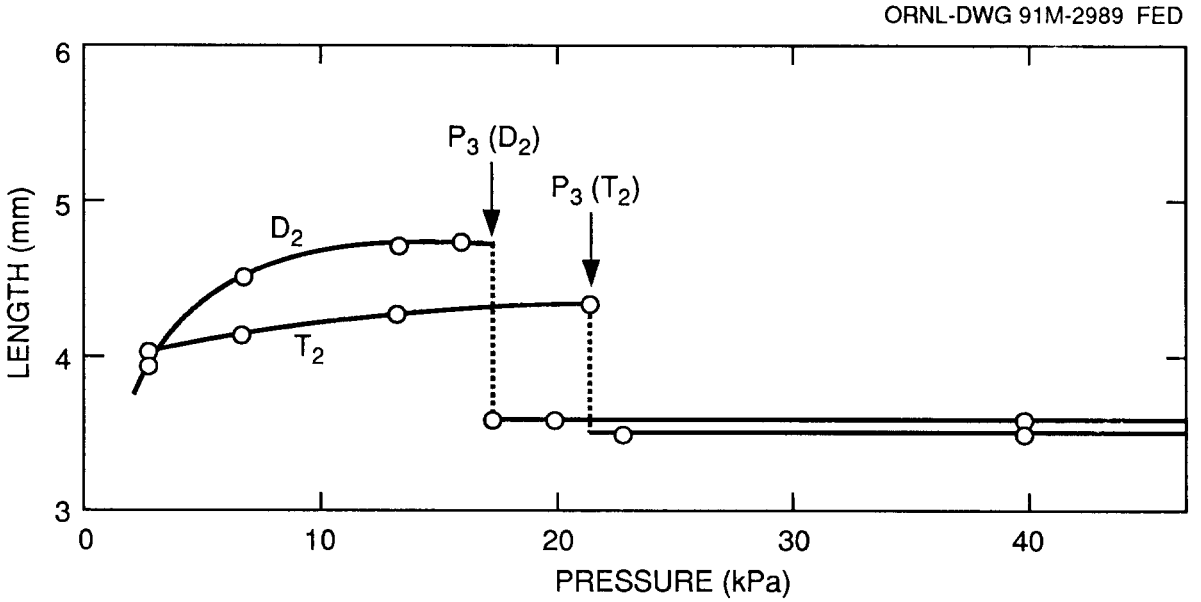

Fig. 3.17. Effect of feed pressure above the triple-point pressure on pellet length.

3.2 PELLET VELOCITY

3.2.1 Diagnostics

Figure 3.18 shows pellet velocity diagnostics (breech pressure, light gates, and shock transducer) for a typical shot. The shot was initiated with a computer-generated trigger pulse to the fast valve power supply at 0 μs. The breech pressure (top curve) begins to rise about 2 ms after the trigger and reaches its peak about 0.5 ms later. The time between the trigger and the appearance of pressure in the breech is a function of both the amount of free travel in the solenoid-driven valve poppet and delays that could be set in the valve power supply. The power supply also controlled the amount of time the valve was held open and the voltage that the solenoid received.[22] Generally, the peak breech pressure varied almost linearly with supply pressure and was 60% to 90% of the supply pressure for supply pressures from 13.9 MPa (2000 psig) to 3.5 MPa (500 psig). Breech pressure became a smaller fraction of supply pressure as the supply pressure was increased because the propellant gas pressure augmented the closing force on the valve poppet. Before velocity scans were made, an effort was made to increase power supply settings until further increases did not increase breech pressure. At this point, breech pressure was limited by valve dynamics alone. However, power supply settings could not be made arbitrarily high because of limitations in the power supply and (for tritium runs) in the amount of propellant that could be released to the vacuum system. Therefore, some

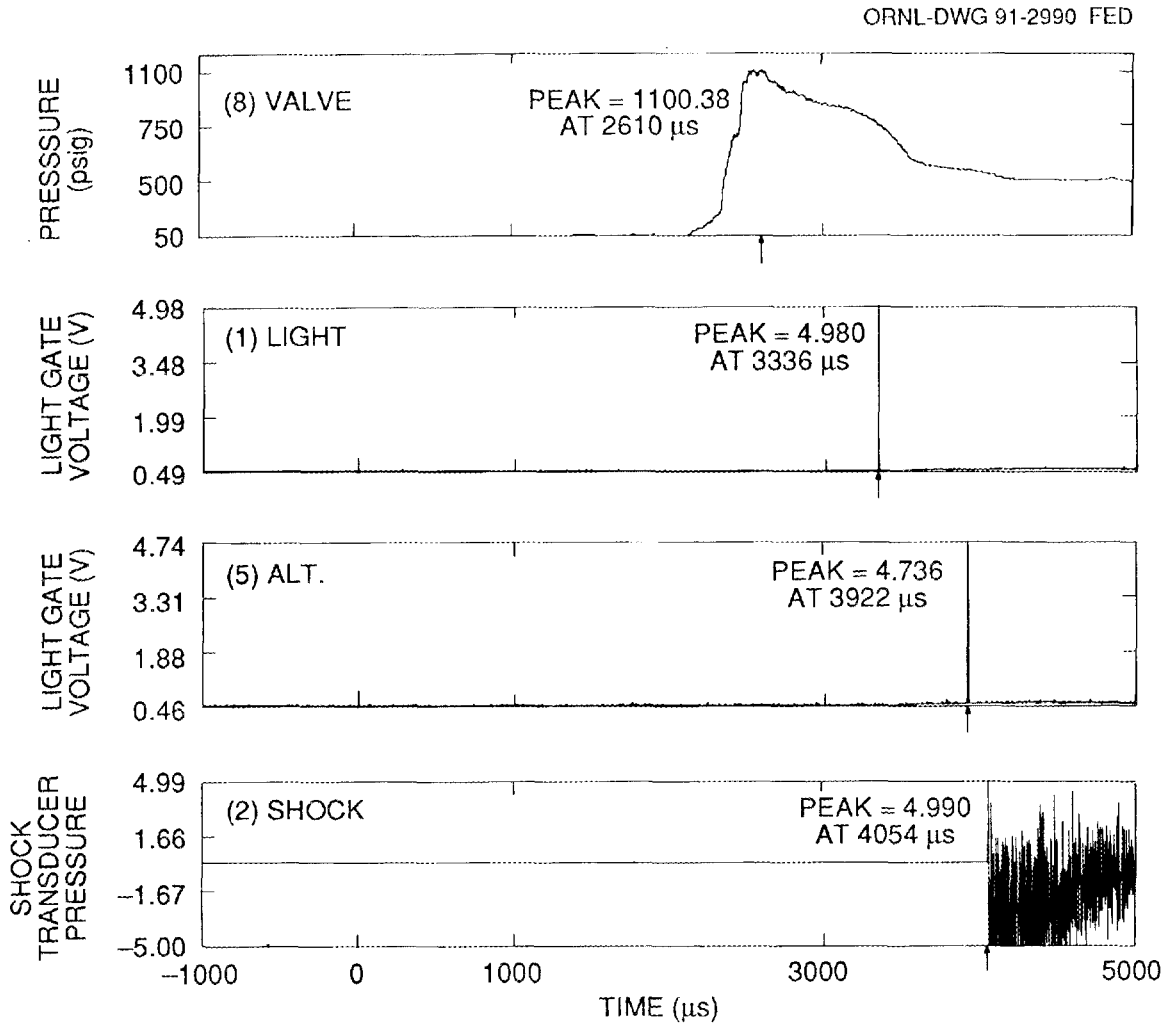

Fig. 3.18. Breech pressure and velocity diagnostics for a typical shot.

additional tailing off of velocities at high supply pressure was unavoidable. However, the effect of power supply and valve dynamics on the results can be reduced by observing the behavior of velocity as a function of breech pressure. Any combination of valve and power supply with a similar time response that delivers the proper breech pressure should produce comparable results. Figure 3.18 also shows the diagnostic signals as the pellet passes the two light gates and strikes the end of the diagnostic line, where the shock was recorded. Pellet velocities shown in Fig. 3.19 were determined from these diagnostics.

3.2.2 Correlation with Theory

Because of the wide range of pellet densities (from hydrogen at 0.087 g/cm^3 to tritium at 0.32 g/cm^3) and breech pressures involved in the TPOP experiment, it is useful

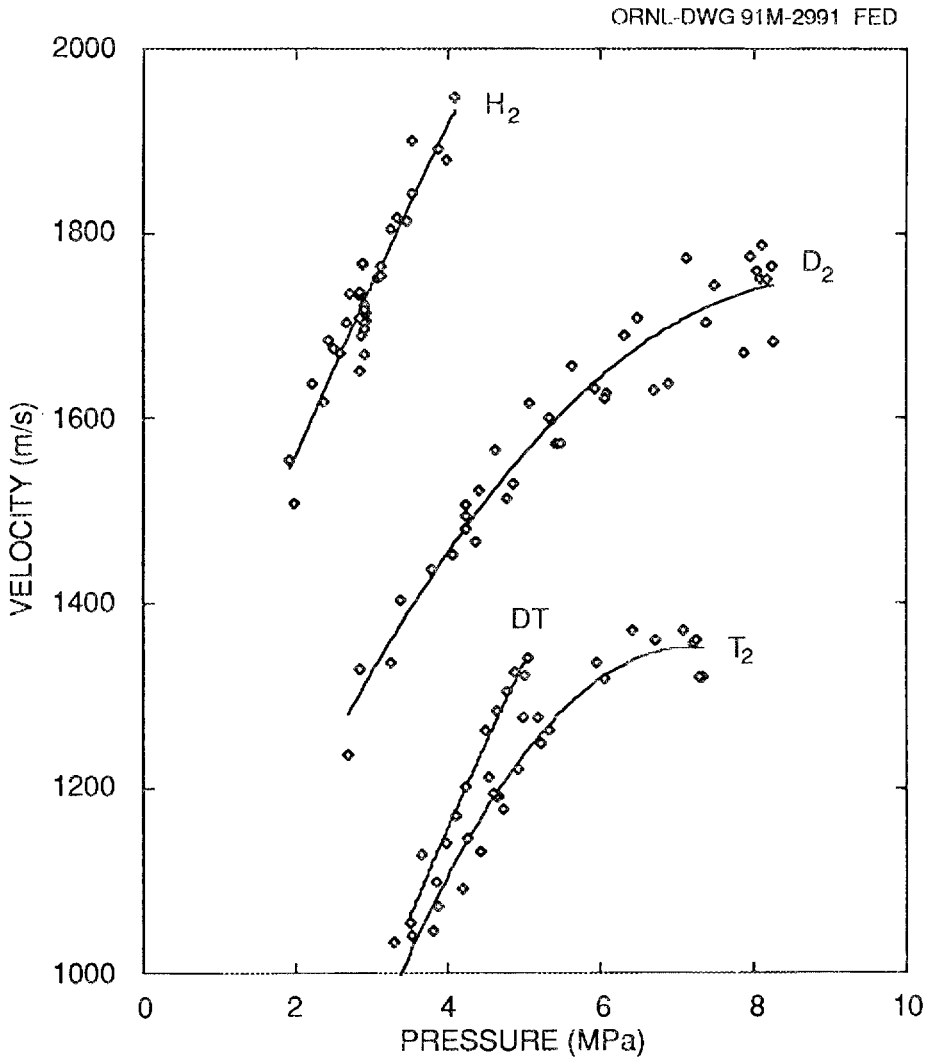

Fig. 3.19. Pellet velocity as a function of peak breech pressure for 4-mm-diam, 4-mm-long H_2 and D_2 pellets and for 4-mm-diam, 5-mm-long DT and T_2 pellets.

to look to theory for guidance in correlating the results. A simple ideal model with an analytical solution has been derived by Landau and Lifshitz.[25] In this model, an infinite tube is assumed to be divided into two sections initially (at $t = 0$) by a frictionless pellet of mass M_p and cross-sectional area A_p located at $x = 0$. To the left of the pellet ($x < 0$) the tube is initially filled with propellant, assumed to be an ideal gas, at a pressure P_0. To the right of the pellet ($x > 0$), the tube is evacuated. The motion of the pellet after its release can be expressed in terms of a dimensionless velocity U^* and a dimensionless initial acceleration a^* as

$$a^* = (\gamma - 1)^2/[2(\gamma + 1)] + [(\gamma - 1)/(\gamma + 1)](1 - U^*)^{-(\gamma+1)/(\gamma-1)} - [(\gamma - 1)/2](1 - U^*)^{-2/(\gamma-1)}, \tag{3.5}$$

where $\gamma = C_p/C_v$. The dimensionless muzzle velocity is the actual muzzle velocity U divided by the maximum ideal velocity U_m,

$$U_m = 2c_0/(\gamma - 1), \tag{3.6}$$

where c_0 is the speed of sound in the propellant gas. The speed of sound in an ideal gas is given by

$$c_0 = \sqrt{\frac{\gamma RT}{M}} \tag{3.7}$$

where R is the ideal gas constant, T is the propellant temperature (assumed constant), and M is the propellant molecular weight. The dimensionless acceleration is given by

$$a^* = a_0 L/U_m^2, \tag{3.8}$$

where L is the barrel length (x position in tube) and a_0 is the initial acceleration,

$$a_0 = (P_0 A_p)/M_p. \tag{3.9}$$

Equations (3.5)–(3.9) show that for an ideal gun the dimensionless muzzle velocity should be a fixed function of the dimensionless initial acceleration. Furthermore, for a given ideal gun in which the barrel length and propellant are not changed, the actual velocity should be a fixed function of the actual initial acceleration.

Figure 3.20 shows velocities for the various hydrogen isotope pellets as a function of initial acceleration calculated from the peak breech pressure and measured pellet mass. Pellet mass varies by almost a factor of five from the 4-mm hydrogen pellets to the 5-mm tritium pellets, yet all the data fall in a narrow band, as predicted by the simple ideal theory. (Isotope density differences are accounted for in the initial acceleration a_0.) Some difference between the hydrogen and deuterium curves at high initial accelerations is probably due to the more severe erosion weight loss for hydrogen at the higher velocities. Nevertheless, the data set appears to be consistent, with none of the isotopes departing

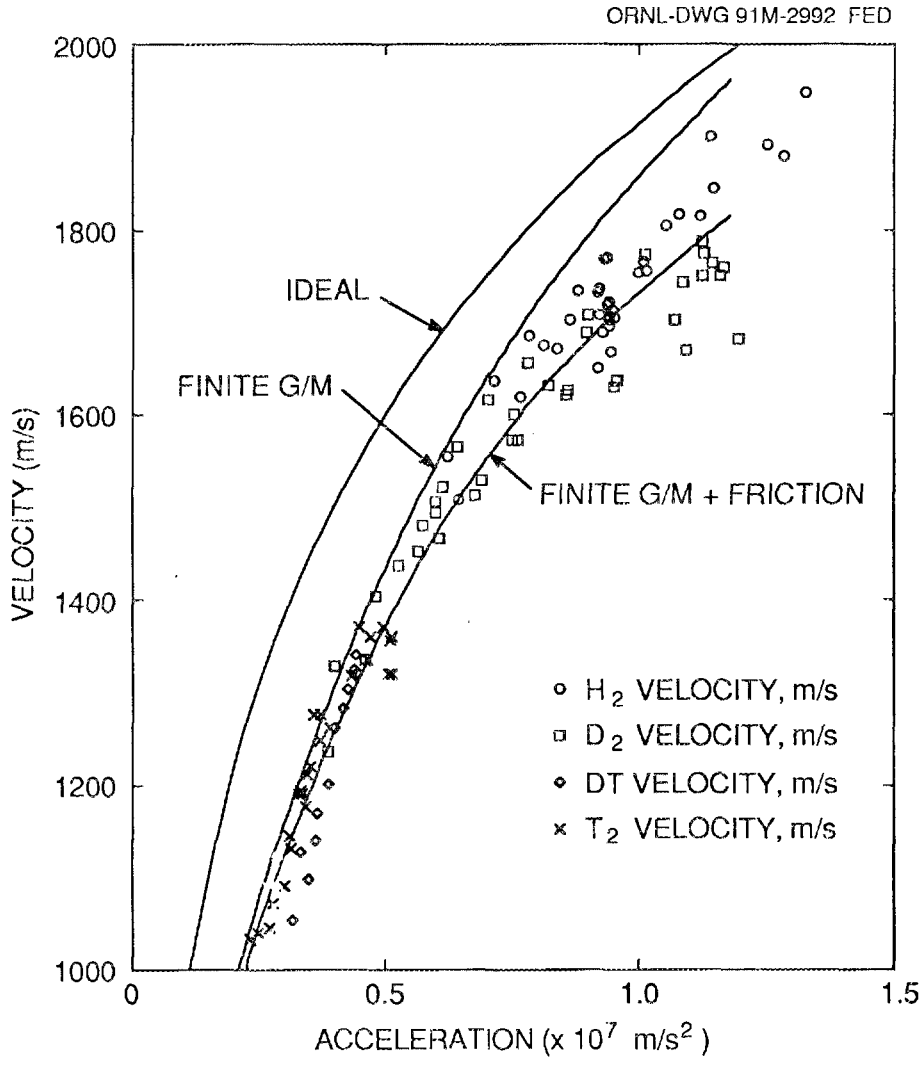

Fig. 3.20. Pellet velocity as a function of initial acceleration.

significantly from expected behavior. Although the ideal theory itself does not give a good prediction of the results, it does give a good representation of the shape of the curve.

It has been shown[26] that for this type of pneumatic gun (single-stage) there are two dominant nonideal effects: at low velocities, the amount of propellant gas available for acceleration limits velocities, and at high velocities, friction becomes important. Seigel[27] made numerical calculations of muzzle velocity using the basic assumptions of the ideal model with the amount of propellant gas being limited by the length of tube behind the pellet. He presents his results in plots of dimensionless velocity (U/c_0) vs dimensionless length of travel (a_0L/c_0^2) for various values of the parameter G/M_p, where G is the weight of propellant gas in the breech of the gun. To estimate the effect of finite G/M_p in the

present experiments, it was assumed that G could be calculated from the amount of propellant trapped between a pellet in the freezing zone of the cryostat and the face of the poppet of the fast valve (a region 21 cm long and 0.4 cm in diameter) and the measured peak breech pressure. Predictions from this model, plotted in Fig. 3.20, show good agreement with the data at low velocities. The effect of friction was estimated from an empirical relationship developed at the U.S. Naval Ordnance Laboratory,[27] in which the ratio of the actual velocity to the predicted frictionless velocity is a function of the dimensionless frictionless velocity. Velocity predictions based on this correlation, shown in Fig. 3.20, are in very good agreement with the data.

3.3 BREAKAWAY PRESSURE

The minimum propellant pressure required to shear the pellet from the wall is referred to as the breakaway pressure. Normally, this pressure cannot be found by evaluating the breech pressure data using the fast propellant valve because the breech pressure increases too rapidly. To observe the breakaway pressure for deuterium pellets, propellant gas flow was restricted by using an ordinary solenoid valve with a needle valve in series to launch the pellet. In addition, the propellant gas was changed to helium, which does not condense and change the pellet size. In these experiments, the propellant pressure was slowly increased until the pellet broke away from the wall. Figure 3.21 shows two typical runs. For the top plot, the supply pressure was set higher than the breakaway pressure, and the pellet was released about 0.2 s after the valve began opening. For the lower curve, the supply pressure was below the breakaway pressure; the pellet sustained the pressure for more than 0.6 s, and when it was finally released its size was significantly reduced, either by melting or breaking. Breakaway pressure measurements for deuterium pellets are listed in Table 3.2. Breakaway pressures for tritium, were not measured in this way, but in several tritium shots the pellet was not released from the barrel. These data are reported in Table 3.2 as being indicative of the breakaway pressure, because other tritium pellets were released at only slightly higher pressures.

The shear strength of the pellet can be calculated by setting the breakaway force exerted on the rear of the pellet equal to the shear force at the wall. When this is done the shear strength σ can be calculated from

$$\sigma = (P_b D_p)/4L_p \,, \tag{3.10}$$

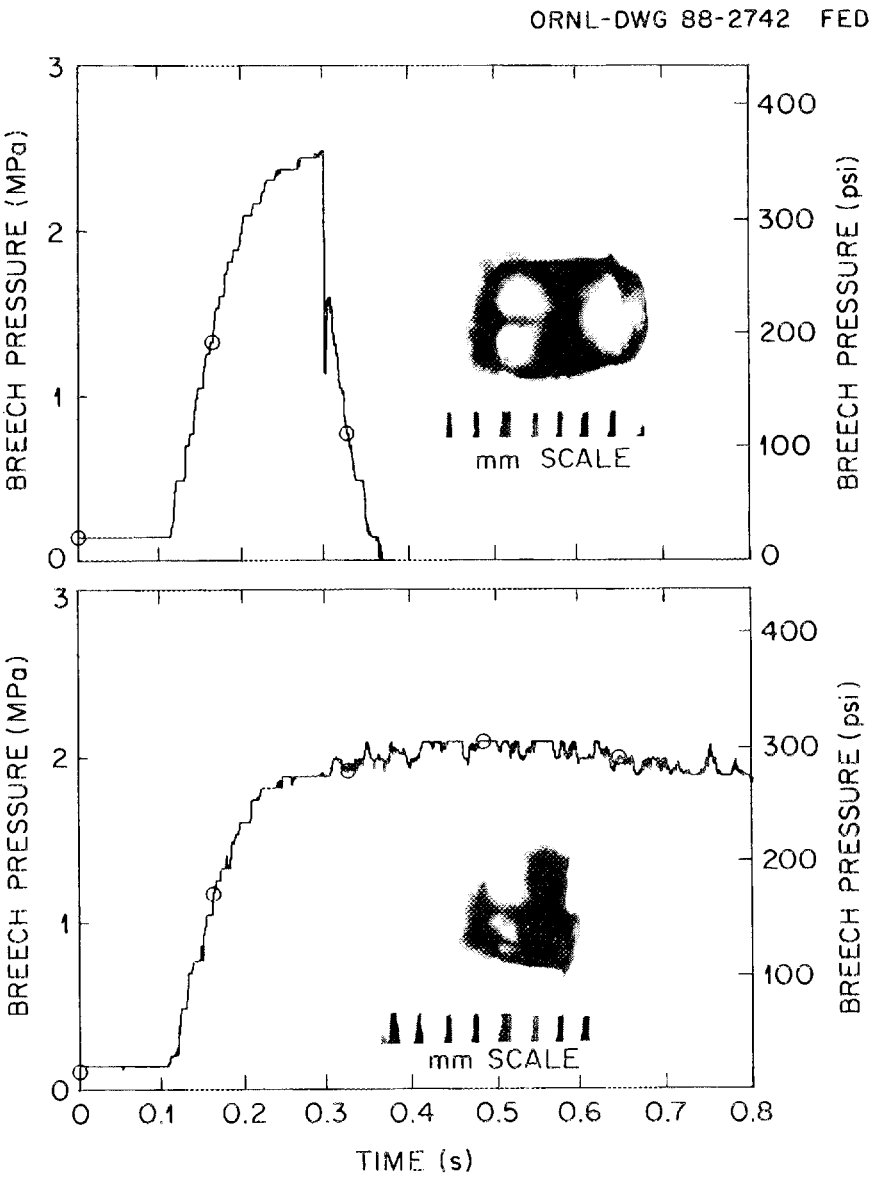

Fig. 3.21. Typical breakaway pressure curves.

where P_b is the breakaway pressure, D_p is the pellet diameter, and L_p is the pellet length. Values of the shear strength are reported in Table 3.2 and presented as a function of temperature in Fig. 3.22. Also shown in Fig. 3.22 are the ultimate tensile strengths of hydrogen[28] and deuterium.[29] Strictly speaking, the shear strength and tensile strength of a material are not necessarily equal. However, the shear strength and tensile strength of deuterium have similar magnitudes and temperature dependences. The value of the shear

Table 3.2. Breakaway pressure data and shear strength

Pressure (psi)	Length (mm)	Temperature (K)	Shear strength (psi)
		Deuterium	
424	4.8	6.0	88
404	4.7	6.0	86
434	4.5	6.0	96
222	4.2	6.0	53
303	4.7	6.0	64
364	5.2	6.4	70
222	4.2	7.9	53
344	4.2	7.9	82
374	4.8	7.9	78
232	3.6	10.0	64
293	4.0	10.0	73
303	4.2	10.0	72
303	4.5	10.0	67
192	3.9	12.0	49
152	3.2	12.0	48
152	3.7	12.0	41
		Tritium	
813	5.2	8.0	156
792	5.3	8.0	149
869	5.1	9.0	170

strength for tritium is about twice that of deuterium at 8 K. This may seem like a large difference between isotopes; however, the tensile strengths of hydrogen and deuterium show similar large differences.

3.4 PELLET EROSION

Pellet diameter can be determined from video images of the pellets. Figure 3.23 shows images of six deuterium pellets formed by filling from the breech and traveling at velocities near 1800 m/s. While images recorded at the second photo station were quite clear, they cannot be used for absolute measurements because the orientation of the pellet relative to the plane of the ruler was not known. At the first photo station the pellet was in the plane of the ruler, so length scales can be readily determined. Because these pellets

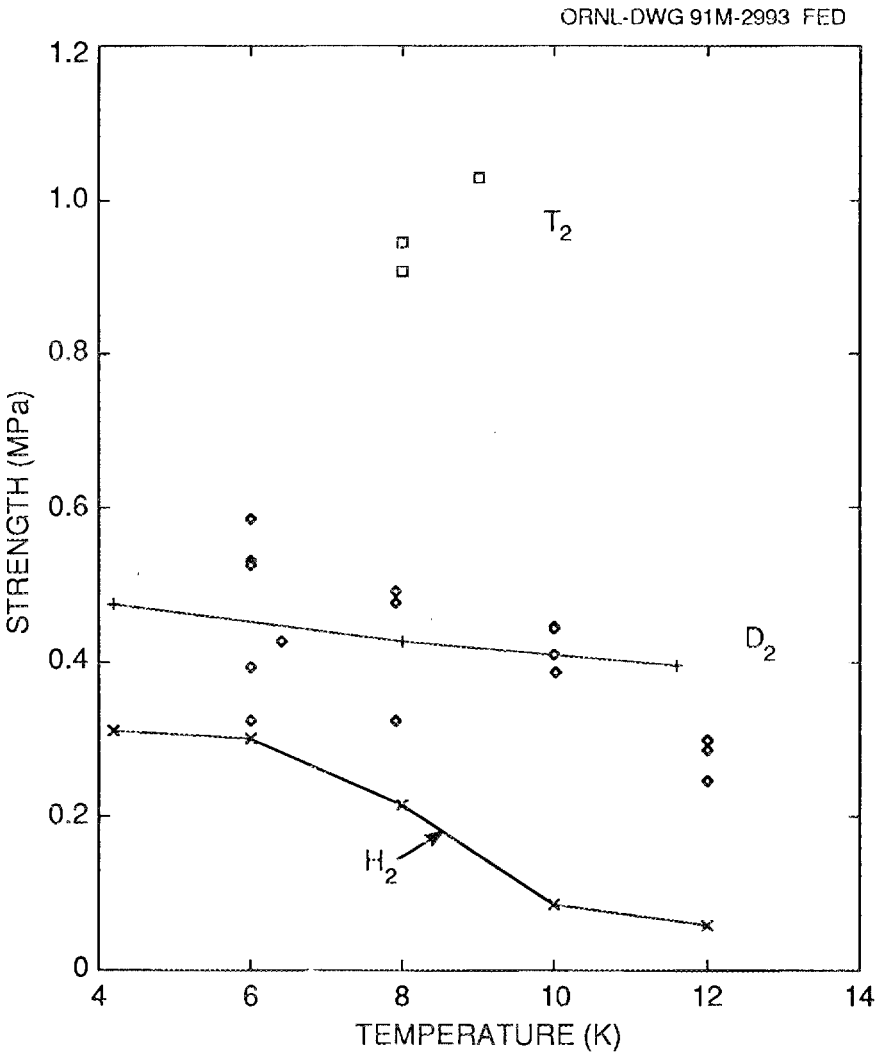

Fig. 3.22. Shear strength of D_2 and T_2 determined from breakaway pressure data. Lines are ultimate tensile strengths of H_2 and D_2.

were filled from the breech, the nose of the pellet occupied the freezing zone of the barrel, and represents the full barrel diameter prior to acceleration. This part of the pellet often appears clear of propellant gas, facilitating measurement of the diameter in images recorded at the first photo station after acceleration. The somewhat conical shape of the rear of the pellet was due to a combination of erosion and the initial shape of the pellet at the time of formation (as described in Sect. 3.1.3). Although this shape was readily observed in images at the second photo station, accurate size measurements could not be made at the first photo station because the back end of the pellet was always obscured by propellant gas.

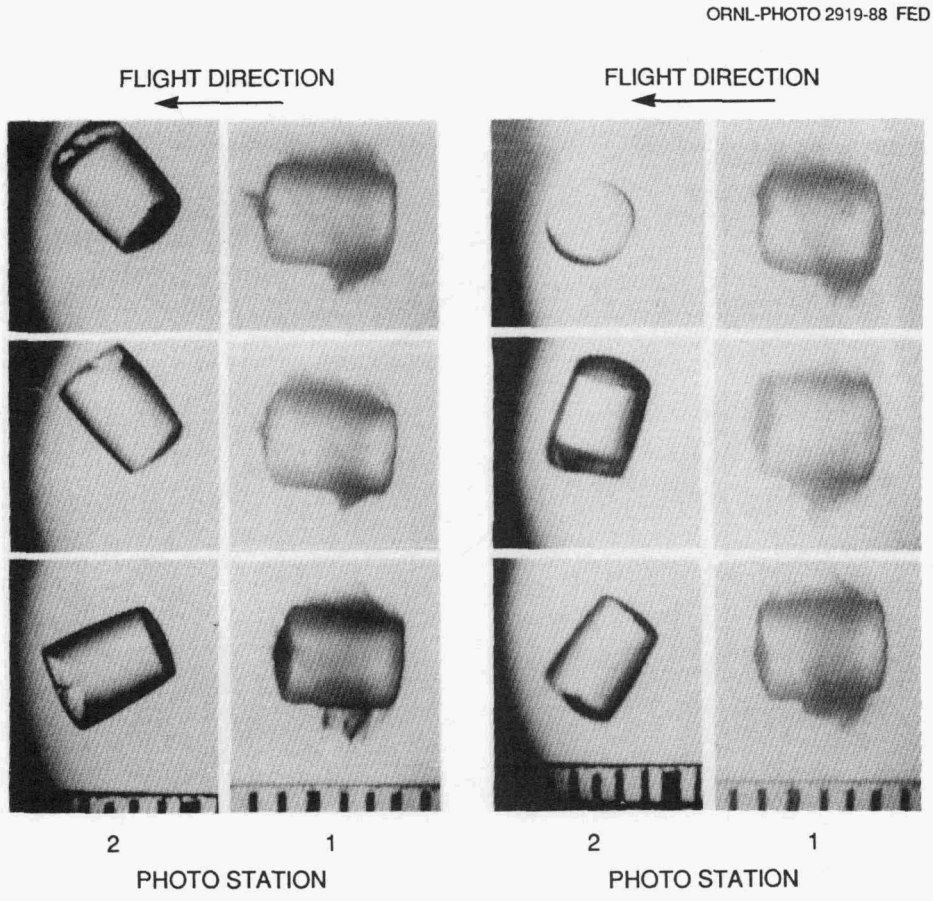

Fig. 3.23. Video images of several deuterium pellets.

Figure 3.24 shows a calibration curve for a rectangular grid pattern (similar in size to a pellet) recorded by the video cameras at various positions in and out of the focal plane. This curve indicates that pellet images shrink as the pellet-to-lens distance increases and that vertical and horizontal length scales were not equal. Lengths measured in the vertical direction were about 10% longer than those measured in the horizontal direction. Since the image of the ruler was measured horizontally and the pellet diameter was measured vertically, pellet diameters appeared to be larger than they actually were. Reported pellet diameters have been corrected for this distortion. Scale size also contracts as the image approaches the edge of the video screen producing the need for an additional correction of 1 to 2% in a few pellets whose images were significantly displaced from the center of the screen.

Figure 3.25 shows pellet diameter as a function of velocity for deuterium and tritium pellets. Lines in the figure are least-squares fit using the slope method, assuming

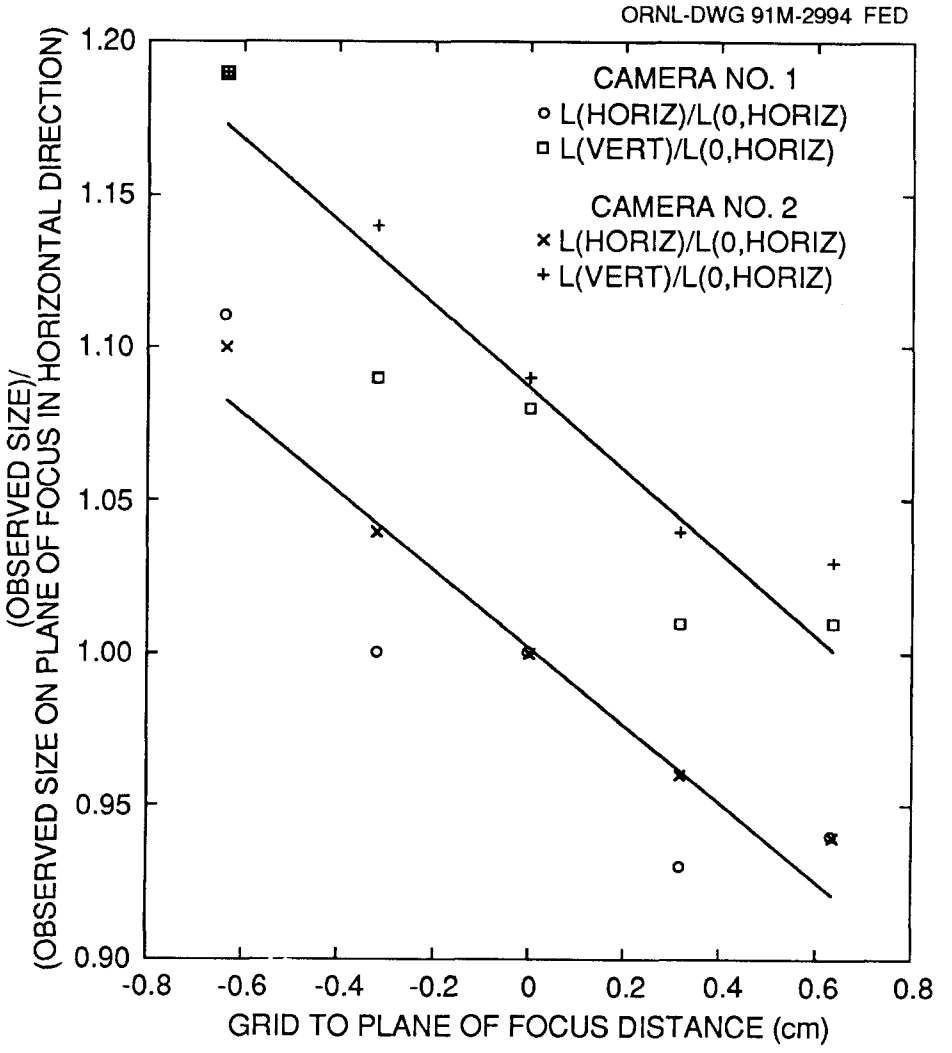

Fig. 3.24. Relative size of a video image of a rectangular grid pattern.

an intercept of 4 mm (the barrel inside diameter) at zero velocity. A least-squares fit of the deuterium data, which encompass a relatively wide range of velocities, using the slope-intercept method has nearly the same slope as the zero-intercept constrained line. Comparison of the deuterium and tritium data indicates that, at a given velocity, tritium will suffer about half the radial erosion loss of deuterium. This is another indication of the greater strength of tritium pellets.

No mechanism existed in this experiment to determine the actual mass of the delivered pellet; however, pellet mass can be inferred by calculating the mass loss as a function of diameter reduction. Figure 3.26 shows estimated fractional weight losses based on this assumption. Weight losses of this magnitude have been observed in other

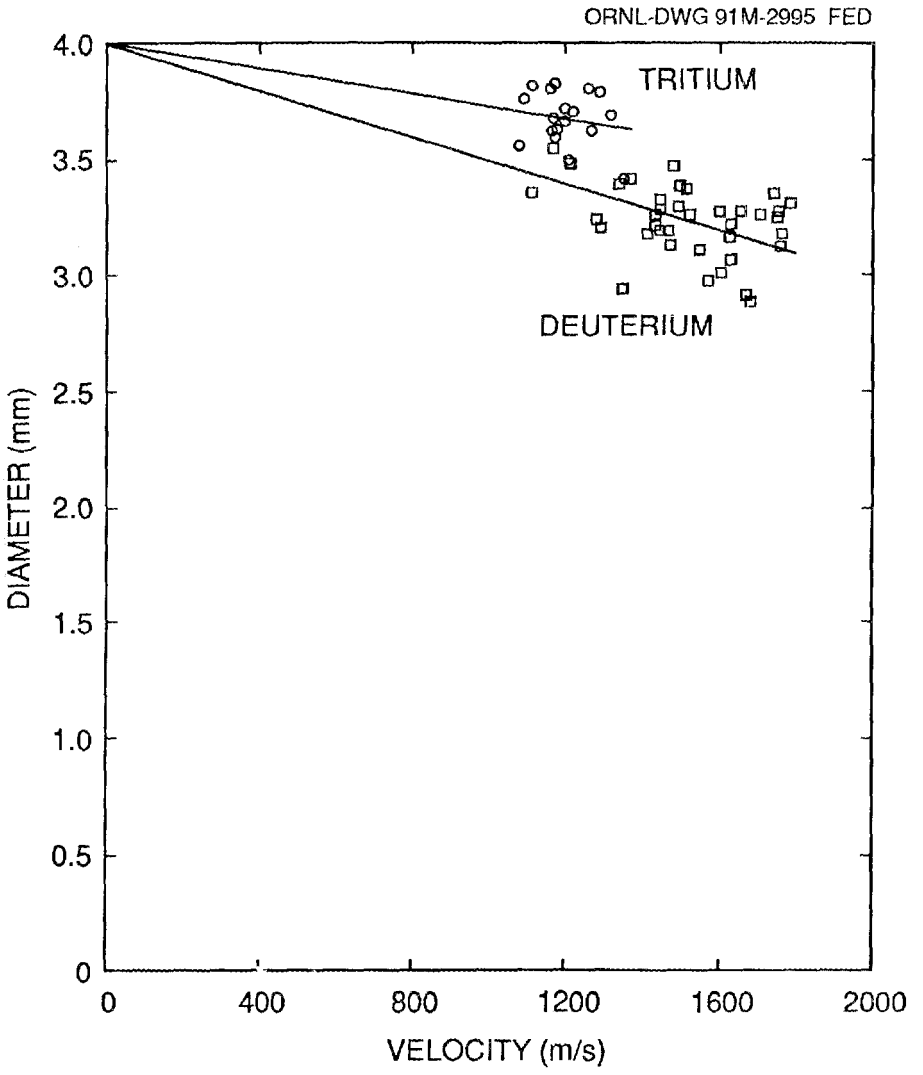

Fig. 3.25. Pellet diameter as a function of velocity.

pneumatic injectors. Milora and co-workers[30] observed a 10% to 30% decrease in the weight of 1000-m/s, 1-mm-diam hydrogen pellets injected into a trapped volume. Büchl and Sandmann[31] observed an 11% mass loss at 400 m/s and a 26% mass loss at 1000 m/s for 0.6-mm-diam deuterium pellets injected into a trapped volume. Watkins and co-workers[32] reported 15% and 30% mass losses for 3.6-mm and 4.6-mm-diam deuterium pellets at velocities of 750–1200 m/s on the basis of observed plasma density increases in the Joint European Torus (JET), and Kamada and co-workers[33] reported 20% to 30% weight losses for 2.7- and 3.8-mm-diam hydrogen pellets on the basis of observed plasma density increases in JT-60. Baylor[34] reported a 0 to 30% mass loss for 2.7- and 4.0-mm

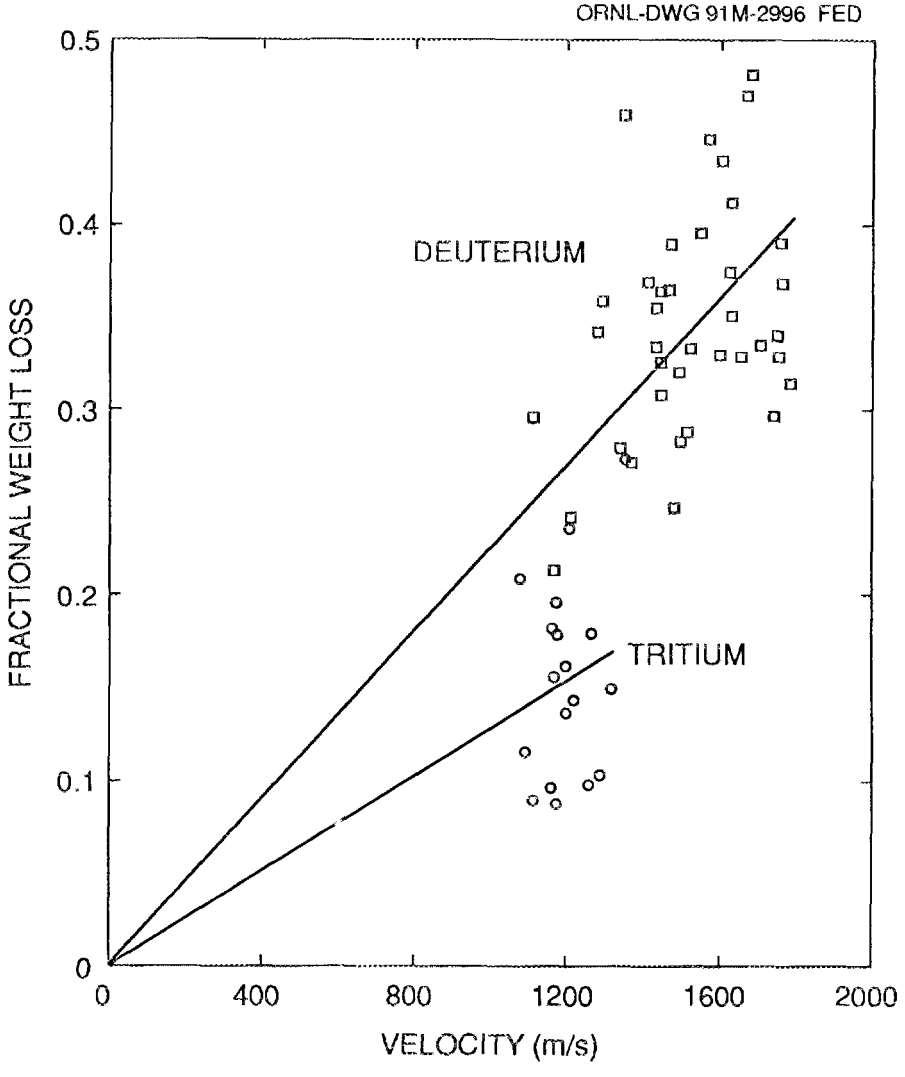

Fig. 3.26. Pellet fractional mass loss, based on diameter reduction, as a function of velocity.

deuterium pellets on the basis of plasma density increases in JET, with an arbitrary assumption of no mass loss for the most efficiently utilized pellets. All of these data for complete injection line losses are of the same order as the TPOP barrel erosion data, indicating that barrel erosion can be the primary loss mechanism in a pneumatic injector.

3.5 SYSTEM RELIABILITY

One mandate of the TPOP program was to track system reliability. Figure 3.27 shows the number of times the valves and pumps in the system were cycled. (A complete description of these elements is given in Sect. 2 of this report.) No failures or leaks

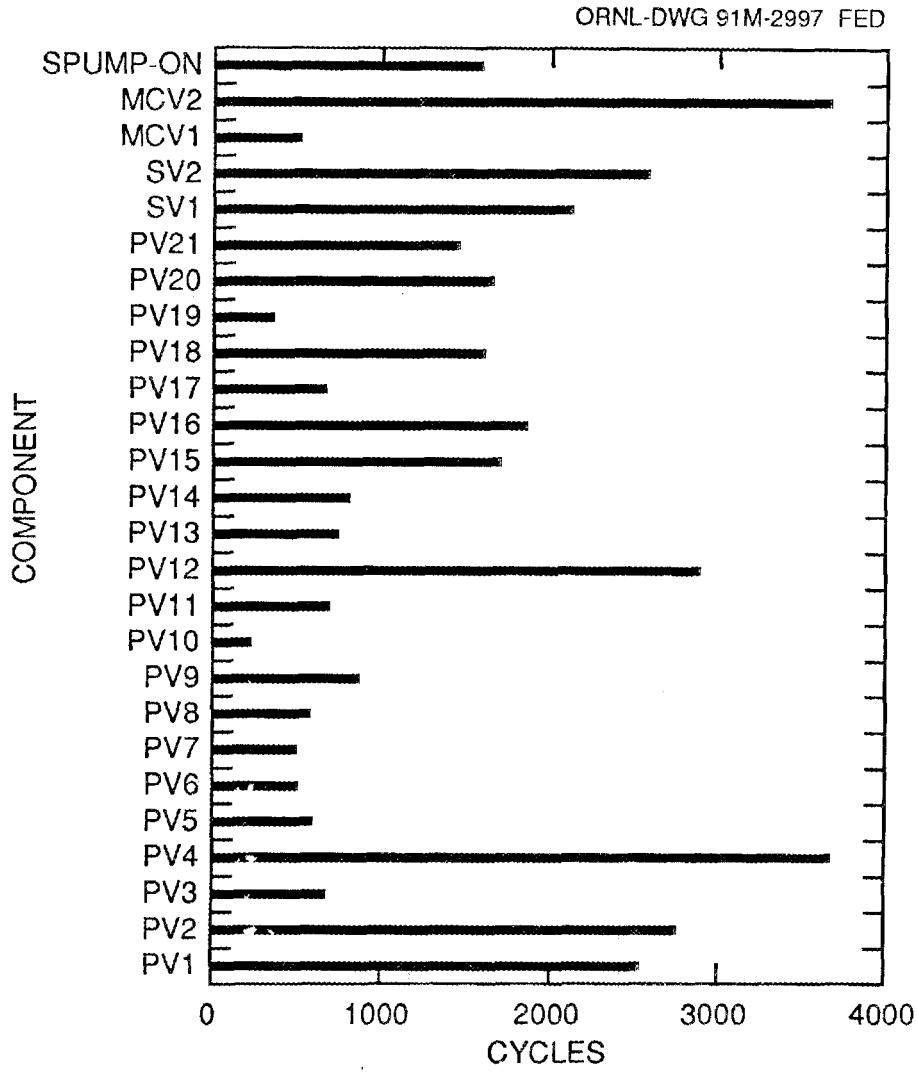

Fig. 3.27. Number of cycles for TPOP system components.

occurred in any of these components during the program. The pumps were run for a total of 772 h. After initial tritium leak testing (which required little time), no tritium leaks developed in the system during operation. Once sealed, the glovebox system had no failures. However, sealing the windows initially was quite time-consuming, and a different window frame design should be considered for future gloveboxes. The hydrogen monitor in the glovebox was of no value because hydrogen levels were virtually always greater than the full-scale value (100 ppm). A less sensitive sensor should be considered in the future.

In early stages of operation with deuterium pellets, a number of bursting disk failures occurred. These failures resulted from excessively high pressure on feed lines to the glovebox and from operator errors. After additional pressure regulators were added to

the feed lines and system operation was automated, no more failures of this type occurred.

One Validyne AP10 pressure transducer failed near the end of the experimental program. The cause of the failure was unknown. During operation, the controllers for these gages drifted and needed zeroing before each day's operation. The fiber-optic transmission and receiving unit also needed at least daily, and sometimes shot-to-shot, adjustment to keep it triggering properly. This digital unit should be replaced with more reliable circuits based on fast analog phototransistors, which were not available when the TPOP was designed. No other transducer failures occurred.

4. CONCLUSIONS AND RECOMMENDATIONS

The TPOP experiment has demonstrated the feasibility of producing and accelerating tritium pellets for fueling fusion reactors. The extremely low ^{3}He levels (<0.005%) needed for production of good pellets can be achieved with cryogenic separation. No deleterious effects were observed if pellets were held in the barrel for up to 0.5 h after formation (longer holding times were not tested). Tritium pellet velocities on the order of 1400 m/s were demonstrated, and higher velocities should be achievable. Both pellet size and velocity were successfully modeled. Higher breech pressures could have been delivered if more powerful power supplies had been used to drive the propellant valve. Alternatively, two-stage drivers could be used in place of the solenoid propellant valve in future work.

The strength of tritium pellets appears to be about twice that of deuterium pellets at temperatures of interest. This could have serious consequences in terms of the extrudability of tritium, and the feasibility of using extrusion-based tritium pellet injectors should be tested. Such extrusion-based pellet injection systems will be required for ITER and fusion reactors because the pulse length of these experiments makes the single-shot pipe-gun injector impractical. Higher ^{3}He levels may be acceptable in extrusion-based injectors because more volume is available inside the extruder for ^{3}He accommodation.

REFERENCES

1. S. L. Milora et al., "Pellet Injection into PDX Diverter Plasmas," *Nucl. Fusion* **22**, 1263 (1982).

2. M. Greenwald et al., "Energy Confinement of High-Density Plasmas in the Alcator C Tokamak," *Phys. Rev. Lett.* **53**, 352 (1984).

3. S. Sengoko et al., "Improvement of Energy Confinement Time by Continuous Pellet Fueling in Beam Heated Doublet III Limiter Discharges," *Nucl. Fusion* **25**, 1475 (1985).

4. S. L. Milora et al., "Confinement of High-Density Pellet-Fueled Discharges in TFTR," *Plasma Phys. Controlled Fusion* **28**, 1435 (1986).

5. S. L. Milora et al., "Summary of Energy and Particle Confinement in Pellet-Fueled, Auxiliary-Heated Discharges in JET," p. 91 in *Controlled Fusion and Plasma Physics: Proceedings of the 16th European Conference,* European Physical Society, Geneva, 1989.

6. S. L. Milora, "Review of Hydrogen Pellet Injection Technology for Plasma Fueling Applications," *J. Vac. Sci. Technol. A* **7**, 925 (1989).

7. M. J. Gouge et al., "The CIT Pellet Injection System: Description and Supporting Research and Development," p. 1240 in *Proceedings of the 13th Symposium on Fusion Engineering, Knoxville, 1989,* vol. 2, Institute of Electrical and Electronics Engineers, New York, 1990.

8. J. R. Gilleland et al., "ITER: Concept Definition," *Nucl. Fusion* **29**, 1191 (1989).

9. P. C. Souers, *Hydrogen Properties for Fusion Energy*, Univ. California Press, Berkeley, 1986.

10. P. C. Souers, "Cryogenic Implications for DT," p. 99 in *Proceedings of the Fusion Fueling Workshop*, Princeton Plasma Physics Laboratory, Princeton, N.J., 1978.

11. P. C. Souers et al., "Anomalous Vapor Pressure over Liquid Deuterium Tritium," *Cryogenics* **22**, 45 (1982).

12. S. L. Milora and C. A. Foster, "Pneumatic Hydrogen Pellet Injection Systems for the ISX Tokamak," *Rev. Sci. Instrum.* **50**, 482 (1979).

13. S. L. Milora, "Review of Pellet Fueling," *J. Fusion Energy* **1**, 15 (1981).

14. S. L. Milora et al., "Development of Hydrogen Pellet Injectors and Pellet Fueling Experiments at ORNL," p. 461 in *Plasma Physics and Controlled Nuclear*

Fusion Research: Proceedings of the 9th International Conference, 1982, International Atomic Energy Agency, Vienna, 1983.

15. S. K. Combs et al., "Development of Hydrogen Pellet Injectors at ORNL," *Nucl. Technol./Fusion* **4**, 666 (1983).

16. J. Lafferanderie et al., "Experimental Test of 6mm Diameter D_2 Pellets Produced by In-Situ Condensation," p. 1387 in *Fusion Technology 1986: Proceedings of the 14th Symposium,* vol. 2, Pergamon Press, Oxford, 1986.

17. S. K. Combs, S. L. Milora, and C. R. Foust, "Simple Pipe Gun for Hydrogen Pellet Injection," *Rev. Sci. Instrum.* **57**, 2636 (1986).

18. H. Sorensen et al., "Simplified Pipe Gun," *Rev. Sci. Instrum.* **58**, 2336 (1987).

19. P. W. Fisher et al., "Tritium Proof-of-Principle Injector Experiment," *Fusion Technol.* **14**, 977 (1988).

20. P. W. Fisher et al., "Tritium Pellet Injector Results," *J. Vac. Sci. Technol. A* **7**, 938 (1989).

21. P. W. Fisher, D. T. Fehling, and S. L. Milora, "Tritium Proof-of-Principle Pellet Injector Results," p. 1236 in *Proceedings of the 13th Symposium on Fusion Engineering, Knoxville, 1989,* vol. 2, Institute of Electrical and Electronics Engineers, New York, 1990.

22. S. L. Milora, S. K. Combs, and C. R. Foust, "Fast Opening Magnetic Valve for High-Pressure Gas Injection and Applications to Hydrogen Pellet Fueling Systems," *Rev. Sci. Instrum.* **57**, 2356 (1986).

23. P. C. Souers, *Cryogenic Hydrogen Data Pertinent to Magnetic Fusion Energy,* UCRL-52628, Lawrence Livermore Laboratory, Livermore, Calif., 1979.

24. Y. S. Touloukian et al., *Thermophysical Properties of Matter,* Vol. 1, *Thermal Conductivity of Metallic Elements and Alloys,* Plenum, New York, 1970.

25. L. D. Landau and E. M. Lifshitz, *Fluid Mechanics*, Addison Wesley, Reading, Mass., 1959.

26. M. J. Gouge et al., "Design Considerations for Single-Stage and Two-Stage Pneumatic Pellet Injectors," *Rev. Sci. Instrum.* **60**, 570 (1989).

27. A. E. Seigel, *The Theory of High Speed Guns*, AGARDograph-91, 1965.

28. L. A. Alekseeva. O. V. Litvin, and I. N. Krupskii, "Temperature Dependence of the Yield Stress of Solid Hydrogen," *Sov. J. Low Temp. Phys.* **8**, 158 (1982).

29. D. N. Bolshutkin, Y. E. Stetsenko, and L. A. Alekseeva, "Plastic Deformation and Stress Relaxation in Solid Normal Deuterium," *Sov. Phys. Solid State* **12**, 119 (1970).

30. S. L. Milora et al., "Results of Hydrogen Pellet Injection Into ISX-B," *Nucl. Fusion* **20**, 1491 (1980).

31. K. Buchl and W. Sandmann, "Launching of D_2-Pellets Through Guide Tubes," p. 1507 in *Fusion Technology 1982: Proceedings of the 12th Symposium*, Pergamon Press, Oxford, 1982.

32. M. L. Watkins et al., "A Model for Pellet Ablation in JET," p. 201 in *Controlled Fusion and Plasma Physics: Proceedings of the 14th European Conference*, European Physical Society, Geneva, 1987.

33. Y. Kamada et al., "Improved Confinement Characteristics of Pellet Fuelled Discharges on JT-60," *Nucl. Fusion* **29**, 1785 (1989).

34. L. R. Baylor, *Particle Transport in Pellet Fueled JET Plasmas*, ORNL/TM-11420, Martin Marietta Energy Systems, Inc., Oak Ridge National Laboratory, 1990.

ORNL/TM-11781
Dist. Category UC-424

INTERNAL DISTRIBUTION

1. J. Sheffield
2. C. C. Baker
3. M. J. Saltmarsh
4. L. A Berry
5. B. A. Carreras
6. R. A. Dory
7. J. L. Dunlap
8. H. H. Haselton
9. M. S. Lubell
10. T. E. Shannon
11. R. P. Leinius
12–13. Laboratory Records Department
14. Laboratory Records, ORNL-RC
15–16. Central Research Library
17. Document Reference Section
18. Fusion Energy Division Library
19–20. Engineering Technology/Fusion Energy Division Publications Office
21. ORNL Patent Office
22–26. P. W. Fisher
27. S. L. Milora
28. M. J. Gouge
29. M. L. Bauer
30. L. R. Baylor
31. S. K. Combs
32. D. T. Fehling
33. C. A. Foster
34. J. S. Watson

EXTERNAL DISTRIBUTION

35. Office of the Assistant Manager for Energy Research and Development, U.S. Department of Energy Field Office, Oak Ridge, P.O. Box 2000, Oak Ridge, TN 37831
36. N. A. Davies, Director, Office of Fusion Energy, Office of Energy Research, ER-50 Germantown, U.S. Department of Energy, Washington, DC 20545
37. M. Roberts, International Programs, Office of Fusion Energy, Office of Energy Research, ER-52 Germantown, U.S. Department of Energy, Washington, DC 20545
38. D. E. Baldwin, Institute for Fusion Studies, The University of Texas at Austin, RLM 11.222, Austin, TX 78712-1060
39. R. W. Conn, Mechanical, Aerospace, and Nuclear Engineering Department, 6291 Boelter Hall, University of California, Los Angeles, CA 90024-1597
40. R. Parker, Plasma Fusion Center, Massachusetts Institute of Technology, 167 Albany St., NW16-288, Cambridge, MA 02139
41. K. I. Thomassen, L-637, Lawrence Livermore National Laboratory, P.O. Box 5511, Livermore, CA 94550
42. J. D. Callen, Department of Nuclear Engineering, University of Wisconsin, Madison, WI 53706-1687
43. S. O. Dean, Fusion Power Associates, Inc., 2 Professional Drive, Suite 248, Gaithersburg, MD 20879
44. H. K. Forsen, Bechtel Group, Inc., Research Engineering, P.O. Box 3965, San Francisco, CA 94119
45. R. W. Gould, Department of Applied Physics, California Institute of Technology, Pasadena, CA 91125

46. R. A. Gross, Plasma Research Laboratory, Columbia University, New York, NY 10027
47. R. J. Hawryluk, Princeton Plasma Physics Laboratory, P.O. Box 451, Princeton, NJ 08543
48. D. M. Meade, Princeton Plasma Physics Laboratory, P.O. Box 451, Princeton, NJ 08543
49. W. M. Stacey, School of Nuclear Engineering and Health Physics, Georgia Institute of Technology, Atlanta, GA 30332
50. D. Steiner, Nuclear Engineering Department, NES Building, Tibbetts Avenue, Rensselaer Polytechnic Institute, Troy, NY 12181
51. R. Varma, Physical Research Laboratory, Navrangpura, Ahmedabad 380009, India
52. Bibliothek, Max-Planck Institut für Plasmaphysik, Boltzmannstrasse 2, D-8046 Garching, Germany
53. Bibliothek, Institut für Plasmaphysik, KFA Jülich GmbH, Postfach 1913, D-5170 Jülich, Germany
54. Bibliothek, KfK Karlsruhe GmbH, Postfach 3640, D-7500 Karlsruhe 1, Germany
55. Bibliotheque, Centre de Recherches en Physique des Plasmas, Ecole Polytechnique Fédérale de Lausanne, 21 Avenue des Bains, CH-1007 Lausanne, Switzerland
56. R. Aymar, CEN/Cadarache, Departement de Recherches sur la Fusion Contrôlée, F-13108 Saint-Paul-lez-Durance Cedex, France
57. Bibliothèque, CEN/Cadarache, F-13108 Saint-Paul-lez-Durance Cedex, France
58. Library, JET Joint Undertaking, Abingdon, Oxfordshire OX14 3EA, England
59. Library, FOM-Instituut voor Plasmafysica, Rijnhuizen, Edisonbaan 14, 3439 MN Nieuwegein, The Netherlands
60. Library, National Institute for Fusion Science, Chikusa-ku, Nagoya 464-01, Japan
61. Library, International Centre for Theoretical Physics, P.O. Box 586, I-34100 Trieste, Italy
62. Library, Centro Richerche Energia Frascati, C.P. 65, I-00044 Frascati (Roma), Italy
63. Library, Plasma Physics Laboratory, Kyoto University, Gokasho, Uji, Kyoto 611, Japan
64. Plasma Research Laboratory, Australian National University, P.O. Box 4, Canberra, A.C.T. 2601, Australia
65. Library, Japan Atomic Energy Research Institute, Naka Fusion Research Establishment, 801-1 Mukoyama, Naka-machi, Naka-gun, Ibaraki-ken, Japan
66. T. V. George, Plasma Technologies Branch, Division of Development and Technology, Office of Fusion Energy, Office of Energy ResearchER-531 Germantown, U.S. Department of Energy, Washington, DC 20545
67. E. Oktay, Division of Confinement Systems, Office of Fusion Energy, Office of Energy Research, ER-55 Germantown, U.S. Department of Energy, Washington, DC 20545
68. H. S. Staten, Plasma Technologies Branch, Division of Development and Technology, Office of Fusion Energy, Office of Energy Research, ER-531 Germantown, U.S. Department of Energy, Washington, DC 20545

69. J. L. Anderson, MS C348, Los Alamos National Laboratory, P.O. Box 1663, Los Alamos, NM 87544
70. J. R. Bartlit, MS C348, Los Alamos National Laboratory, P.O. Box 1663, Los Alamos, NM 87544
71. R. V. Carlson, MS C348, Los Alamos National Laboratory, P.O. Box 1663, Los Alamos, NM 87544
72. G. L. Schmidt, Princeton Plasma Physics Laboratory, P.O. Box 451, Princeton, NJ 08544
73. R. Rossmassler, Princeton Plasma Physics Laboratory, P.O. Box 451, Princeton, NJ 08544
74. P. C. Souers, Lawrence Livermore National Laboratory, P.O. Box 5511, Livermore, CA 94550

75–115. Given distribution as shown in DOE/OSTI-4500-R75, Magnetic Fusion Energy (Category Distribution UC-424, Magnetic Fusion Energy Systems) (41 copies)